Doctoral Dissertation

Monolithic Cellulose Materials and Their Applications for Catalyst Matrix

セルロースモノリス材料の開発と触媒担体への応用

XIE ZHENGTIAN

July 2020

Graduate School of Engineering

Osaka University

Content

General Introduction

Monolithic materials are generally known as single-piece bulk materials with a three-dimensionally connected porous or channel structure. Owing to their high surface area and good flowability, the monolithic materials are considered as the ideal catalyst matrices for constructing flow catalytic devices. The monolithic materials decorated with metal nanoparticles (NPs) such as palladium (Pd), copper (Cu), silver (Ag), and gold (Au) NPs are frequently used in fields including the materials preparation, pharmaceutical synthesis and environmental treatment, [4-9] since they can realize the continuous-flow applications of metal catalysts and offers advantages such as superior heat and mass transfer, good reusability and controllability.[10-12]

In the past two decades, numerous monolithic materials [13-17] were developed for the catalytic application. They were divided into three categories according to their chemical composition: inorganic monoliths, organic monoliths, and hybrid monoliths that combined the characteristic of both inorganic and organic monoliths, [18] as shown in **Table 1.** The silica

Table 1. The categories and characteristics of monolithic materials

Monolithic materials		
Inorganic monolith	**Organic polymer monolith**	**Hybrid monolith**
Main synthesis method • Sol-gel process	**Main synthesis method** • Polymerization • Chemically crosslinking	**Main synthesis method** • Sol-gel process • Polymerization
Advantages • Biocompatible • Cheap	**Advantages** • Not sensitive to pH • Good processability • Chemistry properties can be designed	**Advantages** • Combined the properties of both organic and inorganic monolith
Disadvantages • pH sensitive • Low mechanical resistance	**Disadvantages** • Swelling • Non-biodegradable	**Disadvantages** • Complicated chemical composition

monolith was the commonest inorganic monolith that has been under the spotlight for a few years. [13, 19-23] It was usually prepared by a sol-gel method and posed a typical hierarchically porous structure. The structure of the silica monolith can be well adjusted by controlling the preparation conditions or adding some surfactants. Silica monoliths have been functionalized by different procedures to create active catalytic sites on the surface for various catalytic reactions. [24] It was reported to support catalytic pieces such as MOF, Zeolites, and MNPs including Pd, Ag, and Au NPs as monolithic catalysts and exhibited high catalytic efficiency.[22, 25-28] However, Silica-based monoliths are restricted to application in pH 2~8 due to their dissolution under alkaline conditions. Moreover, most of the inorganic columns without incorporation with other soft materials are usually fragile and easy to be crushed under compression. [29-31] The break of monolith in the flow reaction may lead to unreliable activity or even lose efficacy. Different from the inorganic monolith, the organic polymer monoliths have superior processability and good designation in structure and function. They can be fabricated from selective monomers through a polymerization process in a closed mold. The porous structure can be adjusted by the polymerization conditions including the time, temperature, solvent selection, and monomer concentrations.[32] The active groups for anchoring metal catalysts can be introduced in either the polymerization step or the post-modification process. For example, the Au NPs were deposited on the polyurethane (PU) sponge [33] by a copolymer coating method. Resulted monolithic materials can be used to efficiently reduce 4-nitrophenol with good stability. Monolithic polymers such as the polyamide-imide (PAI) [34], polymethylmethacrylate PMMA[35], polystyrene (PS) [36], polystyrene-poly(ethylene glycol) (PS-PEG) resin [37] and polyelectrolyte [38] were also reported to be decorated with MNPs to fabricate catalytic systems. The stability and the catalytic reactivity of these catalysts were therefore fundamentally improved. One of the drawbacks of the polymer monoliths is that the well-designed polymer skeletons usually suffer the swelling problem in some organic solvent even it was chemically crosslinked, which results in an increase of backpressure in the flow process.[39] Moreover, the majority of the reported MNPs decorated polymer catalytic systems are unbiodegradable and hard to recycle, which are inconsistent with the requirements of

energy-saving and environment protection.

With the improving awareness of cost-saving and environmental protection, an increasing number of recent researches trends to fabricate flow catalytic devices from renewable and biofriendly biomaterials, since the bioresource generally features low price and easy accessibility and biodegradability. Among various biomass-based monolithic materials, the monolithic cellulose materials, due to their renewable, inexpensive, non-toxic, and biodegradable characteristics, were increasingly considered as an ideal candidate to support MNPs as high-efficiency catalysts. [40-43] Besides the merits of monolithic materials mentioned above, using monolithic cellulose materials as catalyst matrices may include following advantages: (1) good thermal stability and insolubility in both water and most organic solvent, which ensures the enhanced stability of catalysts supported on them; (2) the natural surface of cellulose bears a large amount hydroxyl groups, which could be easily functionalized for immobilization of catalyst; (3) the high crystalline order and chiral properties may participate in catalytic events; (4) available industrially in large scale.

Although numerous efforts have been devoted to developing cellulose catalytic system, the majority of the previous researches loaded the metal NPs on the powdery [44 45] or fibrous cellulose, [42, 46, 47] the use of the monolithic cellulose as a matrix for catalytic applications is still in its infancy. Since the cellulose is insoluble in common solvents and it cannot be easily polymerized from its corresponding monomer, the cellulose monolith can hardly be fabricated by traditional strategies such as the sol-gel process, and polymerization-induced phase separation. [48-50] Therefore, the current methods for fabricating monolithic cellulose usually

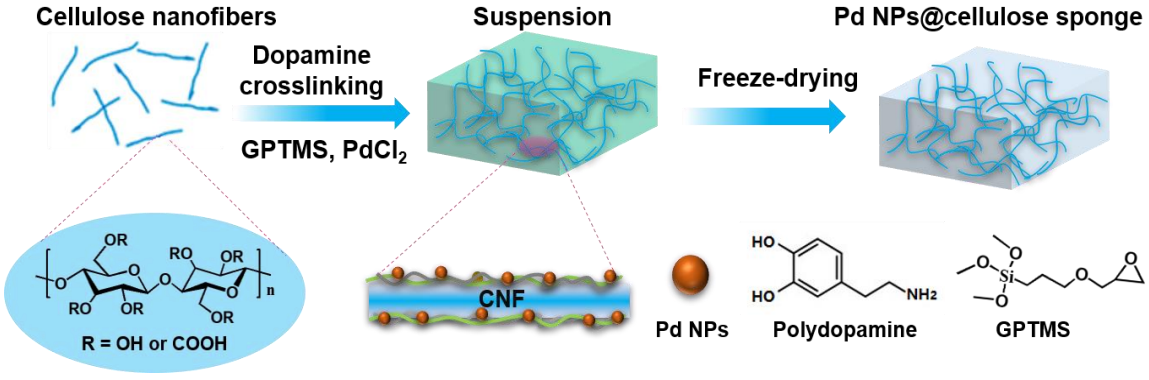

Fig. 1 Schematic of the stepwise formation of cellulose sponge-Pd catalysts. [3]

based on the crosslinking of the cellulose nanofibers or cellulose nanocrystals. [51] For example, the monolithic cellulose sponges were prepared by dual-cross-linking cellulose nanofiber (CNF) with γ-glycidoxypropyltrimethoxysilane (GPTMs) and polydopamine (PDA) and used as carriers of Pd NPs. (**Fig. 1**) The resultant Pd-monolith has shown remarkable catalytic activity and excellent recyclability in Suzuki and Heck cross-coupling reactions. Since some cellulose derivatives such as the 2,2,6,6-Tetramethylpiperidinyloxy (TEMPO)-oxidized cellulose can be dissolved in water, and thus the monolithic cellulose can also be fabricated by crosslinking of these soluble cellulose deriatives. The chemical crosslinking methods require the suitable crosslinking agents or modifers, the chemistry composition is therefore, different with the orignial cellulose. The cellulose dissolved in some special solvent systems such as the ionic liquid, *N*-Methylmorpholine-*N*-oxide monohydrate (NMMO), NaOH/urea, and LiCl/N,N-dimethyl acetamide (DMAc) solvent systems, can also be used to prepare monolithic porous cellulose by a gelation and freeze-drying method. These strategies are heavily relied on the solvent. The ice-templated method can also be used to fabricate porous monolithic cellulose, but few researches reported to use the ice-templated monolithic cellulose to fabricate flow reactor, which may be resulted from its relatively weak mechanical properties.

Recently, a facile temperature-induced phase separation (TIPS) method [2] was developed to prepare the cellulose monolith from cellulose acetate (CA). Unlike crystalline cellulose, CA is a commercially available derivative of cellulose. Owing to the partial acetylation of their hydroxyl groups on the side chains, CA shows a good solubility toward some organic solvents such as acetone and DMF. Therefore, the porous CA monolith can be easily fabricated through a dissolution and phase separation induced by temperature. In this method, the morphology of the final CA monolith can be controlled by changing the conditions such as the initial CA concentration and quench temperature. After deacetylation, the cellulose monolith can be easily obtained. The cellulose monolith prepared via TIPS has a hierarchically porous structure. (**Fig. 2**) This method escapes from the chemical crosslinking steps and the product kept the original chemical structure of cellulose. Moreover, the obtained cellulose monolith can be easily functionalized with reactive groups such as epoxy, primary amine, and aldehyde. [2] Thus, it was

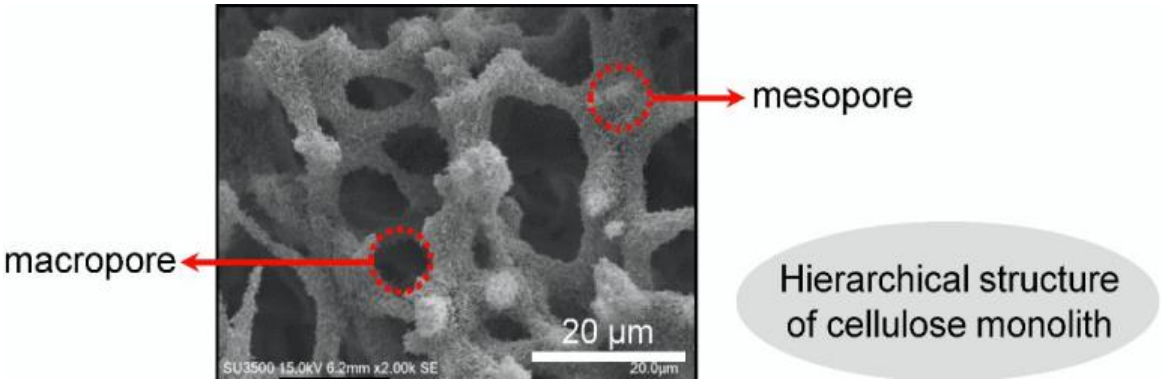

Fig. 2 SEM image of the cellulose monolith prepared via TIPS. [2]

regarded as a promising matrix candidate for supporting metal NPs to efficiently develop green and high-efficiency catalytic systems.

To decorate the MNPs on the cellulose matrix, the current methods can be classified into two strategies including the "graft-to" and "*in situ* synthesis" strategies. In the "graft-to" strategy, the metal NPs were previously prepared and then transferred onto the cellulose. In NPs preparation steps, some ligand or stabilizer such as polyvinylpyrrolidone (PVP) [52] is usually added to adjust the size and shape of the obtained NPs, but the ligand or stabilizer attached on the metal surface may affect the deposition process since it will shield the interaction between metal NPs and cellulose support. Moreover, the existence of ligand or stabilizer might lead to a decrease in the catalytic activity due to the coverage of the active metal sites. [53] Therefore, suitable post-treatment for removing the stabilizer may be necessary for improving the catalytic performance of the MNPs after supported on the monolith.

In terms of the "*in situ* synthesis" strategy, the metal NPs were directly synthesized on cellulose support from the metal precursors. This method can reduce the preparation steps and avoid the use of an excess stabilizer. As shown in **Fig. 3**, there are generally three approaches to *in situ* synthesis metal NPs on cellulose. The first and most common approach is to use an external reducing agent to reduce a metal precursor to form metal NPs on the surface of cellulose support. [1] The sodium borohydride ($NaBH_4$) is one of the most used reducing agents. Schlesinger et al. [54] demonstrated that the size of metal NPs increases with the increase of the metal salt concentration. The majority of the reducing agent such as the $NaBH_4$ and hydrazine (NH_2NH_2) have a fast and efficient reducing capacity, but some of the reducing agents are

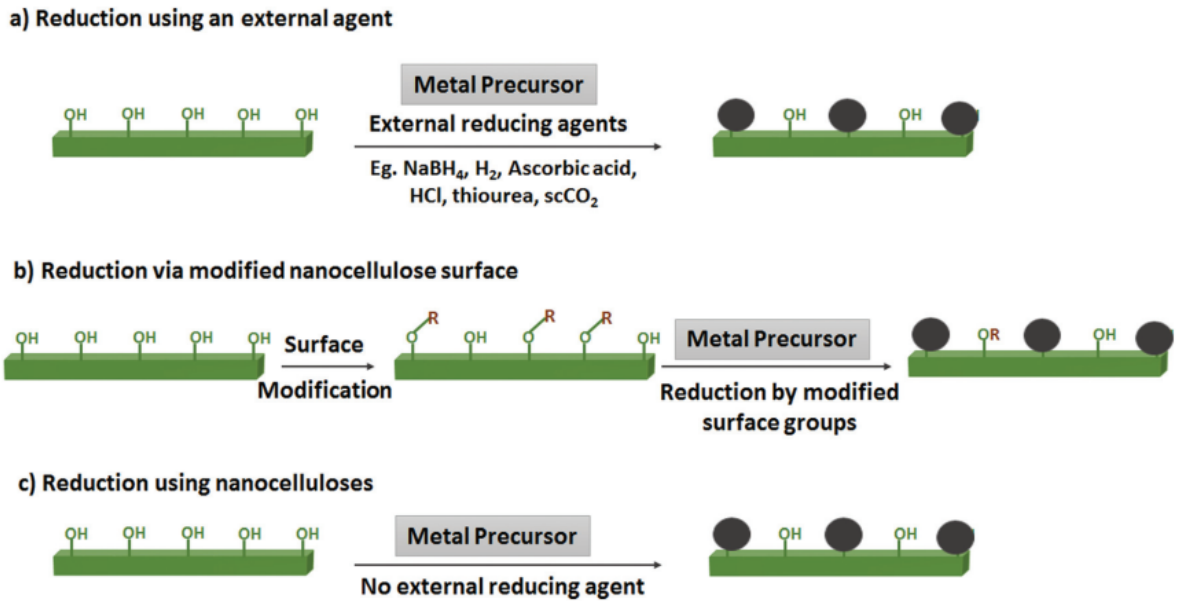

Fig. 3 Three approaches for synthesis of metal NPs-cellulose hybrid composite: (a) reduction using an external agent, (b) reduction via modified nanocellulose surface, and (c) reduction using nanocelluloses. [1]

either expensive or toxic, which are not conducive to the sustainable development of green cellulose catalytic systems.

The second approach for using cellulose as a matrix is to modify the surface of cellulose by attaching chemical groups that have reducing/coordinating capabilities. These functionalized celluloses can be used to generate metal NPs from their corresponding salts, without the use of any external reducing agent. For example, the polydopamine-modified cellulose was reported to synthesize Ag NPs on cellulose using dopamine as a reducing agent. [55] Other chemicals such as the aldehyde groups and thiol groups are also showed reducibility to some metal ions including the Ag and Au ions, and thus these groups are also be grafted on the cellulose to act as reducing agent. [56 57] This method combined the reduction of metal ions and immobilization of the formed metal NPs in one step, but it relied on the special surface functionalization of cellulose. The eventual chemical properties of the cellulose are changed during the modification.

The third approach is to use the surface hydroxyl groups on the celluloses itself for reducing metal precursors into metal NPs. Different from the methods described above, this method is very simple and needs not any surface modification. It can combine the reduction, stabilization, and support into one process and eliminate the addition of a reducing agent and

stabilizer.[52, 58-62] This strategy also minimizes the remaining chemicals attached to the MNP surface after immobilization and reduces the effect of impurities on the catalytic performance of metal NPs. Some recent researches indicated that cellulose could directly reduce noble metal ions including Pd [63, 64], Pt [65-67], Ag [68, 69], and Au [61, 62], but these reduction reactions usually need reaction conditions such as introducing the supercritical CO_2 or energy-consuming steps like hydrothermal treatment.

Although many methods have been reported for introducing metal catalysts on cellulose materials, the majority of them are established based on the powdery or fibrous cellulose. A more specialized method that faces on the monolithic cellulose is still needed to be studied, because: (1) some conditions for powdery or fibrous cellulose may not suitable for monolithic cellulose. For example, the hydrothermal method for synthesizing metal NPs on cellulose can hardly be used for monolithic cellulose since it may lead to the damage of the pore structure of monolith. (2) Different from the common methods conducted in a batch fashion, the connected pore structure of monolithic cellulose enables the continuous-flow synthesis of metal NPs in the monolith. Therefore, more effective methods may be designed based on the structural features of cellulose monolith. (3) The interaction between cellulose and the metal NPs may be affected by the surface morphology of cellulose support, thus the metal NPs formed on monolith may show different stability from that on powdery or fibrous cellulose. Considering these facts above, the suitable method for cellulose monolith is still wait to be established.

In this thesis, the author aimed at the develop efficient strategies for fabricating flow catalytic devices using the monolithic cellulose materials as green catalyst matrices. Specifically, the cellulose monolith prepared via TIPS will be used as the main catalytic matrix in this research, and then three strategies from three perspectives were introduced to construct a flow reactor based on cellulose monolith. Chapter 1 describes the preparation process of cellulose monolith and then reports a surface modification strategy to support of metal catalysts. Chapter 2 focuses on the deposition of narrow-dispersed Au NPs on cellulose. It was realized by depositing the PVP-stabled Au NPs and then removing PVP. Chapter 3 aims at the direct generation and supporting of Au NPs on monolithic cellulose without the surface modification

or the addition of stabilizer or surfactant. This method was very facile and easy to extend to other monolithic cellulose-based materials. In chapter 4, the natural wood and the waste cigarette filter were converted to flow reactors by the method established in Chapter 3. The obtained flow reactors had a typical channel structure and fibrous structure, respectively. Consequently, the obtained reactors showed good flowability and catalytic capacity. These fabrication strategies established in this thesis may provide a guidance for the future develop sustainable flow reactors based on biodegradable monolithic cellulose materials.

Outline of this thesis

In this thesis, the author aimed at developing efficient methods for fabricating catalytic devices using monolithic cellulose materials as green catalyst matrices. This thesis includes 4 chapters.

Chapter 1 Amino modification of cellulose monolith for supporting palladium nanoparticles as flow reactor

The fabrication process of the cellulose monolith from cellulose acetate (CA) via TIPS method was described in this chapter. The branched polyethylenimine (bPEI) was grafted on the pore surface of the monolith to immobilize the Pd NPs. The obtained cellulose-Pd monolith was applied as a flow reactor for continuously catalyzing the reduction reaction of 4-nitrophenol (an important reaction in water treatment) without any post-treatment or regeneration of catalysts. The catalytic performance was calculated and the catalytic mechanism of the monolithic cellulose flow reactor was discussed. By the way, due to the good bio-infinity of bPEI molecules. the bPEI-modified monolith can also be applied to other flow applications such as the bacteria capture in water, which was also investigated in this Chapter.

Chapter 2 Transfer the narrow-dispersed gold nanoparticles on cellulose monolith without surface modification

In this part of research, the poly(vinylpyrrolidone) (PVP)-stabilized Au NPs with a narrow

size distribution were deposited on cellulose monolith. After the removal of the attached PVP by washing with the $NaBH_4$ solution, the obtained sample can be used as a flow reactor in water. This method realized the deposition of the narrow size distribution of Au catalysts and avoided the chemical modification of the cellulose monolith surface.

Chapter 3 Cellulose monolith generating and supporting gold nanoparticles under continuous-flow condition

Chapter 3 introduced a facile method, in which the cellulose monolith was employed to directly reduce Au ions and *in situ* immobilize the formed Au NPs in a continuous-flow fashion. This process was conducted without any surface modification or the addition of a reduction agent. The obtained cellulose- Au monolith was directly applied as a green flow reactor in both water and organic solvents and exhibited good catalytic efficiency and stability.

This method was facile and easy to extend to other monolithic cellulose-based materials such as wood and cigarette filter, which was conducted in Chapter 4.

Chapter 4 Facile fabrication of monolithic cellulose reactor from the natural wood and the used cigarette filter

The method in chapter 3 for generating Au NPs on cellulose monolith was extended to other cellulose-based monolithic materials. As proof of concept, two kinds of monolithic cellulose materials were utilized to fabricate catalytic systems. First is the natural wood material, the most abundant cellulose resource in society. It has a naturally channel structure, which is accessible for flow application. It was converted to a flow reactor after delignification. Second is the used cigarette filter, a common cellulose-derived waste in the daily life. It shows a typical anisotropic structure with a large amount of cellulose acetate fibers bunched together. It was applied to generate and support Au NPs for water treatment. Both these confirmed that the continuous-flow method for generation metal NPs using monolithic cellulose as reducing agent has a great potential for developing flow catalytic devices.

References:

1. M. Kaushik and A. Moores, *Green Chemistry*, 2016, **18**, 622-637.
2. Y. Xin, Q. Xiong, Q. Bai, M. Miyamoto, C. Li, Y. Shen and H. Uyama, *Carbohydrate polymers*, 2017, **157**, 429-437.
3. Y. Li, L. Xu, B. Xu, Z. Mao, H. Xu, Y. Zhong, L. Zhang, B. Wang and X. Sui, *ACS applied materials & interfaces*, 2017, **9**, 17155-17162.
4. P. Marín, F. V. Díez and S. Ordóñez, *Chemical Engineering and Processing - Process Intensification*, 2019, **135**, 175-189.
5. D. K. B. Mohamed, X. Yu, J. Li and J. Wu, *Tetrahedron Lett.*, 2016, **57**, 3965-3977.
6. J. P. McMullen, M. T. Stone, S. L. Buchwald and K. F. Jensen, *Angewandte Chemie*, 2010, **49**, 7076-7080.
7. H. Nakamura, Y. Yamaguchi, M. Miyazaki, H. Maeda, M. Uehara and P. Mulvaney, *Chem Commun (Camb)*, 2002, DOI: 10.1039/b208992k, 2844-2845.
8. A. Molnar, *Chem. Rev.*, 2011, **111**, 2251-2320.
9. M. Irfan, T. N. Glasnov and C. O. Kappe, *ChemSusChem*, 2011, **4**, 300-316.
10. A. Odedra and P. H. Seeberger, *Angewandte Chemie*, 2009, **48**, 2699-2702.
11. R. P. Jumde, M. Marelli, N. Scotti, A. Mandoli, R. Psaro and C. Evangelisti, *Journal of Molecular Catalysis A: Chemical*, 2016, **414**, 55-61.
12. M. A. Bañares, *Catalysis Today*, 1999, **51**, 319-348.
13. C. H. Pelisson, T. Nakanishi, Y. Zhu, K. Morisato, T. Kamei, A. Maeno, H. Kaji, S. Muroyama, M. Tafu, K. Kanamori, T. Shimada and K. Nakanishi, *ACS applied materials & interfaces*, 2017, **9**, 406-412.
14. A. Cybulski and J. A. Moulijn, *Catalysis Reviews*, 1994, **36**, 179-270.
15. J. Chakraborty, I. Nath, S. Song, S. Mohamed, A. Khan, P. M. Heynderickx and F. Verpoort, *Journal of Photochemistry and Photobiology C: Photochemistry Reviews*, 2019, **41**.
16. R. Poupart, D. Grande, B. Carbonnier and B. Le Droumaguet, *Progress in Polymer Science*, 2019, **96**, 21-42.
17. M. Nasrollahzadeh, M. Sajjadi, M. Shokouhimehr and R. S. Varma, *Coordination Chemistry Reviews*, 2019, **397**, 54-75.
18. M. R. Gama, F. R. P. Rocha and C. B. G. Bottoli, *TrAC, Trends Anal. Chem.*, 2019, **115**, 39-51.
19. A. Taguchi and F. Schüth, *Microporous and mesoporous materials*, 2005, **77**, 1-45.

20. W. Zhang, D. Wang and R. Yan, *Selective Nanocatalysts and Nanoscience: Concepts for Heterogeneous and Homogeneous Catalysis*, 2011, 29-71.
21. Y. T. Lai, T. C. Chen, Y. K. Lan, B. S. Chen, J. H. You, C. M. Yang, N. C. Lai, J. H. Wu and C. S. Chen, *ACS Catalysis*, 2014, **4**, 3824-3836.
22. C.-H. Pélisson, T. Nakanishi, Y. Zhu, K. Morisato, T. Kamei, A. Maeno, H. Kaji, S. Muroyama, M. Tafu and K. Kanamori, *ACS applied materials & interfaces*, 2016, **9**, 406-412.
23. B. P. Bastakoti, Y. Li, N. Miyamoto, N. M. Sanchez-Ballester, H. Abe, J. Ye, P. Srinivasu and Y. Yamauchi, *Chemical Communications*, 2014, **50**, 9101-9104.
24. A. Galarneau, A. Sachse, B. Said, C.-H. Pelisson, P. Boscaro, N. Brun, L. Courtheoux, N. Olivi-Tran, B. Coasne and F. Fajula, *Comptes Rendus Chimie*, 2016, **19**, 231-247.
25. A. Sachse, N. Linares, P. Barbaro, F. Fajula and A. Galarneau, *Dalton transactions*, 2013, **42**, 1378-1384.
26. M. T. Alotaibi, M. J. Taylor, D. Liu, S. K. Beaumont and G. Kyriakou, *Surf. Sci.*, 2016, **646**, 179-185.
27. S. S. Bharadwaj, C. Yokoyama and L. D. Schmidt, *Applied Catalysis A: General*, 1996, **140**, 73-97.
28. N. Moitra, A. Matsushima, T. Kamei, K. Kanamori, Y. H. Ikuhara, X. Gao, K. Takeda, Y. Zhu, K. Nakanishi and T. Shimada, *New J. Chem.*, 2014, **38**, 1144-1149.
29. A. El Kadib, R. Chimenton, A. Sachse, F. Fajula, A. Galarneau and B. Coq, *Angewandte Chemie International Edition*, 2009, **48**, 4969-4972.
30. J. Łojewska, A. Kołodziej, J. Żak and J. Stoch, *Catalysis today*, 2005, **105**, 655-661.
31. N. Linares, S. Hartmann, A. Galarneau and P. Barbaro, *ACS Catalysis*, 2012, **2**, 2194-2198.
32. F. Svec, *J. Chromatogr. A*, 2010, **1217**, 902-924.
33. Y. Yu, W. Xiao, T. Zhou, P. Zhang, C. Yan and Z. Zheng, *Materials Chemistry Frontiers*, 2017, **1**, 482-486.
34. Y. He, F. Rezaei, S. Kapila and A. A. Rownaghi, *ACS applied materials & interfaces*, 2017, **9**, 16288-16295.
35. M. Nandi and H. Uyama, *RSC Advances*, 2014, **4**, 20847-20855.
36. R. Greco, L. Caciolli, A. Zaghi, O. Pandoli, O. Bortolini, A. Cavazzini, C. De Risi and A. Massi, *Reaction Chemistry & Engineering*, 2016, **1**, 183-193.
37. T. Suzuka, K. Kimura and T. Nagamine, *Polymers*, 2011, **3**, 621-639.
38. Y. Mei, Y. Lu, F. Polzer, M. Ballauff and M. Drechsler, *Chemistry of Materials*, 2007,

19, 1062-1069.

39. R. J. Groarke and D. Brabazon, *Materials (Basel)*, 2016, **9**.
40. X. Wu, Z. Shi, S. Fu, J. Chen, R. M. Berry and K. C. Tam, *ACS Sustainable Chemistry & Engineering*, 2016, **4**, 5929-5935.
41. M. A. Lucchini, E. Lizundia, S. Moser, M. Niederberger and G. Nystrom, *ACS applied materials & interfaces*, 2018, **10**, 29599-29607.
42. J. Tan, R. Liu, W. Wang, W. Liu, Y. Tian, M. Wu and Y. Huang, *Langmuir*, 2009, **26**, 2093-2098.
43. M. Kaushik and A. Moores, *Green Chemistry*, 2016, **18**, 622-637.
44. F. Quignard and A. Choplin, *Chemical Communications*, 2001, 21-22.
45. M.-Y. Zhou, Y.-Q. Li and X.-M. Xu, *Journal of Chemical Research*, 2003, **2003**, 134-135.
46. X. Wu, C. Lu, Z. Zhou, G. Yuan, R. Xiong and X. Zhang, *Environmental Science: Nano*, 2014, **1**, 71-79.
47. W. Li, R. Liu, H. Kang, Y. Sun, F. Dong and Y. Huang, *Polymer Chemistry*, 2013, **4**, 2556-2563.
48. V. L. Budarin, J. H. Clark, R. Luque, D. J. Macquarrie and R. J. White, *Green Chemistry*, 2008, **10**, 382-387.
49. J. L. Williams, *Catalysis Today*, 2001, **69**, 3-9.
50. Q. Lin, X. Hou and C. Ke, *Angewandte Chemie*, 2017, **56**, 4452-4457.
51. T. Saito, S. Kimura, Y. Nishiyama and A. Isogai, *Biomacromolecules*, 2007, **8**, 2485-2491.
52. K. M. Koczkur, S. Mourdikoudis, L. Polavarapu and S. E. Skrabalak, *Dalton transactions*, 2015, **44**, 17883-17905.
53. Y. Borodko, H. S. Lee, S. H. Joo, Y. Zhang and G. Somorjai, *The Journal of Physical Chemistry C*, 2009, **114**, 1117-1126.
54. M. Schlesinger, M. Giese, L. K. Blusch, W. Y. Hamad and M. J. MacLachlan, *Chem Commun (Camb)*, 2015, **51**, 530-533.
55. Z. Shi, J. Tang, L. Chen, C. Yan, S. Tanvir, W. A. Anderson, R. M. Berry and K. C. Tam, *J Mater Chem B*, 2015, **3**, 603-611.
56. N. Drogat, R. Granet, V. Sol, A. Memmi, N. Saad, C. Klein Koerkamp, P. Bressollier and P. Krausz, *J. Nanopart. Res.*, 2010, **13**, 1557-1562.
57. S. M. Ansar, R. Haputhanthri, B. Edmonds, D. Liu, L. Yu, A. Sygula and D. Zhang, *The Journal of Physical Chemistry C*, 2010, **115**, 653-660.

58. N. Moitra, K. Kanamori, T. Shimada, K. Takeda, Y. H. Ikuhara, X. Gao and K. Nakanishi, *Advanced Functional Materials*, 2013, **23**, 2714-2722.
59. H. Nakao, H. Shiigi, Y. Yamamoto, S. Tokonami, T. Nagaoka, S. Sugiyama and T. Ohtani, *Nano Lett.*, 2003, **3**, 1391-1394.
60. J. Turkevich, P. C. Stevenson and J. Hillier, *Discussions of the Faraday Society*, 1951, **11**, 55-75.
61. J. Van Rie and W. Thielemans, *Nanoscale*, 2017, **9**, 8525-8554.
62. X. Wu, C. Lu, Z. Zhou, G. Yuan, R. Xiong and X. Zhang, *Environmental Science: Nano*, 2014, **1**, 71.
63. X. Wu, C. Lu, W. Zhang, G. Yuan, R. Xiong and X. Zhang, *Journal of Materials Chemistry A*, 2013, **1**, 8645.
64. M. Rezayat, R. K. Blundell, J. E. Camp, D. A. Walsh and W. Thielemans, *ACS Sustainable Chemistry & Engineering*, 2014, **2**, 1241-1250.
65. K. Benaissi, L. Johnson, D. A. Walsh and W. Thielemans, *Green Chem.*, 2010, **12**, 220-222.
66. X. Lin, M. Wu, D. Wu, S. Kuga, T. Endo and Y. Huang, *Green Chem.*, 2011, **13**, 283-287.
67. L. Johnson, W. Thielemans and D. A. Walsh, *Green Chemistry*, 2011, **13**, 1686.
68. F. Fu, J. Gu, J. Cao, R. Shen, H. Liu, Y. Zhang, X. Liu and J. Zhou, *ACS Sustainable Chemistry & Engineering*, 2017, **6**, 738-748.
69. J. Cai, S. Kimura, M. Wada and S. Kuga, *Biomacromolecules*, 2009, **10**, 87-94.

Chapter 1

Amino modified cellulose monolith for supporting metal nanoparticles as flow reactor

1.1 Introduction

The monolithic flow catalytic devices in forms of porous or hollow materials decorated with metal nanoparticles (NPs) are frequently used in fields such as materials preparation, pharmaceutical synthesis and environmental treatment, [1-6] since they make the metal catalysts reusable, controllable and the reproducible.[7-9] Although numerous porous materials [10-14] have been attempted to immobilize the metal NPs on solid substrates to construct reusable catalysts, developing highly effective, environmentally friendly, cost-effective and easily-performed MNPs supported catalytic system with good mechanical property and long-term stability is still on the road.

The ecofriendly polymers from renewable resources like cellulose [15-17], starch [18, 19], chitosan [20], alginate [21], and gelatin [22] recently aroused intensive research interests to exploit them for supported catalysis due to their widely available, inexpensive, non-toxic, and biodegradable characteristics. Among all of the biomass, cellulose is the most abundant renewable biomass in nature which has been produced on an industrial scale and used for developing novel functional materials.[23-25] For example, Wu et al. recently modified cellulose nanocrystals (CNCs) by coating melamine-formaldehyde on its surface and dispersing the Palladium (Pd) NPs on its surface as high-performance nanocatalysts. [16] The obtained catalyst composites exhibited high catalytic activity with a turnover frequency (TOF) of 3168 h^{-1} and can be reused after recovery treatment. Despite the high catalytic efficiency, the separation and recovery process of the CNCs supported catalysts requires multiple steps such as chemical treatment, ultrafiltration and repeatedly washing, which pose an obstacle in scale-up applications. Actually, the powdery or fibrous cellulose such as cellulose nanofibers (CNFs) and CNCs will inevitably aggregate together during the application. As a result, the catalyst

composites will gradually lose the catalytic activity. Moreover, the recovery procedure and post treatment of catalysts may lead to the loss of catalyst and the unreliable catalytic activity. To address these drawbacks, it is highly desirable to develop novel ways to construct the cellulose supported MNPs catalytic system, which not only makes the MNPs stably immobilized and exhibit superior catalytic performance but also guarantee the good stability and continuous-flow use of catalyst without additional recovery treatment.

In this chapter, the thermally-induced phase separation (TIPS) method was used to fabricate cellulose monolith from cellulose acetate (CA). After surface modified with amino groups, the monolith was used to support Pd NPs to construct flow catalytic devices. The obtained flow reactor can be used without additional post-treatment or the tedious recycling process of catalysts. Results indicated that the prepared microreactor had high catalytic efficiency for the typical reduction reaction of 4-nitrophenol (4-NP).

1.2 Experiment

1.2.1 Materials

The cellulose diacetate powder (CA, L_{30}) with an acetylation degree of 55% was friendly provided by DAICEL Co., Ltd. Japan. Epichlorohydrin (EC) with a purity of 99%, branched Polyethylenimine (bPEI, average molecular weight is about 600), Sodium tetrahydroborate ($NaBH_4$), *N,N*-dimethylformamide (DMF), 1-hexanol, and Pd(II) acetate ($Pd(Ac)_2$) were purchased from FUJIFILM Wako Pure Chemical Corporation, Japan. 4-NP was supplied by Tokyo Chemical Industry Co., Ltd. *Escherichia coli* MG1655 and *Bacillus subtilis* 168 were cultured in LB broth (Lennox) medium (Sigma-Aldrich, St Louis, MO, USA). PBS (137 mM NaCl, 2.7 mM KCl, 10 mM Na_2HPO_4 and 1.8 mM KH_2PO_4, pH 7.4) was used as the buffer. Other chemicals were all chemically purified and commercially available.

1.2.2 Preparation of Cellulose-bPEI-Pd monolith

The cellulose acetate monolith was prepared by TIPS method reported in the previous work. [26] The detailed process was as follows: First, 2.5 g of CA powder was completely dissolved into 10 mL of DMF by stirring at 90 ºC. Then 15 mL of 1-hexanol was added dropwise into the mixed solution with gentle stirring. After the mixture becomes transparent, the mixture was put into mold and maintained at 25 ºC for 24 h to complete the phase separation. Finally, the solvent was replaced with ethanol three times, and the obtained CA monoliths were subsequently dried in vacuo at room temperature. The cellulose monoliths were prepared by hydrolyzing the CA monoliths in 0.5 mol/L NaOH solution in methanol at room temperature. After 3 h, the hydrolyzed cellulose monoliths were rinsed with water and methanol successively and dried in vacuo.

For the surface modification of cellulose monoliths, EC was previously used to graft the epoxy groups onto the monoliths. The cellulose monoliths were firstly immersed into 5 wt% NaOH solution in methanol and kept for 3 h at room temperature under gentle shaking and then washed with DMSO. Subsequently, the obtained monoliths were immersed into EC/DMSO solution (30%, v/v) to take the grafting reaction. Here the amount of the epoxy group was 10

times overdose. This reaction was performed for 3 h at 30 °C. The obtained monoliths (cellulose-EC) were washed thoroughly with water until the eluate became neutral and then dried in vacuo. The Cellulose-EC monoliths were further modified with bPEI in ethanol. For this reaction, the Cellulose-EC was immersed into the bPEI/Ethanol solution (30%, v/v) for 24

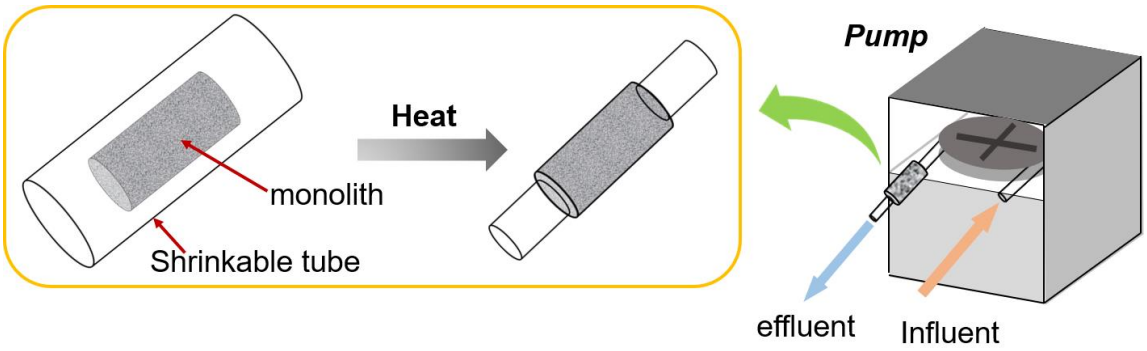

Fig. 1-1. Schematic diagram of the structure of the microreactor and the flow process.

h at 50 °C. The acquired Cellulose-bPEI monoliths were thoroughly rinsed with water and then dried in vacuo. The diameter of the obtained Cellulose-bPEI column was about 0.6 cm.

The Pd supported cellulose monolith (Cellulose-bPEI-Pd) was obtained by allowing the $Pd(OAc)_2$/toluene solution to flow through the Cellulose-bPEI monolith. The Cellulose-bPEI monolith was first cut to relatively small columns with a length of 0.8 cm and fixed in a polytetrafluoroethylene (PTFE) heat-shrinkable tube (**Fig. 1-1**). Then a peristaltic pump was employed to pump the $Pd(OAc)_2$ solution to pass through the monolith followed by repeated washing with toluene. Subsequently, the Pd was *in situ* reduced by the Sodium Borohydride ($NaBH_4$) in the monolith. After drying, the Cellulose-bPEI-Pd monoliths were ready to be used as microreactors.

1.2.3 Catalytic performance test

The reduction reaction of 4-NP was used to test the catalytic performance of the monolithic microreactor. 4-NP (10.0 mmol/L) was mixed with the reducing agent ($NaBH_4$ aqueous solution, 0.2 mol/L) and then the mixture was pumped to flow through the microreactor. After being flowed through the monolith, the effluent was collected and tested by UV-*vis* measurement. The standard solutions of 4-NP were tested to build the standard curve as a reference. According to the standard curve, the concentration of 4-NP in the effluent was calculated. Based on the concentration change of 4-NP and the flow rate, the catalytic

efficiency of the microreactor could be evaluated. The flow rate in this work was corrected by the real volume of the effluent outflowed per minute. To evaluate the stability of obtained reactor, the deionized water was continuously flowed through the reactor with a flow rate of 1 mL/min. After flowed for 1 h, the 4-NP (10 mmol/L) reactants was flowed through the reactor with the flow rate of 1 mL/min to take reaction. The reaction conversion was calculated based on the UV-vis measurements. By repeating the process above, the reaction conversion at each hour was recorded and compared.

1.2.4 Bacterial capture test

E. coli and *B. subtilis* were cultured in LB broth (Lennox) medium with constant shaking at 37 °C. The bacteria were collected by centrifugation at 6000 G and washed three times with PBS buffer to remove the culture medium. The concentration of bacterial suspension was adjusted to 3×10^8 CFU/mL for the flow system. Monolith was cut into 1.5 cm × ϕ 6 mm columns and fixed into a polyolefin heat shrinkable tube (THT-8.0 N). A peristaltic pump was used to flow the bacterial suspension through the monolith with different flow velocities 0.2 mL/min, 1 mL/min, and 3 mL/min. The effluent was collected every few minutes. Bacteria in effluent were counted with a hemocytometer (Sunlead Glass Corp., Japan) following the JHS Standard of Japanese Blood Products Association. Bacteria adhered to the monolith surfaces were fixed with 2.5% glutaraldehyde (in PBS) at 37 °C for 24 h. After rinsing with PBS twice, the samples were dehydrated in an ethanol series (10%, 30%, 50%, 60%, 70% and 80%, 5 min each, and followed by 90% and 100%, 10 min each) and dried under vacuum overnight for the SEM observation.

1.2.5 Characterization

Fourier transform infrared (FTIR) measurements of the samples were performed using the Thermo Scientific (Yokohama, Japan) Nicolet iS5 spectrometer equipped with iD5 ATR attachment. A Hitachi S-3000N scanning electron microscope (SEM), Tokyo, Japan, operated at 15 kV, has been used for the observation of the microstructure of the monoliths. Prior to the measurements, the monolith samples have been slivered into thin sections and adhered to the

probe followed by their coating with a thin layer of gold using an ion sputter apparatus, E-1010 Hitachi Ltd, Tokyo, Japan. Surface elemental composition was captured by Energy-dispersive X-ray spectroscopy (EDX) (HITACHI, Miniscope TM 3000 equipped with Swift ED 3000). The grain size of Pd NPs as well as their distribution in Cellulose-bPEI-Pd monolith were investigated by Transmission electron microscope (TEM, JEOL JEM-2010), with the accelerating voltage of 100 kV. The XRD patterns of cellulose, Cellulose-bPEI, and Cellulose-bPEI-Pd were obtained by using an X-Pert diffractometer, at the wavelength of 1.54 Å. The generator voltage was 45 kV and the generator current was 200 mA. The concentration change of 4-NP in flow reaction was measured by UV-*vis* spectrophotometer (HITACHI, U-2910). The absorbance curve was collected at the wavelengths ranging from 250 to 600 nm. The atomic content of Pd in the samples was detected by inductively coupled plasma atomic emission spectrometry (ICP-AES) with SHIMADZU, ICPS-8100. Pd standards with the atomic concentration of 0.5, 1, 2, 5, and 10 ppm were used for the calibration. The mechanical performance of the monolith was evaluated on a universal testing machine (EZ Graph, SHIMADZU) with a compression speed of 1 mm/min in water. The maximum compression strain (ε) was set to 70%.

1.3 Results and discussion

1.3.1 Fabrication and modification of monolithic cellulose

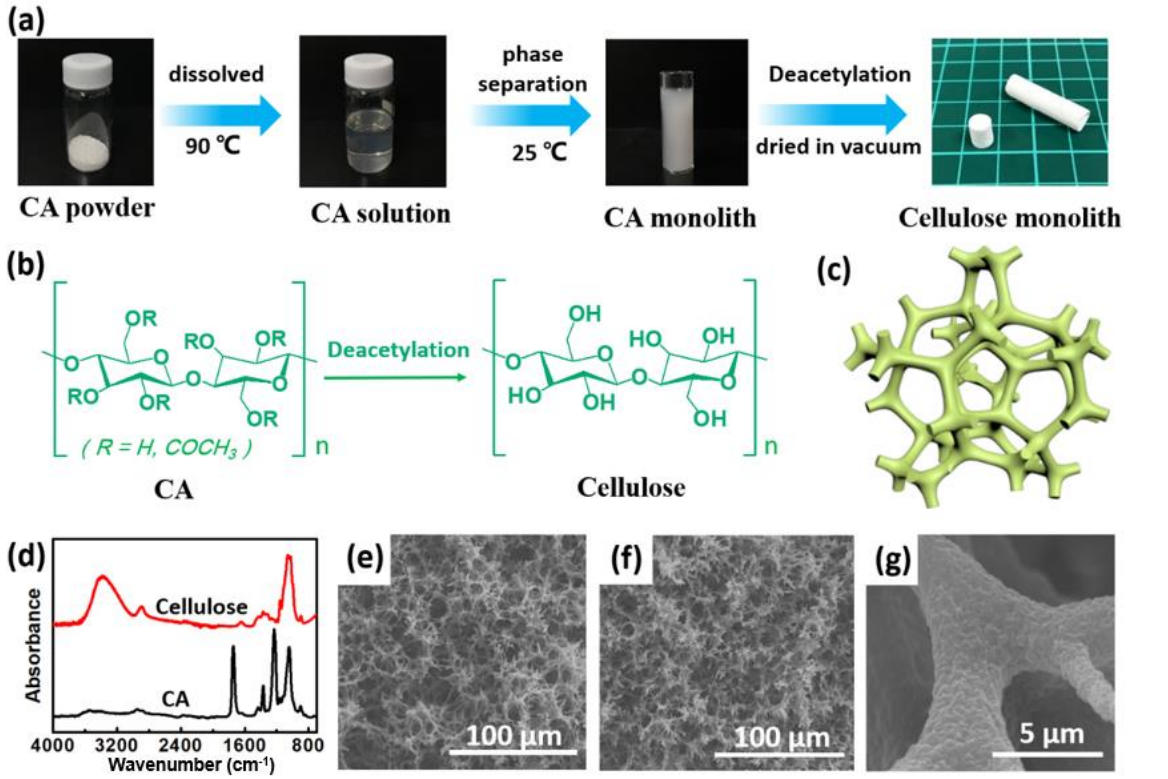

Fig. 1-2. (a) Fabrication process of cellulose monolith by TIPS method. **(b)** Scheme of the deacetylation reaction of cellulose acetate. **(c)** Schematic picture of the skeleton of porous cellulose monolith. **(d)** FTIR spectrums of monoliths before and after deacetylation; SEM images of the micro morphologies of **(e)** CA monolith, **(f)** and **(g)** Cellulose monolith at different scale.

The hierarchically porous cellulose monolith was fabricated according to a simple, inexpensive, and scalable TIPS method reported in the previous work. Unlike crystalline cellulose, CA as a commercially available derivative of cellulose, due to the partial acetylation of the hydroxyl groups on the side chains, shows a good solubility toward some organic solvents such as acetone and DMF. As shown in **Fig. 1-2 (a)**. the CA powder was firstly dissolved into a mixed solvent of DMF and 1-hexanol at 90 °C, then the solution was transferred into a mold and kept at 20 °C. During this process, the phase separation occurred in the mold and the porous CA monolith formed. After deacetylation, the cellulose monolith could be easily obtained from CA monolith. (**Fig. 1-2 (b)**). SEM observation revealed that the obtained cellulose monolith poses a three-dimensionally (3D) continuous macro-pore structure

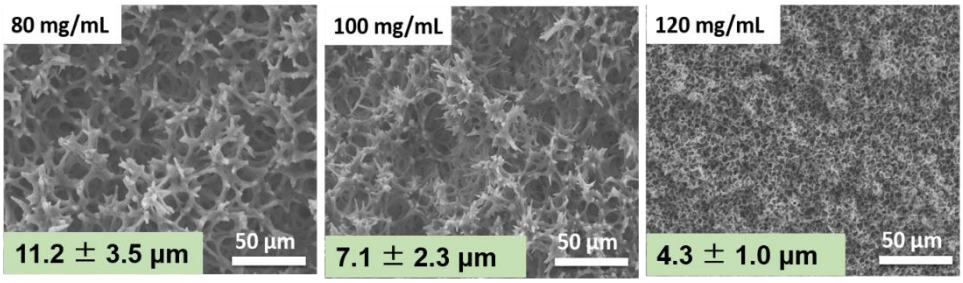

Fig. 1-3. The SEM images of monoliths prepared with different CA concentration. The average macro-pore size was illustrated in the green blank. (**Note**: in all of the later experiments, the concentration of 100 mg/mL was used, except where noted.)

(**Fig. 1-2 (c, e)**). In fact, the macro-pore size can be certainly controlled by changing the fabrication conditions such as the CA concentration. As shown in **Fig. 1-3**, the increase of the CA concentration resulted in the decrease of the pore size. In this thesis, the monolith prepared with the CA concentration of 100 mg/mL was used. Besides of the macro-pores, the monolith has a large number of mesopores with size 3-20 nm according to the non-local density functional theory (NLDFT), [27, 28] which was confirmed by the nitrogen adsorption/desorption experiment. (**Fig. 1-4**) Such a special continuous pore structure not only endows monolith with a relatively high surface area that is conducive to the efficient surface modification and the absorption of metal NPs on the monolith, but also allows the fluidic application of cellulose monolith. To confirm the successful preparation of cellulose monolith, the FTIR experiments was conducted by using ATR mold. The obtained spectrums of CA monolith and deacetylated monolith (cellulose monolith) were collected and compared in **Fig. 1-2 (d)**. It can be found that

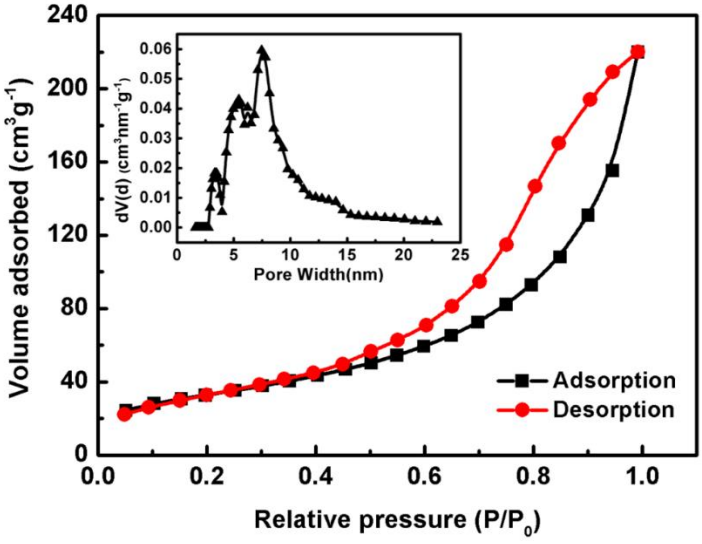

Fig. 1-4 Nitrogen adsorption/desorption isotherms of cellulose monolith. Inset: pore size distribution plots of cellulose monolith.

the characteristic peak of CA at 1232 cm^{-1} and 1743 cm^{-1}, corresponding to the acetate groups, disappeared at the curve of the hydrolyzed monolith. On the other hand, a board new peak centered at 3300 nm, which was attributed to the hydroxide groups, appeared after deacetylation. [29] Both of these indicated that the CA monolith has been successfully converted to cellulose monolith. Considering that the deacetylation reaction of CA was carried out in NaOH solution, the cleavage of the main chain of CA may occur by alkaline hydrolysis; however, the use of methanol as a solvent under mild reaction conditions (at room temperature) enabled the selective hydrolysis of the side chain in CA. After the hydrolysis, the monolith remained a good columnar shape and showed similar porous microstructure with the CA monolith, despite a slight shrinkage of pore size (**Fig. 1-2 (e)** and **(f)**). As illustrated in **Fig. 1-2 (g)**, the skeleton of cellulose monolith posed a relatively rough surface after the deacetylation process. In this process, the acetyl groups were converted to hydroxide groups, which allows for further surface modification of the monolith to supported Pd NPs for catalytic application.

To stably immobilize the Pd NPs on cellulose monolith, a two-step strategy was adopted, including surface modification of monolith and the deposition of Pd accompanied by *in situ* reductions of Pd on the monolith. (**Fig. 1-5 (a)**). In the first step, the monolith was previously treated by EC, then the bPEI, a branched molecule bearing a large number of amino groups (**Fig. 1-5 (b)**), was grafted onto monolith by the reaction between amino groups and epoxy groups of EC. This reaction is easy to take place in ethanol and has already been reported in many previous works. [30, 31] After modification, the monolith was washed repeatedly by water and the dried sample was tested by EDX. **Fig. 1-5 (c)** illustrated the distribution map of nitrogen element on the cross-section of the monolith, it can be found that a great number of nitrogen atoms distributed on the surface of the monolith, indicating that the bPEI molecules were successfully grafted onto the cellulose monolith. FTIR spectrums of cellulose monolith and bPEI modified monolith (Cellulose-bPEI) were also collected by using ATR mold and investigated in **Fig. 1-5 (e)**. Compared to the unmodified cellulose monolith, the spectrum of Cellulose-bPEI shows a new peak at 1570 cm^{-1}, which was resulted from the vibration of primary amine groups of bPEI. [32, 33] Moreover, the peak at 1460 cm^{-1}, corresponding to the methylene groups, [34, 35] became stronger than that of cellulose monolith, which can be attributed to the increase of methylene groups caused by the introduction of bPEI. Because the samples

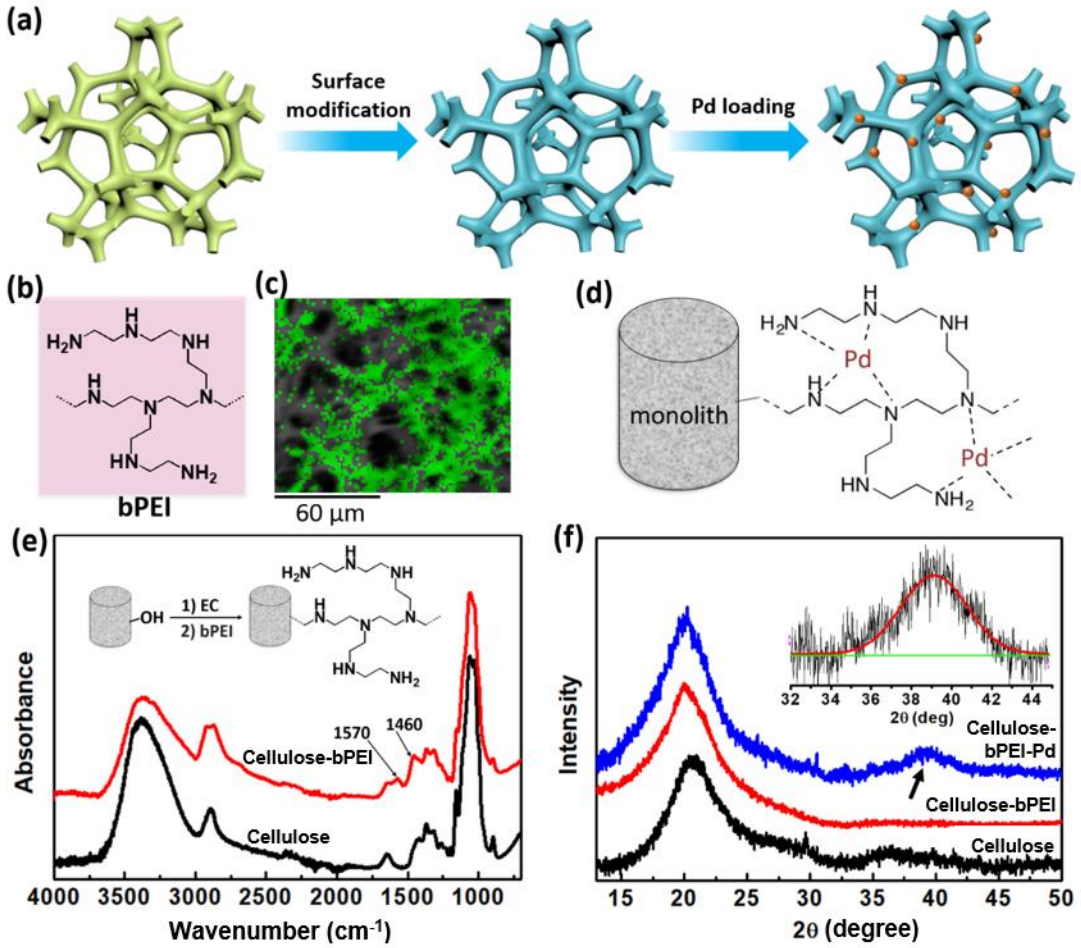

Fig. 1-5. (a) Schematic diagram of the modification and the Pd loading on the pore surface of cellulose monolith. **(b)** Chemical structure of bPEI. **(c)** N elemental mapping (green color) on the cross section of Cellulose-bPEI monolith. **(d)** Chemical structure of the modified cellulose-bPEI-Pd monolith, Pd was anchored by the amino groups of bPEI grafted on the pore surface of monolith. **(e)** FTIR spectrums of the cellulose monolith and bPEI modified cellulose (Cellulose-bPEI). **(f)** XRD spectrums of cellulose, Cellulose-bPEI and Cellulose-bPEI-Pd. The inserted figure is the magnification of the crystal peak around 39° (as noted in arrow).

were washed repeatedly to remove any residual free bPEI molecules, these newly emerged peaks demonstrated the successful modification with bPEI. The grafted bPEI molecules could absorb and anchor Pd on the monolith by the complexation between Pd and amino groups, as shown in **Fig. 1-5 (d).** In the second step, Pd was deposited on the surface of the skeleton of monolith by the circulatory flowing of the $Pd(OAc)_2$/toluene solution through the modified monolith via a pump. During this process, the Pd atoms will be gradually absorbed and anchored by the amino groups on the Cellulose-bPEI monolith. After the *in situ* reductions of Pd in the monolith by $NaBH_4$, the obtained Cellulose-bPEI-Pd monolith could be used as a catalytic reactor.

To quantify the Pd loading in the monolith, the dried Cellulose-bPEI-Pd column (36 mg) was cut to pieces and completely dissolved into aqua regia to be tested by ICP. Results showed the content of Pd in monolith was about 0.07 wt%. Thanks to the sufficient amino groups on the modified monolith and the low concentration of the $Pd(OAc)_2$ solution used in this experiment (30 μmol/L, 10 mL), most of Pd was deposited on monolith and the deposition ratio was calculated to be ~80%. XRD was conducted to study the Pd crystals in the monolith. **Fig. 1-5 (f)** presented the resulted curves of cellulose, Cellulose-bPEI, and Cellulose-bPEI-Pd monolith. Cellulose-bPEI showed very little difference from the cellulose, suggesting that the modification process does not affect the crystallography of cellulose. After the deposition of Pd, the Cellulose-bPEI-Pd presented a new peak centered at $2\theta=39^{o}$ (the insert in **Fig. 1-5 (f))**, which can be indexed to the (111) plane of the face-centered cubic (fcc) structure of Pd. According to the *Bragg's low*, d-spacing of the (111) plane of Pd crystal was calculated to be 0.234 nm, which matched the reported results in other literature and confirmed the formation of Pd NPs crystals. The size and distribution of Pd NPs as well as the morphology of Cellulose-bPEI-Pd monolith were further investigated by SEM and TEM. **Fig. 1-6 (a)** and **(b)** presented the SEM images of cellulose monolith and Cellulose-bPEI-Pd monolith, it can be found that the surface of Cellulose-bPEI-Pd was rougher than that of unmodified cellulose monolith, which may result from the surface modification and the deposition process of Pd NPs. Despite this, the continuous porous structure of monolith was still clearly observed. These results also confirmed that the modification and the preparation process of Pd NPs will not destroy the skeleton structure of cellulose monolith. On the other hand, the TEM images (**Fig. 1-6 (c** and **d)**) demonstrated that the Pd NPs were dispersed in the skeleton surface of Cellulose-bPEI-Pd monolith with relatively uniform grain size. To quantitatively investigate the grain size and its distribution of Pd NPs, the TEM images were further analyzed by the *Image J* program. The distribution result indicates that the mean diameter of Pd NPs in monolith is 1.7 nm (**Fig. 1-6 (e)**). The small grain size of Pd NPs may contribute to the high catalytic efficiency of the Cellulose-bPEI-Pd monolith. It should be noted that the particle density over various parts of the monolith is not uniform. From **Fig. 1-6 (f)** it can be seen that the Pd NPs were mainly distributed on the surface of the skeleton (which was the pore wall of monolith), while the

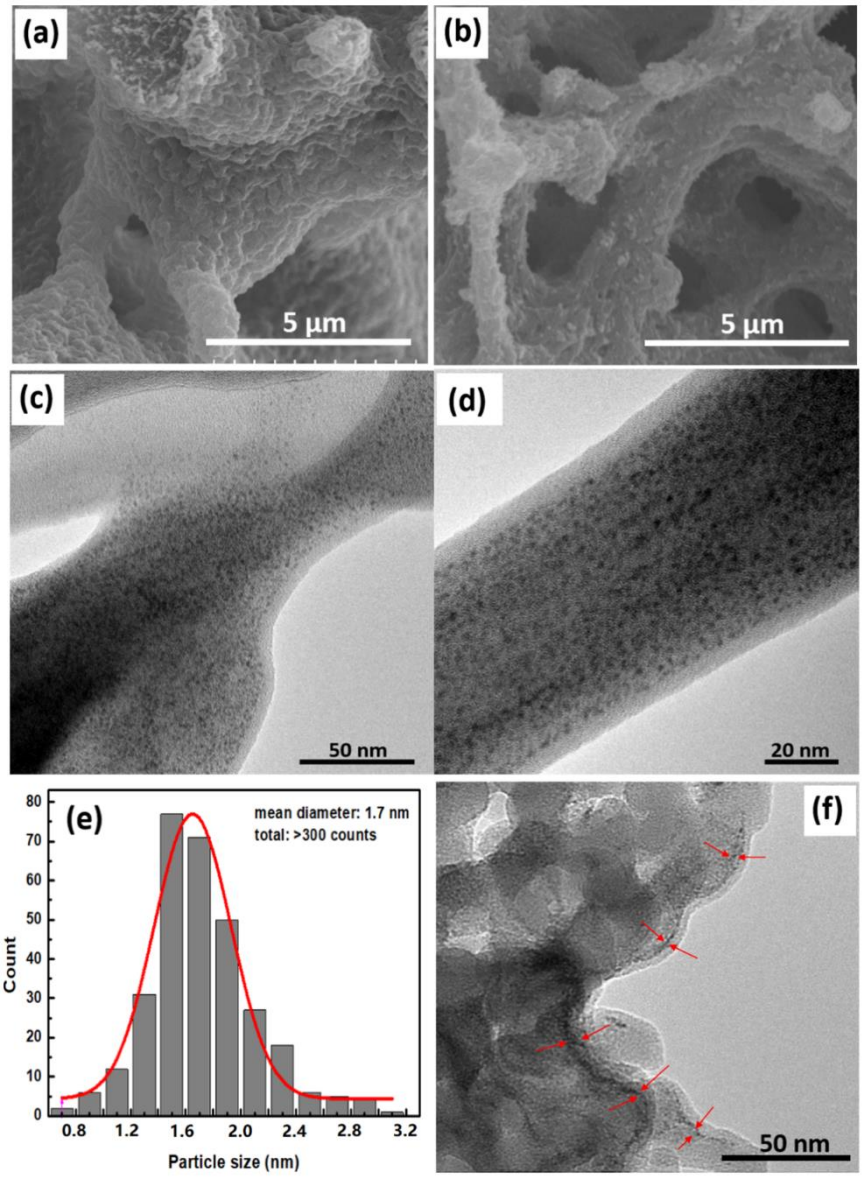

Fig. 1-6. Morphology of the modified monolith: **(a)** and **(b)** are the SEM images of monoliths before and after modification with bPEI. **(c, d** and **f)** TEM images of the different areas of Cellulose-bPEI-Pd monolith. The red arrows in Fig. (f) indicates the Pd NPs on sample. **(e)** the statistic of the size of Pd NPs.

density of Pd NPs inside of the skeleton was relatively lower than the surface of skeleton. Since the deposition of Pd was achieved by passing the Pd solution through the cellulose column, it is understandable that the Pd NPs tend to be immobilized on the pore wall of monolith rather than inside of skeleton. Actually, this inhomogeneous distribution of Pd may be good for enhancing overall catalytic efficiency since the Pd NPs inside the skeleton will not be in contact with the reactants during the catalytic process and will not contribute to the catalytic efficiency.

1.3.2 Mechanical properties

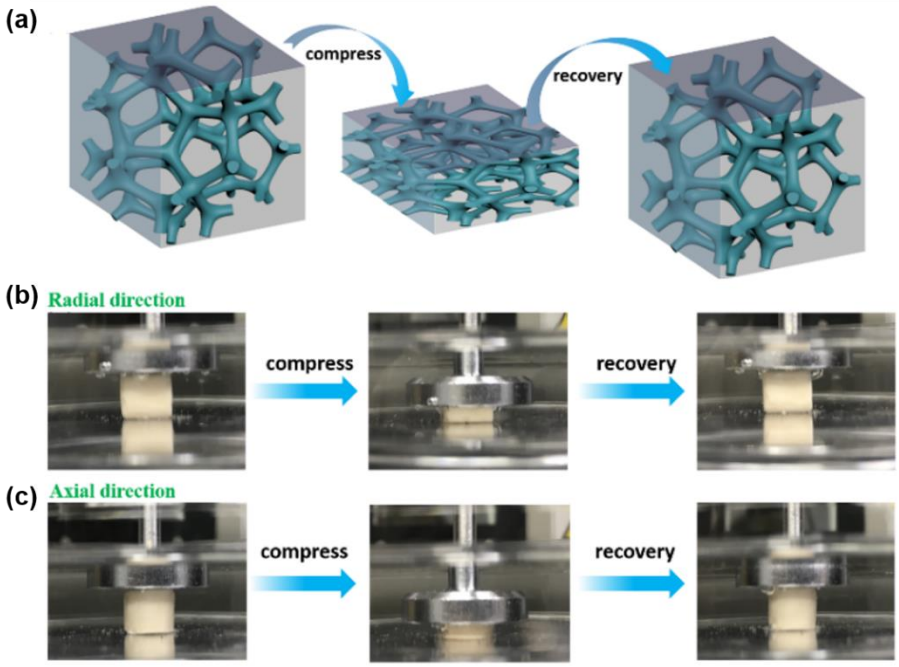

Fig. 1-7 Mechanical properties of Cellulose-bPEI-Pd monolith: **(a)** the schematic picture of the structural change of monolith under compression. the compression and recovery process at the **(b)** radial direction and **(c)** axial direction.

For the practical catalytic application of the monolith as flow reactor, the good mechanical properties especially the shape resilience of monolith is necessary since the damage of monolith in use process may not only cause a sharp and irreversible decrease of the catalytic performance but also result in the leaching of catalysts and the contamination of the product. Here the mechanical performance of the Cellulose-bPEI-Pd monolith was tested by compression experiment in water. The monolith was firstly compressed to the strain of 70%, then released. As shown in **Fig. 1-7**, at both radial and axial directions, the monolith will not be crushed even under the maximum compression strain. After the release of load, the monolith could instantly recover to the original shape, which suggested that the cellulose monolith (Cellulose-bPEI-Pd) overcame the brittleness of the crystalline cellulose and could bear a 70% reduction in volume under applied pressure. The excellent shape resilience may result from the unique continuous pore structure of monolith which can endure the deformation of shape. Moreover, the modification process may destroy a part of the crystalline of cellulose and endow the monolith with flexibility in the water. The excellent mechanical properties ensured that the microreactor can be used in a circulatory fashion in a severe environment.

1.3.3 Catalytic performance

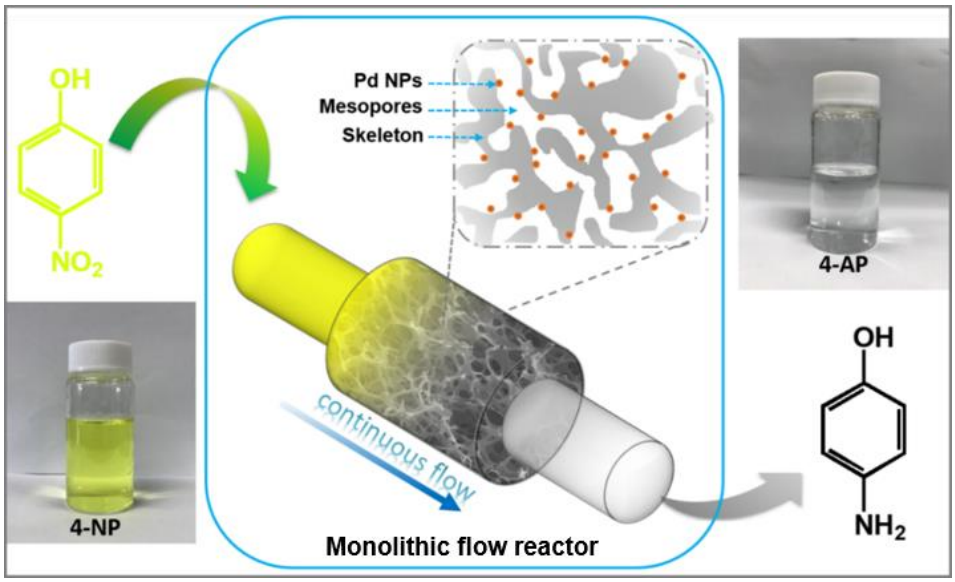

Fig. 1-8. The schematic image of the microfluidic reactor: A pump was used to flow the react agent pass through the monolith to take reaction under the catalyst of monolith, in the monolith the 4-NP was reduced to 4-AP and the color of reactants was gradually changed from yellow to colorless.

As shown in **Fig. 1-8**, the as-prepared Cellulose-bPEI-Pd monolith was fixed into a heat shrinkable tube to construct a flow catalytic system, in which a peristaltic pump was employed to allow the reactants to flow through the monolith. The reduction reaction of 4-NP was used to evaluate the catalytic activity of this monolithic microreactor. This reaction is considered as an ideal model reaction to test the catalytic activity of Pd NPs system because it's widely used in wastewater treatment. Moreover, this reaction can be intuitively observed since the color of the solution will change from yellow to colorless during the reaction, as illustrated in **Fig. 1-8**. The 4-NP solution showed a characteristic peak at 400 nm at the UV-*vis* spectra, and the peak

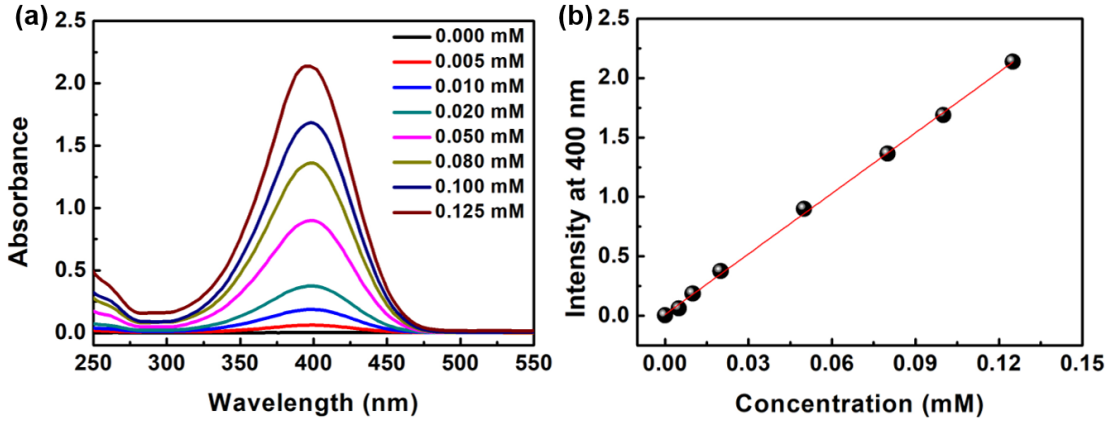

Fig. 1-9 (a) UV-vis absorption spectra of 4-NP with different concentration. **(b)** Standard curve of the concentration of 4-NP in water.

intensity follows a good linear relationship with 4-NP concentration. (**Fig. 1-9**) Thus, this reaction can also monitor by UV-*vis* experiments. Thanks to the well-defined hierarchical porous monolith into which the Pd NPs were homogeneously supported, the flow-through process could force the reactants to effectively contact with the Pd NPs. As a result, the 4-NP will be reduced during the flow process and converted to 4-aminophenol (4-AP) as the reactants flow out of the monolith.

In this experiment, the 4-NP (10.0 mmol/L) was previously mixed with a reducing agent ($NaBH_4$ aqueous solution, 0.2 mol/L) and then the mixture was pumped to flow through the monolith with a speed of 1 mL/min. **Fig. 1-10 (a)** showed the UV spectra of the reactants solution before and after flowing through the Cellulose-bPEI-Pd monolithic microreactor. The characteristic absorbance of 4-NP at 400 nm disappeared after flowing through the microreactor. Meanwhile, a new peak appeared at 292 nm, indicating that the reduction of 4-NP to 4-AP

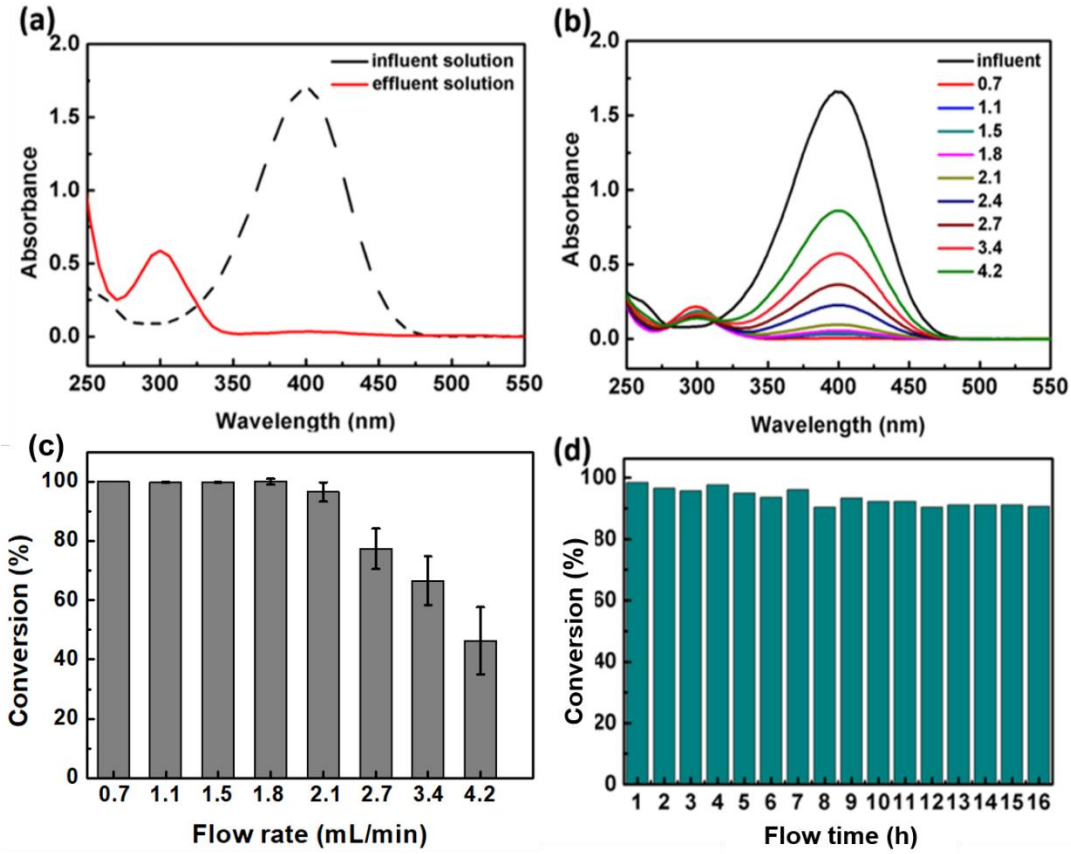

Fig. 1-10. (a) The UV spectrums of the reactants solution before and after flow through the C-bPEI-Pd monolith. The influent solution was diluted by 100 times to be tested. **(b)** The UV spectrums of the effluent at different flow rate. The solutions were diluted by 100 times to be tested. **(c)** The reaction conversion at different flow rate. **(d)** The stability of the monolith microreactor.

could be catalyzed by the Cellulose-bPEI-Pd monolith as predicted. As a contrast, the mixed solution of 4-NP and $NaBH_4$ also flowed through the Cellulose-PEI monolith and the UV-*vis* measurements were carried to investigate the concentration of 4-NP in the influent and the effluent solution. The result showed that the amount of 4-NP adsorbed by the monolith column was very low and could be ignored when compared with the chemically reduced 4-NP. To determine the maximum catalytic ability of the monolithic microreactor, the reduction efficiency of microreactor at different flow rates was systematically studied. **Fig. 1-10 (b)** recorded the UV-*vis* results of the effluent solution outflowed at each speed. When the speed slow than 1.8 mL/min, no obvious peak could be found at 400 nm at the curve of effluent, indicating that the 4-NP could be almost totally reduced. However, with the further increase of flow rate, the characteristic peak of 4-NP appeared and the intensity of this peak gradually increased with the increase of flow rate, which means that the 4-NP cannot be completely reduced under such high flow speed and remained in the effluent solution. Comparing the peak intensity with the UV-*vis* standard curves of 4-NP in water (**Fig. 1-9**), the concentration of 4-NP remained in effluent solution could be obtained and the reaction conversion (X_c) was calculated by the equation:

$$X_c = \frac{C_0 - C}{C_0} \times 100\%$$

where C_0 and C represent the concentration of 4-NP in the influent solution and effluent solution, respectively. The calculated reaction efficiency at different flow speeds was shown in **Fig. 1-10 (c)**. As analyzed above, the reaction efficiency remained almost 100% at low flow speed but decreased when the speed faster than 1.8 mL/min. To quantitatively evaluate the catalytic activity of microreactor, the TOF (defined as the number of moles of 4-NP reduced per mole catalyst per hour) was calculated according to the equation below:

$$TOF = \frac{n_{4-NP}}{t \cdot n_{Pd}} = \frac{(C_0 - C) \cdot \nu}{n_{Pd}}$$

where n is the number of moles. t means reaction time and ν represents the flow rate. Here the n_{pd} in monolith was calculated to be 0.238 μmol according to the ICP results mentioned previously. Taking that the reaction efficiency at the flow speed of 1.8 mL/min was 100% (e. t. C=0), the TOF was calculated to be about 4540 h^{-1}. The catalytic efficiency was much higher than the cellulose nanocrystal supported Pd catalysts (879.5 h^{-1}).[36] Besides the high catalytic

efficiency, the microreactor also showed superior stability. As shown in **Fig. 1-10 (d)**, even after continuously flow for 16 hours, the catalytic efficiency remained very high (>90%). The slight decrease of the catalytic activity may result from two reasons: 1) some micropores/channel in monolith were broken or closed due to the continued high backpressure in the flow process. This may result in a decrease of the effective catalytic surface area. 2) Although the surface modification by PEI could relatively stabilize the Pd NPs on the monolith, some Pd NPs may be leached out during the long-time flowing process. However, the decrease in the catalytic efficiency of this reactor was very slow. It could actually meet the requirement in most cases of practical water treatment.

The superior activity may originate from the special porous structure of monolith, by which the reactants could contact the Pd NPs more sufficiently. As shown in **Fig. 1-11**, for fibers, supported metal NPs, the reaction only occurs on the surface of the solid support. As a result, the reactants around the fibers will be reacted quickly, while the solution far from catalytic surface cannot contact the catalysts and thus remained a high concentration of the reactant. Therefore, the improvement of overall catalytic performance may be actually limited by the diffusion of reactants, especially in the case of low catalysts dosage. Although high-

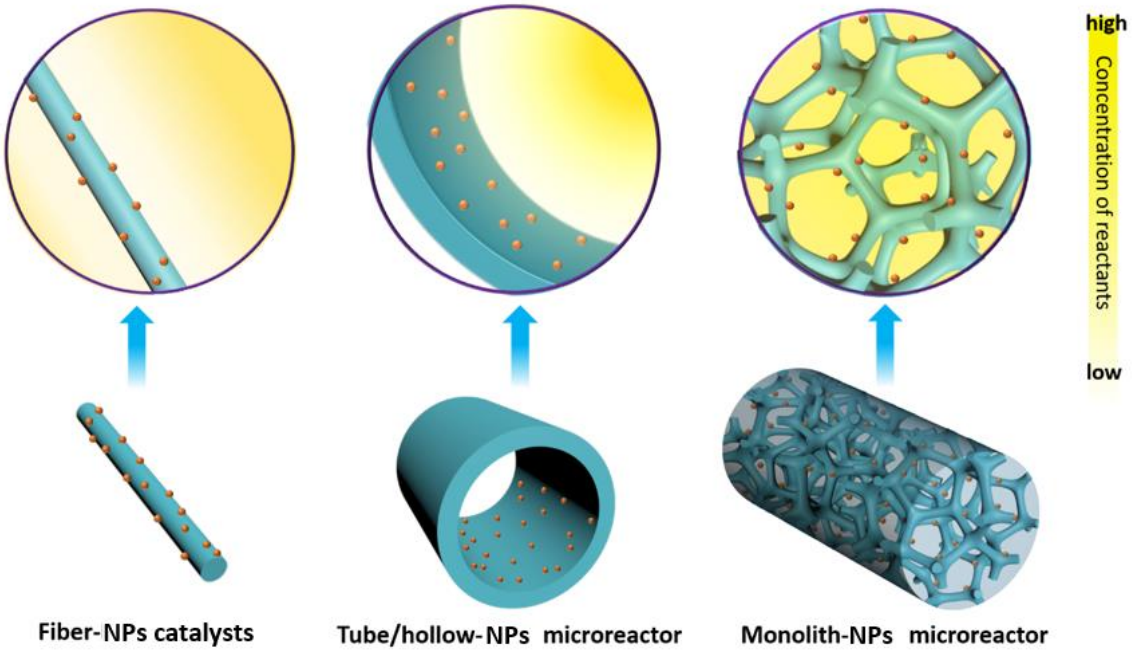

Fig. 1-11. Schematic figure of the different kinds of metal NPs supported systems including fibrous catalysts, tube/hollow reactors and monolithic microreactors. The pictures in the cycles are the corresponding concentration distribution of reactants during the catalyzing process.

speed stirring of solution could accelerate the diffusion process, the vigorous mechanical stirring might lead to the damage of catalysts and in turn, reduce the activity of catalysts. Likewise, the heterogeneous distribution of reactants will also affect the catalytic performance of the tube/hollow reactors. During the flow process, the reactants will show a low concentration near the tube wall but a high concentration at the core of fluid unless the tube diameter is very small or the turbulence of fluid could be achieved by reasonable texture design of the inner surface. Both of these may inevitably increase the preparation difficulty and reduce the accessibility of the reactor. Different from the strategy above, the monolithic microreactor posed a hierarchical porous structure and showed a much bigger surface area in comparison with the fibrous and tubes, which will fundamentally accelerate the mass transfer of reactants and the reactants could get more efficient contact with the NPs during the flow process. Thus, the monolithic cellulose microreactor exhibited superior catalytic performance.

1.3.4 Other flow application of cellulose-bPEI monolith

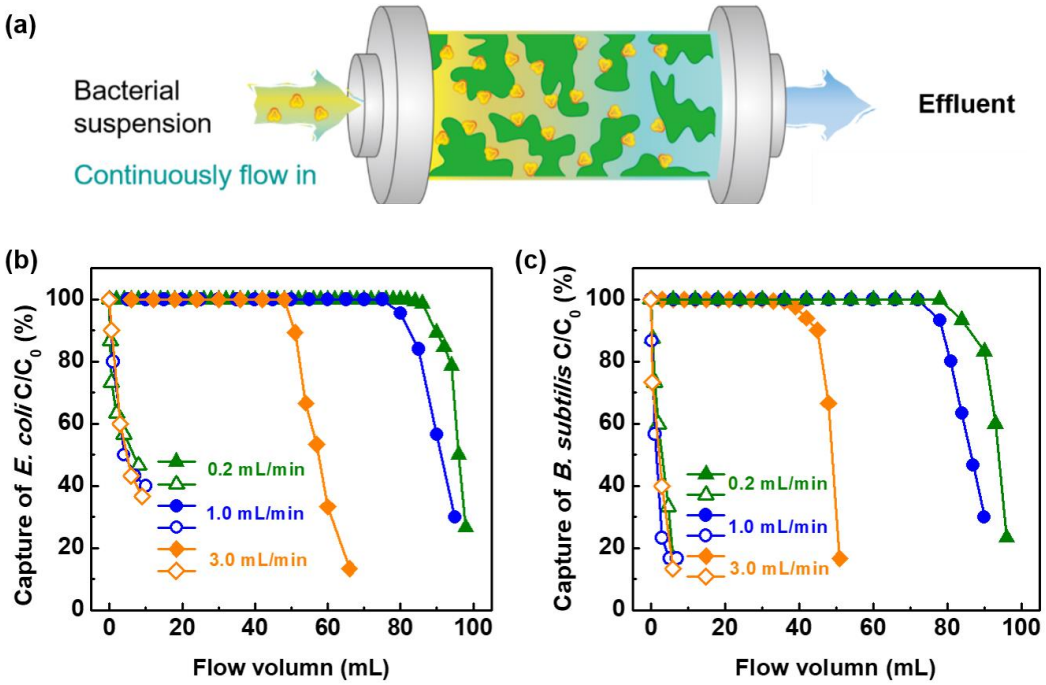

Fig. 1-12. (a) Scheme of the monolith function in a bacterial capture experiment. Bacterial capture efficiencies of monolith with and without bPEI modification, for **(b)** *E. coli* and **(c)** *B. subtilis* at flow velocities of 0.2 mL/min, 1 mL/min, and 3 mL/min. The solid icons indicate samples with bPEI modification, and the hollow icons indicate samples without bPEI modification (*E. coli* and *B. subtilis* suspension concentration: 3×10^8 CFU/mL).

It was worthy to note that the bPEI-modification strategy can also be extended to other flow applications such as the bacteria capture in water, due to the good bio-infinity of bPEI molecules. As a demonstration, the cellulose-bPEI monolith was applied as a capture device to remove bacteria in water. As shown in **Fig. 1-12 (a)**, the cellulose-bPEI monolith was used to capture both gram-negative (*Escherichia coli*) and gram-positive (*Bacillus subtilis*) bacteria. The bacterial capture efficiencies of the monolith at different flow velocities were summarized in **Fig. 1-12 (b,** and **c)**. Both *E. coli* and *B. subtilis* were effectively captured by the cellulose-bPEI monolith and the capacities were calculated to be 3.5×10^{11} CFU/g at 0.2 mL/min, 3.4×10^{11} CFU/g at 1 mL/min, and 1.9×10^{11} CFU/g at 3 mL/min for *E.coli*; and 3.2×10^{11} CFU/g at 0.2 mL/min, 3.2×10^{11} CFU/g at 1 mL/min, and 1.3×10^{11} CFU/g at 3 mL/min for *B. subtilis*. In stark contrast, the monolith without bPEI modification showed negligible capture efficiency, whether at low or high flow velocity. The capture efficiency was negatively affected by increased flow velocity. Increased velocity shortened the residence time of bacteria in the monolith to reduce the exposure to the pore walls and the stability of initial attachments. Because of the insufficient contact of bacteria with pores, the regional surface area of the monolith skeleton was not adequately utilized causing a decrease in capture capacity. Nevertheless, the cellulose-bPEI monolith still revealed a satisfactory capture efficiency for the high concentration of bacteria at high flow velocity.

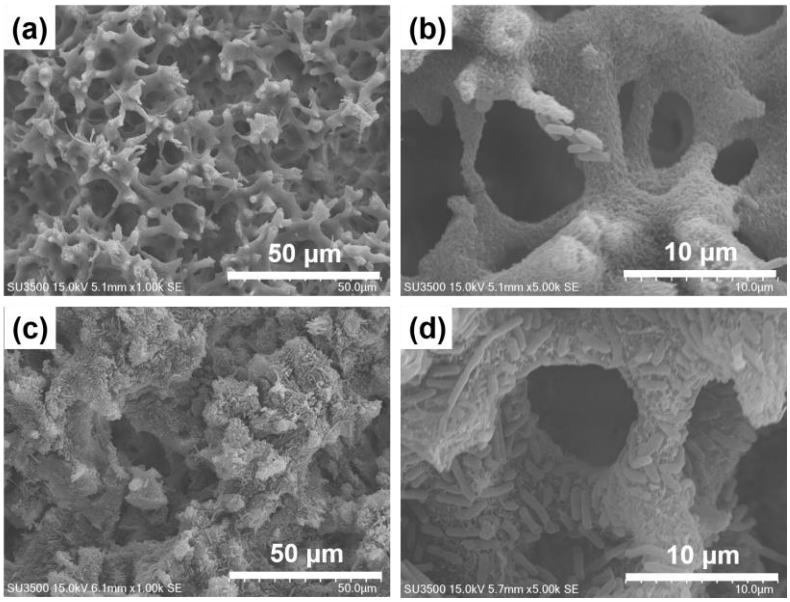

Fig. 1-13. SEM images of bacteria captured by **(a, b)** cellulose monolith and **(b, d)** cellulose-bPEI monolith at different magnification. (flow velocity: 1 mL/min, *E. coli* suspension concentration: 3×10^8 CFU/mL)

The internal structure of monolith after bacterial capture shown in **Fig. 1-13**, few bacteria attached to the skeleton of monolith without modification (**Fig. 1-13 (a** and **b)**) whereas numerous bacteria congested in part of the pores and compactly adhered to the skeleton surface of the cellulose-bPEI monolith (**Fig. 1-13 (c** and **d)**). This also demonstrated the processing capability of cellulose-bPEI for removing microbial contaminants in water supplies.

1.4 Conclusion

In this chapter, the cellulose monolith was prepared from CA by a facile TIPS method. The cellulose monolith prepared by this method had a unique hierarchically porous structure, which was conducive for the catalytic application. A surface modification strategy was conducted to graft bPEI on monolith for supporting Pd NPs. The obtained cellulose-bPEI-Pd monolith exhibited an excellent shape resilience under compression. It was used as a flow reactor and showed high efficiency and good stability for catalyzing the reduction reaction of 4-NP. Besides, due to the good bio-infinity of bPEI molecules, the cellulose-bPEI monolith can also be used to effectively capture bacteria under a continuous-flow condition.

1.5 References

1. P. Marín, F. V. Díez and S. Ordóñez, *Chemical Engineering and Processing - Process Intensification*, 2019, **135**, 175-189.
2. D. K. B. Mohamed, X. Yu, J. Li and J. Wu, *Tetrahedron Lett.*, 2016, **57**, 3965-3977.
3. J. P. McMullen, M. T. Stone, S. L. Buchwald and K. F. Jensen, *Angewandte Chemie*, 2010, **49**, 7076-7080.
4. H. Nakamura, Y. Yamaguchi, M. Miyazaki, H. Maeda, M. Uehara and P. Mulvaney, *Chem Commun (Camb)*, 2002, DOI: 10.1039/b208992k, 2844-2845.
5. A. Molnar, *Chem. Rev.*, 2011, **111**, 2251-2320.
6. M. Irfan, T. N. Glasnov and C. O. Kappe, *ChemSusChem*, 2011, **4**, 300-316.
7. A. Odedra and P. H. Seeberger, *Angewandte Chemie*, 2009, **48**, 2699-2702.
8. R. P. Jumde, M. Marelli, N. Scotti, A. Mandoli, R. Psaro and C. Evangelisti, *Journal of Molecular Catalysis A: Chemical*, 2016, **414**, 55-61.
9. M. A. Bañares, *Catalysis Today*, 1999, **51**, 319-348.
10. C. H. Pelisson, T. Nakanishi, Y. Zhu, K. Morisato, T. Kamei, A. Maeno, H. Kaji, S. Muroyama, M. Tafu, K. Kanamori, T. Shimada and K. Nakanishi, *ACS applied materials & interfaces*, 2017, **9**, 406-412.
11. A. Cybulski and J. A. Moulijn, *Catalysis Reviews*, 1994, **36**, 179-270.
12. J. Chakraborty, I. Nath, S. Song, S. Mohamed, A. Khan, P. M. Heynderickx and F. Verpoort, *Journal of Photochemistry and Photobiology C: Photochemistry Reviews*, 2019, **41**.
13. R. Poupart, D. Grande, B. Carbonnier and B. Le Droumaguet, *Progress in Polymer Science*, 2019, **96**, 21-42.
14. M. Nasrollahzadeh, M. Sajjadi, M. Shokouhimehr and R. S. Varma, *Coordination Chemistry Reviews*, 2019, **397**, 54-75.
15. X. Lin, M. Wu, D. Wu, S. Kuga, T. Endo and Y. Huang, *Green Chemistry*, 2011, **13**, 283-287.
16. X. Wu, Z. Shi, S. Fu, J. Chen, R. M. Berry and K. C. Tam, *ACS Sustainable Chemistry & Engineering*, 2016, **4**, 5929-5935.
17. K. R. Reddy, N. S. Kumar, P. S. Reddy, B. Sreedhar and M. L. Kantam, *Journal of Molecular Catalysis A: Chemical*, 2006, **252**, 12-16.
18. V. L. Budarin, J. H. Clark, R. Luque, D. J. Macquarrie and R. J. White, *Green Chemistry*, 2008, **10**, 382-387.

19. M. J. Gronnow, R. Luque, D. J. Macquarrie and J. H. Clark, *Green Chemistry*, 2005, **7**, 552-557.
20. Z. Xue, X. Sun, Z. Li and T. Mu, *Chemical Communications*, 2015, **51**, 10811-10814.
21. W.-L. Wei, H.-Y. Zhu, C.-L. Zhao, M.-Y. Huang and Y.-Y. Jiang, *Reactive and Functional Polymers*, 2004, **59**, 33-39.
22. X. Zhang, Y. Geng, B. Han, M. Y. Ying, M. Y. Huang and Y. Y. Jiang, *Polymers for Advanced Technologies*, 2001, **12**, 642-646.
23. J. Song, C. Chen, C. Wang, Y. Kuang, Y. Li, F. Jiang, Y. Li, E. Hitz, Y. Zhang and B. Liu, *ACS applied materials & interfaces*, 2017, **9**, 23520-23527.
24. Z. Zhang, G. Sèbe, X. Wang and K. C. Tam, *Carbohydrate polymers*, 2018, **182**, 61-68.
25. A. P. Almeida, J. P. Canejo, S. N. Fernandes, C. Echeverria, P. L. Almeida and M. H. Godinho, *Advanced Materials*, 2018, **30**, 1703655.
26. Y. Xin, Q. Xiong, Q. Bai, M. Miyamoto, C. Li, Y. Shen and H. Uyama, *Carbohydrate polymers*, 2017, **157**, 429-437.
27. P. Tarazona, *Phys Rev A Gen Phys*, 1985, **31**, 2672-2679.
28. P. Tarazona, U. M. B. Marconi and R. Evans, *Mol. Phys.*, 1987, **60**, 573-595.
29. Y. Xin, Q. Xiong, Q. Bai, M. Miyamoto, C. Li, Y. Shen and H. Uyama, *Carbohydr. Polym.*, 2017, **157**, 429-437.
30. M. Chu, C. Dong, H. Zhu, X. Cai, H. Dong, T. Ren, J. Su and Y. Li, *Polymer Chemistry*, 2013, **4**, 2528.
31. Y. Long, L. Zheng, Y. Gu, H. Lin and X. Xie, *Polymer*, 2014, **55**, 6494-6503.
32. J. Martínez Urreaga and M. U. de la Orden, *Carbohydrate Polymers*, 2007, **69**, 14-19.
33. J. Wang, L. Zhao, W. Duan, L. Han and Y. Chen, *Industrial & Engineering Chemistry Research*, 2012, **51**, 13655-13662.
34. M. U. De La Orden, M. C. Matías and J. Martínez Urreaga, *Journal of Applied Polymer Science*, 2004, **92**, 2196-2202.
35. J. Zhao, C. Lu, X. He, X. Zhang, W. Zhang and X. Zhang, *ACS applied materials & interfaces*, 2015, **7**, 2607-2615.
36. X. Wu, C. Lu, W. Zhang, G. Yuan, R. Xiong and X. Zhang, *Journal of Materials Chemistry A*, 2013, **1**, 8645.

Chapter 2

Transfer the narrow-dispersed gold nanoparticles on cellulose monolith without surface modification

2.1 Introduction

The current methods for introducing metal NPs on cellulose support materials mainly include the "in-situ synthesis" [1-5] and "graft to" [6-8] strategies. The "in-situ synthesis" method usually based on the *in situ* reduction of the metal ions on the surface of the support. This method integrates the preparation and the loading of MNPs in one procedure, and thus minimizes the fabrication steps and reduces the usage of chemicals. The drawback is that the size as well as its distribution of the formed Au NPs are actually hard to be controlled in this method. The "graft to" method needs to previously prepare Au NPs and then decorate the obtained NPs onto the surface of support materials. Unlike the *in situ* synthesis method, this method allows to more precisely design and adjust the particle size and structure in the synthesis process. [8]

For the controllable preparation of metal NPs, the external surfactant or stabilizer such as organothiols [9, 10], amines [11], phosphines [12] and polymers like polyvinyl alcohol (PVA) [13] and polyvinylpyrrolidone (PVP) [14] were frequently added to adjust the particle size and prevent the aggregation of the obtained NPs. [15, 16] Among various stabilizers, PVP was most commonly used in the preparation of Au NPs since it could be easily attached to the surface of Au NPs by the carbonyl groups and the nitrogen atoms of PVP. [17] The addition of a certain amount of PVP with suitable molecule weight could realize the controllable synthesize of Au NPs characterized by uniform morphology and narrow size distribution. [8] However, researches proved that the removal of PVP from Au NPs are difficult, and the PVP remained and covered on the surface of metal NPs will not only lead to the impurities during the catalytic reaction but also reduce the catalytic activity of the metal NPs due to the decrease of the active metal sites. [18] Moreover, the stabilizer could also affect the immobilization of the Au NPs on cellulose materials since it

will partially shield the surface of Au NPs and weaken the interaction between metal NPs and cellulose support. As a result, the PVP covered Au NPs are hard to be directly fixed on the cellulose surface.

Some recent researches indicated that the $NaBH_4$ in reaction solution can detach the stabilizers including the organothiols, adenine, and PVP due to a hydride displacement mechanism. [19] The hydride produced by $NaBH_4$ has a relatively higher binding energy with Au NPs than binding energy between PVP and Au NPs. Thus, the PVP absorbed on Au surface can be replaced by hydride and removed from the Au NPs. After removal of the PVP, the catalytic activity can be enhanced due to the exposure of more reactive sites. [20]

In this chapter, a reasonable tans-deposition method was used to immobilize the narrow-dispersed Au NPs on cellulose monolith as a flow reactor. The PVP-stabilized Au nanoparticle (Au:PVP) was first deposited on the cellulose monolith by circularly flow of Au:PVP/Methanol solution. Then the removal of PVP from cellulose monolith was realized by flowing the $NaBH_4$/Methanol solution to continuously wash the monolith. After the removal of PVP, the Au NPs showed enhanced activity and good stability in water.

2.2 Experiment

2.2.1 Materials

The cellulose acetate powder (CA, L30) used in this experiment was supplied by DAICEL Co., Ltd. Japan, and its acetylation degree was approximately 55%. PVP (k-15) was purchased from Tokyo Chemical Industry Co., Ltd. Hydrogen tetrachloroaurate tetrahydrate ($HAuCl_4 \cdot 4H_2O$) with a purity of 99% was purchased from Nacalai Tesque, Inc. Kyoto, Japan. $NaBH_4$ was purchased from FUJIFILM Wako Pure Chemical Corporation, Japan. 4-NP and dimethylphenylsilane ($PhMe_2SiH$) were purchased from Tokyo Chemical Industry Co., Ltd. Methylene blue and methyl orange were purchased from Tokyo Chemical Industry Co., Ltd. Other chemicals including *N*,*N*-dimethylformamide, 1-hexanol, and sodium hydroxide were produced by FUJIFILM Wako Pure Chemical Corporation, Japan, all of which were chemically purified and commercially available. The heat-shrinkage polyolefin tube (THT-8.0N) for fabricating the flow reactors was provided by Denka Electron Co. Ltd., Japan.

2.2.1 Synthesis of Au:PVP with the narrow size distribution.

AU:PVP was prepared by a "seed-mediated" method according to the previous work. [21] First, Au of small size (1.5 nm) was prepared. 10 mg of PVP (K-15) was dissolved in 43 mL deionized water at room temperature. Then 2 mL of $HAuCl_4$ aqueous solution (12.5 mmol/L) was added into the PVP solution at the temperature of 1 ºC to introduce Au atoms. Subsequently, sodium borohydride aqueous solution (157 mg of $NaBH_4$ dissolved in 5 mL deionized water) was used to reduce the Au ions. The resulted solution was treated by centrifugation and repeated washing with water. After dried by freezing drying, the Au:PVP cluster (1.5 nm) was obtained, which was used as a seed to further prepare Au NPs with the size around 7 nm. Briefly, 265 mg of PVP (k-15) was previously dissolved in 15 mL water in a tube, then 10 mg (1.15 mol) of the seed was added in the mixed solution under stirring. The dissolved oxygen in the obtained solution was removed through freeze-thaw treatment 2 times. Subsequently, 0.328 mL of 72.9 mmol/L HAuCl4 aqueous solution was added in the solution followed by the freeze-thaw treatment. The 0.79 mL of 90 mmol/L Na_2SO_3 was introduced in the solution at 27 ºC to

reaction for 3 h under stirring. Finally, the product was treated by centrifugation at 0 °C using a vivaspin (3000 MWCO). After repeatedly washed with water 3 times and freeze-dried for 2 days, the Au:PVP powder (210 mg, 0.025 mmol) was obtained.

2.2.2 Transfer the Au:PVP onto cellulose monolith.

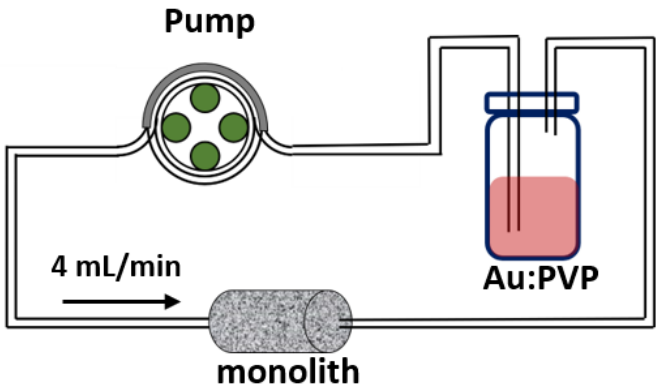

Fig. 2-1 Scheme of the circularly flow of the Au:PVP/Ethanol through cellulose monolith.

The cellulose monolith prepared by the TIPS method described in Chapter 1 was used as the matrix for supporting the Au:PVP. After complete drying in vacuum, the monolith with a length of 1 cm was fixed into a heat-shrinkable tube to be used. A facile continues-flow method was used to immobilize the as-prepared Au:PVP onto the surface of cellulose monolith. In this method, 10 mg of Au:PVP powder was dissolved in 10 mL ethanol. Subsequently, the solution was circularly flowed through the monolith with a speed of 4 mL/min by a peristaltic pump as shown in **Fig. 2-1**. After flow for 10 min, the sample (named CM-Au:PVP) was obtained.

Furthermore, 30 mL of 1 mmol/L $NaBH_4$/Methanol solution circularly flowed through the CM-Au:PVP for 1 h to wash out the PVP attached to the Au NPs. The washing solution was collected to be detected by FTIR and ICP-AES. After washed by $NaBH_4$ solution, the sample was further washed with ethanol for 0.5 h to remove any remained $NaBH_4$. Finally, the ethanol in monolith was exchange to water by the flow of 30 mL of water with 0.5 mL/min. The sample after removal of PVP was named as CM-Au. To test the stability of the Au NPs on the monolith, 20 mL water circularly flowed through the sample for 1 h. The washing solution was collected to be detected by ICP-AES measurement. As a comparison, the CM-Au:PVP without washed with $NaBH_4$ solution was also tested by the same procedure.

2.2.3 Catalytic performance test.

The catalytic performance of the CM-Au:PVP and CM-Au was evaluated by the oxidation reaction of $PhMe_2SiH$ to dimethylphenylsilanol ($PhMe_2SiOH$) in DMF. In this experiment, 0.1 mmol of $PhMe_2SiH$ and 25 μL of H_2O were dissolved in 3 mL of DMF, and the mixture was circularly flowed through the reactor at a constant flow rate (3 mL/min) to take reaction in the air at room temperature. After reacting for 15 min, 20 μL of the reactant solution was taken out and dissolved in 1 mL of deuterated dimethyl sulfoxide (DMSO-D6, with 5 wt % of tetramethylsilane) to be tested by ^1H NMR.

2.2.4 Characterization

The FTIR test was conducted on a Thermo Scientific (Yokohama, Japan) Nicolet iS5 spectrometer equipped with an iD5 ATR attachment. UV-*vis* spectrophotometer (HITACHI, U-2910) was used to monitor the concentration of Au ions in the Au deposition process. The absorbance curve was collected at wavelengths ranging from 250 to 800 nm. X-ray photoelectron spectroscopy (XPS, JEOL JPS-9010MC) was applied to study the surface chemistry consistent with the samples, using monochromatized Al-Kα radiation (1486.6 eV). The XPS results were collected by at fixed analyzer pass energies of 160 eV and 10 eV, respectively. The residual pressure inside the analysis chamber was in the 10^{-7} Pa range. The binding energies were referred to as C-H (sp^3) carbon for the C1s peak set at 284.8 eV. The morphologies of the monoliths were observed using a SEM (Hitachi S-3000N) at 15 kV. Before the observation, the samples were slivered into sections and coated with a thin layer of Au by using an ion sputter apparatus (E-1010, Hitachi Ltd.). The size of the Au NPs and their dispersion state in the monolith were detected by TEM (JEOL JEM-2010) at an acceleration voltage of 100 kV. The sample was ground and dispersed into methanol, then deposited on a copper grid coated with carbon (NP-C15, Okenshoji, Co., Ltd.) for testing. The crystalline states of the cellulose monolith with and without Au loading were studied through XRD experiments conducted with an X-Pert diffractometer (SmartLab, RIGAKU) using graphite-monochromatized Cu-Kα radiation ($\lambda = 1.54$ Å). The generator voltage and current were set at 45 kV and 200 mA, respectively. The atomic content of Au in the samples was detected by

inductively coupled plasma atomic emission spectrometry (ICP-AES) with SHIMADZU, ICPS-8100. Au standards with the atomic concentration of 0.5, 1, 2, 5, 10, 20, and 50 ppm were used for the calibration. The reaction conversion of the oxidation of $PhMe_2SiH$ was determined by proton nuclear magnetic resonance (^1H NMR) spectroscopy using DMSO-D6 as a solvent, with JNM-ECS400 (400 MHz, JEOL Ltd., Tokyo, Japan). The scanning time was set to 32 times.

2.3 Results and discussion

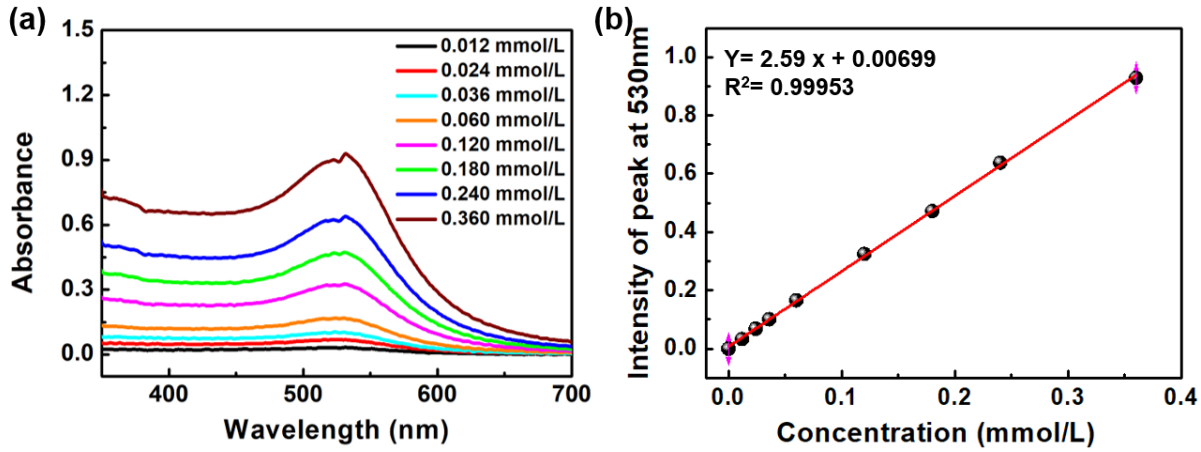

Fig. 2-2 (a)UV-vis absorption spectra of Au:PVP (7nm) methanol solution with different concentration and the standard curves; **(b)** standard curve of intensity vs. concentration.

Since the UV-*vis* curve of Au:PVP (7nm)/methanol solution showed a surface plasma resonance (SPR) peak at the 530 nm and the intensity of this peak depends on the concentration of the solution, UV experiments were conducted to monitor the deposition process of Au NPs on the monolith. To quantitatively determine the Au loading on the monolith, the standard curve was previously established between the intensity at 530 nm and the concentration by collecting a serious of UV dates of Au solution with different concentrations. As shown in **Fig. 2-2 (a)**, the peak centered on 530 nm reduced with the decrease of the concentration. **Fig. 2-2 (b)** plots the standard curves between the UV peak height and the concentration, it can be found that it followed a pretty good linear relationship.

During the deposition process, the cellulose monolith with a length of about 1 cm was fixed to the heat-shrinkable tube, and the Au/methanol solution was flowed through the tube to achieve the deposition of Au:PVP NPs on the monolith. During this process, the monolith

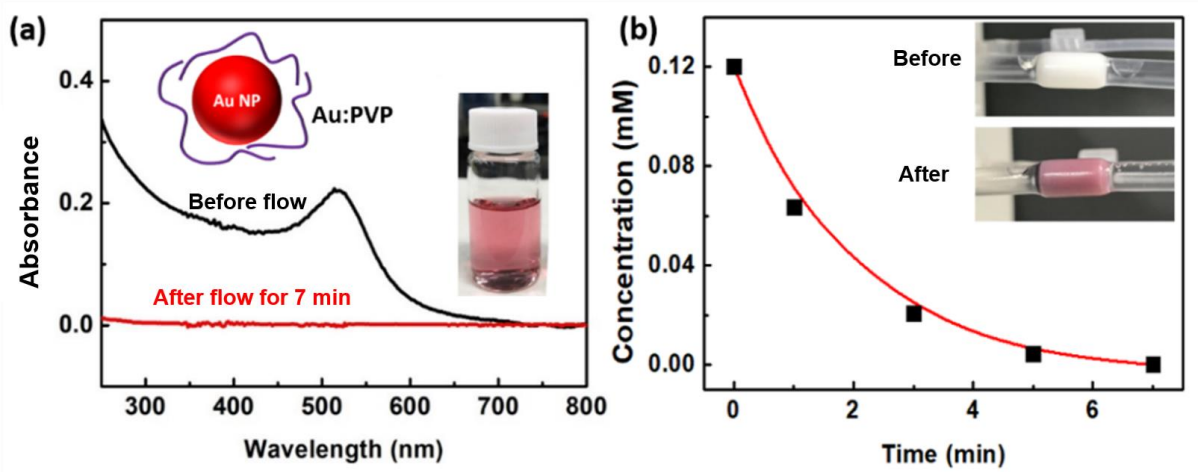

Fig. 2-3 (a) UV-vis spectra of Au:PVP solution before and after deposition for 10 min. **(b)** Concentration change of Au:PVP during the flow process.

gradually became red, while the color of the flow solution faded and changed to colorless after flow for 7 min. This indicated that the Au:PVP in solution was successfully transferred onto the cellulose monolith. To quantitatively investigate the deposition process, the UV-*vis* was used to monitor the concentration change of Au:PVP in methanol solution. As shown in **Fig. 2-3 (a)**, the peak at 530 nm disappeared at the curve of the solution after flow for 7 min, which indicated the Au:PVP was completely transferred on the monolith. Specifically, the concentration at different flow time was tested and plotted in **Fig. 2-3 (b)**. It can be found that the Au:PVP consuming speed is fast at the beginning and then slowed down due to the decrease of the concentration. The Au:PVP was absorbed on monolith only in 7 min. A large amount of the hydroxyl groups on monolith may play an important role in deposition of the Au:PVP. To demonstrated this point, the CA monolith without deacetylation was applied to conduct the deposition experiment under the same conditions. The result showed that the Au:PVP cannot be deposited on the CA monolith even prolonged the flow time to 3 h, suggesting that the

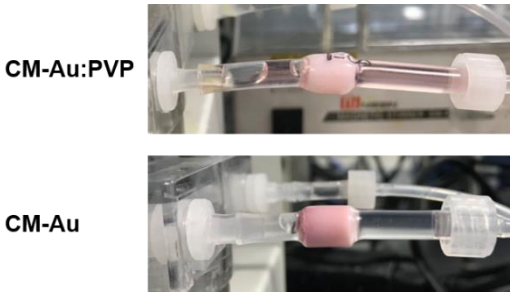

Fig. 2-4. Digital photos of CM-Au:PVP and CM-Au in the water flow process.

hydroxyl groups of cellulose were essential for the absorption of the Au:PVP NPs on cellulose monolith in the flow deposition process.

It should be noted that the Au:PVP deposited on the CM-Au:PVP is not stable. As shown in **Fig. 2-4**. When the deionized water flowed through the monolith, the leaching of Au NPs was visually observed. The monolith gradually changed from red to white and the washing solution became reddish. After continuous flow with water for 3 h, the Au NPs are almost removed from the monolith. The low stability of Au:PVP on monolith can be attributed to the PVP molecules attached to Au NPs, which may act as a barrier that shields the interaction between Au NPs and the hydroxyl groups of cellulose. As a result, the Au:PVP cannot be immobilized by the cellulose monolith and will be washed out when flowed with water. To improve the stability of Au NPs on cellulose monolith, the removal of PVP after deposition is

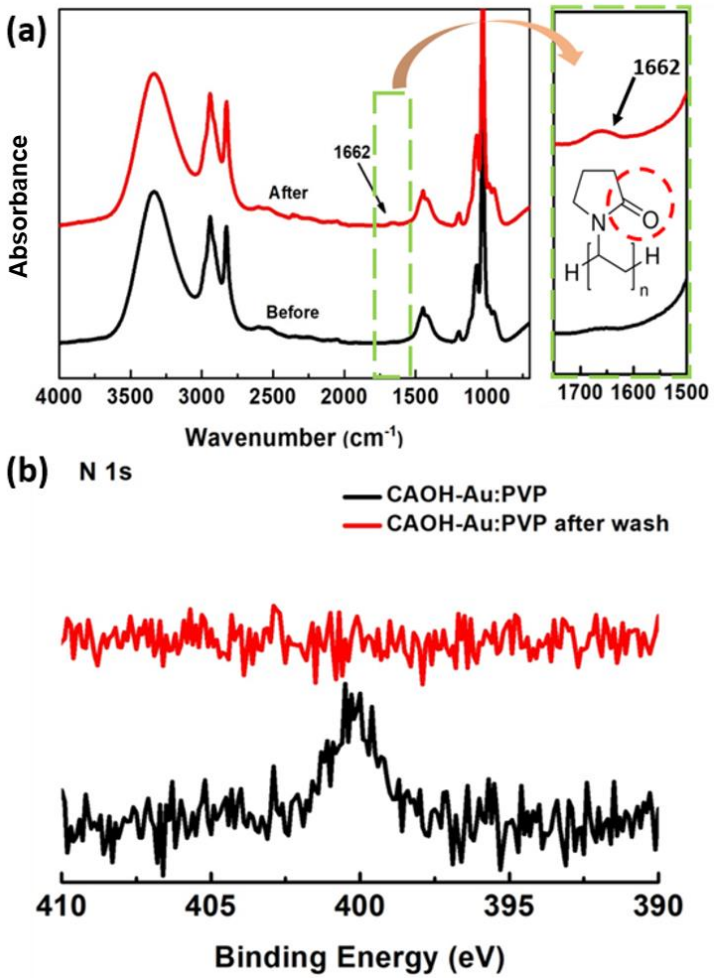

Fig. 2-5 (a) FTIR spectra of the $NaBH_4$/methanol solution before and after circularly flowing through the CM-Au:PVP monolith for 2 h. **(b)** XPS N 1s spectra of sample before and after wash.

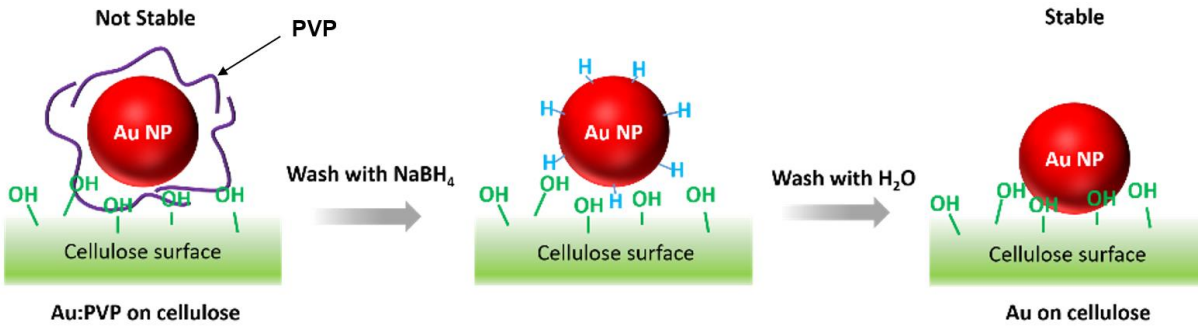

Fig. 2-6. Scheme of the microstructure of interface between cellulose and Au NPs.

necessary. Some recent research reported that the adsorbates, including the PVP, covered on Au NPs can be detached when the reaction solution contains $NaBH_4$.[19, 20] They proposed that the hydride derived from sodium borohydride has a higher binding affinity to AuNPs than most of the other absorbers such as PVP and organothiols. Thus, it can displace the adsorbates from AuNPs. Based on this fact, the $NaBH_4$ was used to remove the PVP by circularly flowing the $NaBH_4$/methanol solution through the CM-Au:PVP monolith for 2 h. To confirm the successful removal of PVP, the washing solution was tested by FTIR. As a comparison, the methanol without the addition of $NaBH_4$ was also tested after the same flow process. As shown in **Fig. 2-5 (a)**, a new peak at 1662 cm^{-1}, corresponding to the "C=O" bond of PVP, was found at the curve of $NaBH_4$ washing solution, which indicated that the PVP was removed from the Au NPs surface and remained in solution. Moreover, the XPS was collected to compare the surface chemical change before and after washing with $NaBH_4$. The high-resolution N 1s curves (**Fig. 2-5 (b)**) demonstrated that the Nitrogen element cannot be detected in the sample after washing, suggesting the complete removal of PVP. After the removal of PVP, the obtained sample (CM-Au) can be used in water. (**Fig. 2-4**). It can be interpreted that the removal of PVP allows the Au NPs to more close contact with cellulose. As shown in **Fig. 2-6**, when washed with $NaBH_4$ solution, the $NaBH_4$ will react with the gold nanoparticles and transfer the surface-hydrogen species to the surface of the gold particles, by which the PVP was detached and removed. [2] Without the coverage of PVP, the Au NPs can more inficiently interact with oxygen-containing groups of cellulose and stabilized by chelation effect. Since a large number of hydroxyl groups are born on the skeleton of cellulose monolith, the most majority of the Au NPs were

immobilized on monolith but not leached out. ICP-AES results showed that about 83 % of Au NPs was remained after removal of PVP.

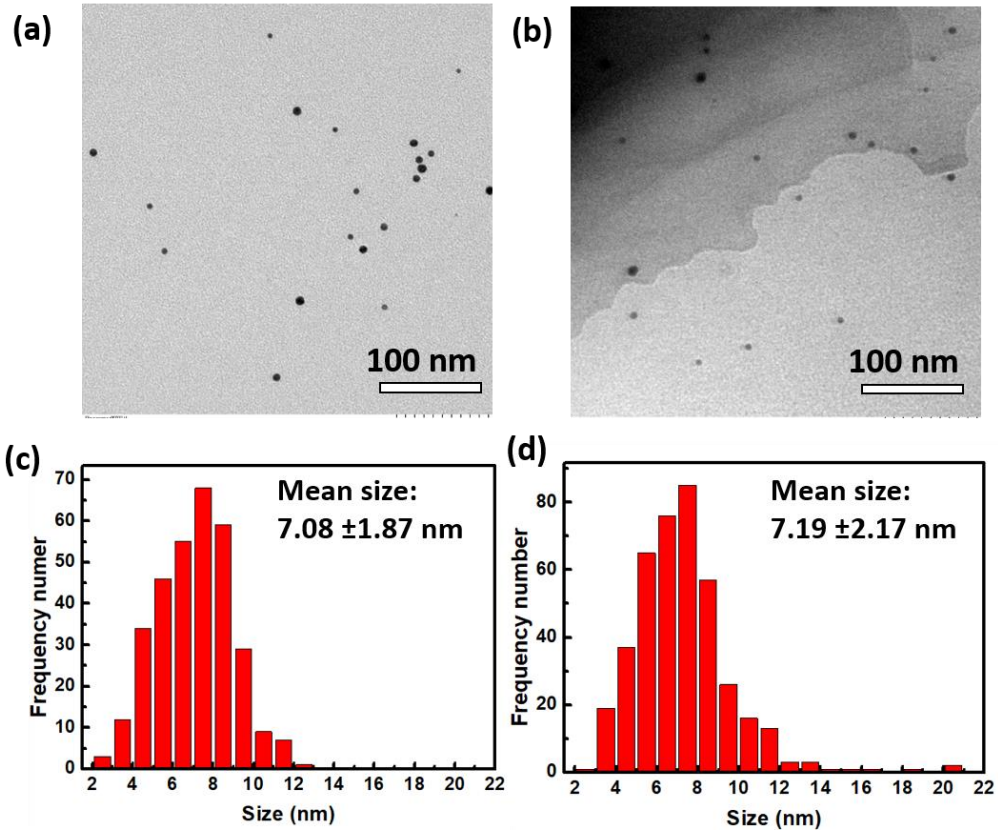

Fig. 2-7 TEM image and the size distribution of **(a, c)** Au:PVP and **(b, d)** Au NPs on cellulose monolith.

The size and its distribution of metal NPs in Au:PVP and CM-Au were observed by TEM to investigate the size change after the transfer process. Compare the images illustrated in **Fig. 2-7 (a** and **b)**, it can be seen the Au NPs after immobilization is still showed a sphere shape without obvious aggregation. According to the statistics of the Image-J program, the size dispersion was obtained and shown in **Fig. 2-7 (c** and **d)**. The average size of the Au NPs on CM-Au was calculated to be 7.19 ± 2.17 nm, which is similar to that of original Au:PVP (7.08 ±1.87 nm). Although it seems a little bigger after deposition and washing, the relatively narrow-dispersed size almost remained. This can be attributed to the stabilization of the numerous hydroxyl groups on cellulose monolith, which anchored the Au NPs and avoided the obvious aggregation after removing of PVP. On the other hand, the rough skeleton surface of the cellulose monolith may contribute to the immobilization of Au NPs by fixing the NPs in micro/mesopores or caves.

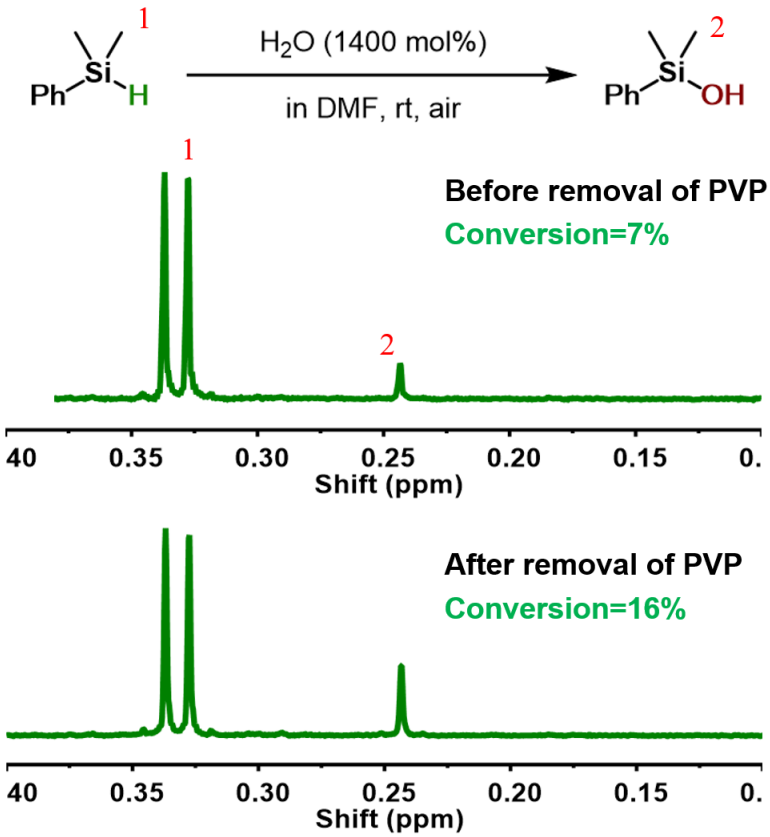

Fig. 2-8 ^{1}H NMR spectra of the product catalyzed by reactor before and after removing PVP.

To evaluate the catalytic performance before and after remove PVP. The oxidation reaction of $PhMe_2SiH$ to $PhMe_2SiOH$ in DMF (As shown in **Fig. 2-8 (a)**) was conducted using the CM-Au and CM-Au:PVP as a flow reactor, respectively. The 3 mL of DMF solution with 0.1 mmol $PhMe_2SiH$ and 2 μL H_2O was circularly flowed through the monolith to take reaction. After reaction for 15 min, 20 μL of reactant solution was taken out and dissolved in 1 mL DMSO-d_6 to tested by ^{1}H NMR. The resulted spectra were compared in **Fig. 2-8 (b** and **c)**. The double peak at 3.3 ppm was assigned to the hydrogen of methyl groups on $PhMe_2SiH$. After the reaction, this peak will become a single peak and shifted to 0.24 ppm, which corresponding to the methyl groups $PhMe_2SiOH$. According to the ratio of the integrated area of these two peaks, the conversion of the reaction can be calculated. As a result, the CM-Au showed a conversion of about 16%, which is higher than that of CM-Au:PVP (7%). This indicated that the Au NPs after remove of PVP have enhanced catalytic activity. It can be interpreted that more active metal sites were exposed without the coverage of PVP.

2.4 Conclusion

In this Chapter, the narrow-dispersed Au:PVP NPs were prepared by a "seed-mediated" method using PVP as a stabilizer. The obtained Au:PVP NPs were successfully transferred onto the cellulose monolith by a facile continuous-flow method. The $NaBH_4$/methanol solution was used to wash the as-prepared CM-Au:PVP to remove PVP from Au NPs surface. The successful removal of PVP was demonstrated by FTIR and XPS. After removing PVP, the Au NPs were immobilized on cellulose monolith by the chelation interaction between metal NPs and hydroxyl groups of cellulose. The CM-Au after remove PVP was more stable in water compared with the CM-Au:PVP. Finally, the CM-Au monolith was used as a flow reactor to catalyze the oxidization reaction of $PhMe_2SiH$. Results showed that the sample without PVP had an enhanced catalytic activity, which may be attributed to the exposure of more active metal sites after removing of PVP from Au NPs surfaces.

2.5 References

1. E. Lam, S. Hrapovic, E. Majid, J. H. Chong and J. H. Luong, *Nanoscale*, 2012, **4**, 997-1002.
2. R. J. Pinto, P. A. Marques, M. A. Martins, C. P. Neto and T. Trindade, *J. Colloid Interface Sci.*, 2007, **312**, 506-512.
3. M. Schlesinger, M. Giese, L. K. Blusch, W. Y. Hamad and M. J. MacLachlan, *Chem Commun (Camb)*, 2015, **51**, 530-533.
4. H. Koga, E. Tokunaga, M. Hidaka, Y. Umemura, T. Saito, A. Isogai and T. Kitaoka, *Chem Commun (Camb)*, 2010, **46**, 8567-8569.
5. Y. Shin, I.-T. Bae, B. W. Arey and G. J. Exarhos, *The Journal of Physical Chemistry C*, 2008, **112**, 4844-4848.
6. H. Chanzy, B. Henrissat and R. Vuong, *FEBS Lett.*, 1984, **172**, 193-197.
7. D. F. Siqueira Petri, S. Choi, H. Beyer, T. Schimmel, M. Bruns and G. Wenz, *Polymer*, 1999, **40**, 1593-1601.
8. S. Haesuwannakij, T. Poonsawat, M. Noikham, E. Somsook, Y. Yakiyama, R. N. Dhital and H. Sakurai, *Journal of Nanoscience and Nanotechnology*, 2017, **17**, 4649-4657.
9. M. C. Daniel and D. Astruc, *Chem. Rev.*, 2004, **104**, 293-346.
10. B. Kim, G. Han, B. J. Toley, C. K. Kim, V. M. Rotello and N. S. Forbes, *Nat Nanotechnol*, 2010, **5**, 465-472.
11. J. D. Newman and G. J. Blanchard, *Langmuir*, 2006, **22**, 5882-5887.
12. W. W. Weare, S. M. Reed, M. G. Warner and J. E. Hutchison, *Journal of the American Chemical Society*, 2000, **122**, 12890-12891.
13. Y. Zhao, L. Jia, J. A. Medrano, J. R. H. Ross and L. Lefferts, *ACS Catalysis*, 2013, **3**, 2341-2352.
14. K. M. Koczkur, S. Mourdikoudis, L. Polavarapu and S. E. Skrabalak, *Dalton transactions*, 2015, **44**, 17883-17905.
15. P. Sonstrom and M. Baumer, *Physical chemistry chemical physics : PCCP*, 2011, **13**, 19270-19284.
16. C. J. Jia and F. Schuth, *Physical chemistry chemical physics : PCCP*, 2011, **13**, 2457-2487.
17. J. Xian, Q. Hua, Z. Jiang, Y. Ma and W. Huang, *Langmuir*, 2012, **28**, 6736-6741.
18. Y. Borodko, H. S. Lee, S. H. Joo, Y. Zhang and G. Somorjai, *The Journal of Physical Chemistry C*, 2009, **114**, 1117-1126.

19. S. M. Ansar, F. S. Ameer, W. Hu, S. Zou, C. U. Pittman, Jr. and D. Zhang, *Nano letters*, 2013, **13**, 1226-1229.
20. B. Donoeva and P. E. de Jongh, *ChemCatChem*, 2018, **10**, 989-997.
21. H. Tsunoyama, H. Sakurai and T. Tsukuda, *Chem. Phys. Lett.*, 2006, **429**, 528-532.

Chapter 3

Cellulose monolith generating and supporting gold nanoparticles for green catalyst

3.1 Introduction

From the last two decades, numerous efforts [1-8] have been attempted to decorate the metal NPs on monoliths to develop high-efficiency flow catalytic systems. Many strategies for preparing monolith-supported reactors usually involves the external reducing agent or stabilizer, which leads to increased production cost and environmental pollution.[9-13] From the green chemistry perspective, a more eco-friendly and efficient method for fabricating metal NPs-supported monolithic flow reactor is still required.

Recently, directly reducing metal ions by the support materials has been considered as a reasonable strategy, as it can combine the reduction, stabilization, and support into one process and eliminate the addition of a reducing agent and stabilizer.[3, 14-18] This strategy also minimizes the remaining chemicals attached to the MNP surface after immobilization and reduces the effect of impurities on the catalytic performance of metal NPs. Indeed, some materials such as hydrogen silsesquioxane,[3] aniline,[15] citrate[16], chitosan[19, 20], and cellulose[17, 18] have already been proven to serve as both reducing and stabilizing agents in the preparation of heterogeneous metal catalysts. Among them, cellulose as the most abundant biomass in nature,[21] is considered as one of the most promising supporting materials because of its inexpensive, biodegradable, nontoxic and chemical-resistant characteristics.[22]

The current state of synthesis of Au NPs using cellulose as a reducing agent usually involves the reaction conditions such as introducing the supercritical CO_2 [23] or steps such as hydrothermal treatment.[24, 25] Moreover, most previous studies have been conducted on powdery or fibrous cellulose, and the obtained products can hardly be used as continuous-flow reactors. Fortunately, no study has reported the use of porous cellulose sponges to directly reduce and support the metals to construct a green catalytic system. This is probably because

most porous cellulose sponges are prepared based on the crosslinking of the modified cellulose, such as carboxymethyl cellulose (CMC) [26] and 2,2,6,6-tetramethylpiperidine-1-oxyl radical (TEMPO)-oxidized cellulose.[27] The modification treatment and the crosslinking process would inevitably complicate the chemical properties of cellulose, making the investigation of the reaction between cellulose sponge and metal ions difficult.

Unlike the cellulose sponge fabricated by the chemical crosslinking of surface-modified cellulose, the cellulose monolith prepared via TIPS has a simple chemical composition that remains the original chemical structure of cellulose, thus it was considered as a promising candidate of supporting materials for directly reducing the metals to efficiently develop green and high-efficiency flow catalytic systems.

In this chapter, a continuous-flow method was developed for the monolithic cellulose to reduce Au ions and stabilize the formed Au NPs at room temperature without adding any other reducing agent or surfactant. This strategy realized a combination of the green preparation of metal NPs and their facile immobilization on the renewable cellulose materials by using a simple and moderate method. The product was applied as a continuous-flow reactor in both water and organic solvent.

3.2 Experiment

3.2.1. Materials

The cellulose acetate powder (CA, L30) used in this experiment was supplied by DAICEL Co., Ltd. Japan, and its acetylation degree was approximately 55%. Hydrogen tetrachloroaurate tetrahydrate ($HAuCl_4 \cdot 4H_2O$) with a purity of 99% was purchased from Nacalai Tesque, Inc. Kyoto, Japan. Sodium borohydride ($NaBH_4$) was purchased from FUJIFILM Wako Pure Chemical Corporation, Japan. 4-NP and dimethylphenylsilane ($PhMe_2SiH$) were purchased from Tokyo Chemical Industry Co., Ltd. Methylene blue and methyl orange were purchased from Tokyo Chemical Industry Co., Ltd. Other chemicals including *N*,*N*-dimethylformamide, 1-hexanol, and sodium hydroxide were produced by FUJIFILM Wako Pure Chemical Corporation, Japan, all of which were chemically purified and commercially available. The heat-shrinkage polyolefin tube (THT-8.0N) for fabricating the flow reactors was provided by Denka Electron Co. Ltd., Japan.

3.2.2 Preparation of Au NPs on the cellulose monolith

The porous cellulose monolith was fabricated according to the method described in Chapter 1. The as-prepared cellulose monolith was directly applied to reduce $HAuCl_4$ and anchor the formed Au NPs. First, the cellulose monolith with a length of 1 cm was fixed in a heat-shrinkable tube, and then, the $HAuCl_4$ aqueous solution (0.2 mmol/L, 5 mL, pH was adjusted to 13 with 1 mol/L aqueous NaOH solution) was pumped to circularly flow through the monolith by using a peristaltic pump. During the continuous flow, the Au ion was gradually reduced to Au NPs. After being flowed for 3 h, the sample was washed with deionized water (200 mL) and then dried under vacuum for 24 h to obtain the cellulose-Au monolith.

As a comparison, the reduction experiment was also conducted in a batch fashion, in which the cellulose monolith was immersed in the $HAuCl_4$ aqueous solution to react under stirring; the other reaction conditions were the same as those in the flow fashion. After reaction for 3 h, the sample was taken out and washed with deionized water, and then dried under vacuum for 24 h to be tested.

3.2.3 Catalytic performance test

The obtained cellulose-Au monolith was fixed in a shrinkable tube to construct the circulation flow reactor. The 3 mmol/L 4-NP aqueous solution and freshly prepared 0.5 mol/L aqueous solution of $NaBH_4$ was mixed, and then immediately flowed through the reactor at a certain flow rate to react. After being flowed through the monolith, the effluent was collected and diluted by 30 times with deionized water to be tested by UV-*vis* measurement. The standard solutions of 4-NP were previously tested to build the standard curve as a reference. According to the standard curve, the concentration of 4-NP in both the influent and effluent was calculated. Then, the catalytic efficiency was estimated by using the concentration change and flow rate. In this experiment, the flow rate was corrected by the real volume of the effluent outflowing per unit time.

The catalytic performance of the reactor in an organic solution was evaluated by the oxidation reaction of $PhMe_2SiH$ to dimethylphenylsilanol ($PhMe_2SiOH$) in DMF. In this experiment, 0.1 mmol of $PhMe_2SiH$ and 25 μL of H_2O were dissolved in 3 mL of DMF, and the mixture was circularly flowed through the reactor at a constant flow rate (3 mL/min) to take reaction in air at room temperature. After reacting for a certain time (0.5, 1, 2, and 3 h), 20 μL of the reactant solution was taken out and dissolved in 1 mL of deuterated dimethyl sulfoxide (DMSO-D6, with 5 wt % of tetramethylsilane) to be tested by ^1H NMR. To test the reusability, the same monolithic reactor was employed to repeat the reaction and the catalytic performance was evaluated. In each cycle, 0.1 mmol of $PhMe_2SiH$ and 25 μL of H_2O were dissolved in 3 mL of DMF, and the mixture was circularly flowed through the reactor to take reaction. After 1 h of reaction, 20 μL of the obtained reactant solution was taken out and dissolved in 1 mL of DMSO-D6 to be tested by ^1H NMR.

3.2.4 Characterization

The chemical change of the monolith was investigated through FTIR measurements on a Thermo Scientific (Yokohama, Japan) Nicolet iS5 spectrometer equipped with an iD5 ATR attachment. A UV-*vis* spectrophotometer (HITACHI, U-2910) was used to monitor the concentration of Au ions in the preparation process of Au NPs. The absorbance curve was

collected at wavelengths ranging from 250 to 500 nm. Before the measurement, the solution was adjusted to pH = 1 using 1 mol/L HCl aqueous solution. The concentration of UV specimen was determined according to the peak intensity and calibrated based on the volume change caused by the pH adjustment. $HAuCl_4$ standard solutions with the concentration of 0, 0.02, 0.05, 0.1, 0.15 and 0.2 mmol/L were prepared as follows: Firstly, 0, 0.02, 0.05, 0.1, 0.15 and 0.2 mL of the standard 5.00 mmol/L $HAuCl_4$ aqueous solution were added in vials respectively, and to each vial was added aqueous HCl solution (1 mol/L, 0.5 mL). Subsequently, the deionized water was added to adjust the volume to be 5.0 mL. The concentration change of 4-NP in the catalytic reaction was also determined by UV-*vis* experiments. The absorbance curve was collected at the wavelengths ranging from 250 to 600 nm. XPS (JEOL JPS-9010MC) was applied to study the surface chemical composition of the monolith, using monochromatized Al-Kα radiation (1486.6 eV). The XPS results were collected by at fixed analyzer pass energies of 160 eV and 10 eV, respectively. The residual pressure inside the analysis chamber was in the 10^{-7} Pa range. The binding energies were referred to as C-H (sp^3) carbon for the C1s peak set at 284.8 eV. The morphologies of the monoliths were observed using a SEM (Hitachi S-3000N) at 15 kV. Before the observation, the samples were slivered into sections and coated with a thin layer of Au by using an ion sputter apparatus (E-1010, Hitachi Ltd.). In addition, the size of the Au NPs and their dispersion state in the monolith were detected by TEM (JEOL JEM-2010) at an acceleration voltage of 100 kV. The sample was deposited on a copper grid coated with carbon (NP-C15, Okenshoji, Co., Ltd.) for testing. The crystalline states of the cellulose monolith with and without Au loading were studied through XRD experiments conducted with an X-Pert diffractometer (SmartLab, RIGAKU) using graphite-monochromatized Cu-Kα radiation (λ = 1.54 Å). The generator voltage and current were set at 45 kV and 200 mA, respectively. The atomic content of Au in the samples was detected by inductively coupled plasma atomic emission spectrometry (ICP-AES) with SHIMADZU, ICPS-8100. Au standards with the atomic concentration of 0.5, 1, 2, 5, 10, 20, and 50 ppm were used for the calibration. The reaction conversion of the oxidation of $PhMe_2SiH$ was determined by proton nuclear magnetic resonance (^{1}H NMR) spectroscopy using DMSO-d_6 as a solvent, with JNM-ECS400 (400 MHz, JEOL Ltd., Tokyo, Japan).

3.3 Results and discussion

3.3.1 Preparation of Au NPs on cellulose monolith

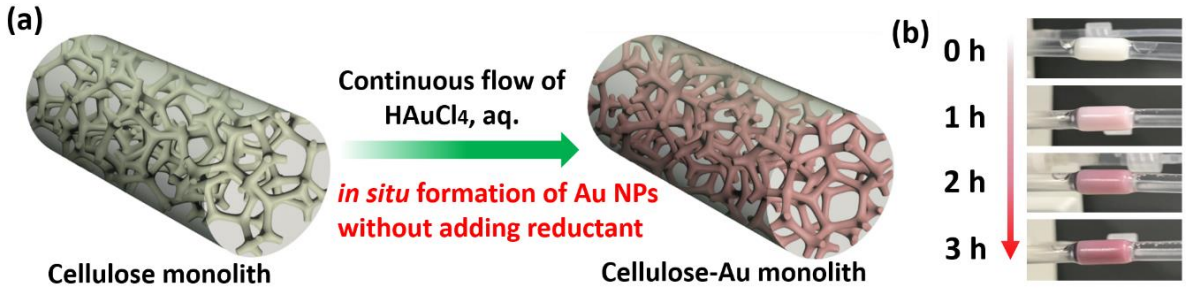

Fig. 3-1 (a) Schematic diagram of the reduction of Au ions by cellulose monolith without adding any external reducing agent. **(b)** Digital pictures of the monolith after different reaction times during the continuous-flow reaction with $HAuCl_4$ aqueous solution.

The cellulose monolith was prepared according to the previously reported procedure based on the TIPS method.[28] The obtained cellulose monolith possessed a uniform column shape with a diameter of around 0.8 cm. It had three-dimensional continuous macropores with sizes of approximately 10–30 μm, and a rough surface. The nitrogen adsorption/desorption isotherm experiments in Chapter 1 demonstrated that the cellulose monolith had a mesopore structure with a pore size of 5–15 nm according to the non-local density functional theory (NLDFT). [29, 30] Such a hierarchical pore structure not only endows the monolith with a high surface area suitable for the efficient reduction of Au^{3+} and immobilization of Au NPs on the monolith but also allows it to be applied in the flow system. Moreover, the cellulose monolith has a very simple chemical composition compared to the cellulose sponge prepared by the crosslinking of surface-modified cellulose. All these advantages make it a promising supporting material for constructing a green catalytic flow reactor. As shown in **Fig. 3-1 (a)**, the cellulose monolith was applied to reduce the $HAuCl_4$ without adding any reducing agent. In a typical experiment, a monolith with a length of 1 cm is fixed in a shrinkable tube and the aqueous Au ion solution is continuously flowen through the monolith using a peristaltic pump. The color of the monolith gradually changes to reddish in the flow process, indicating the formation of Au NPs (**Fig. 3-1 (b)**).

To more specifically investigate this process, the concentration of Au ions in solution was

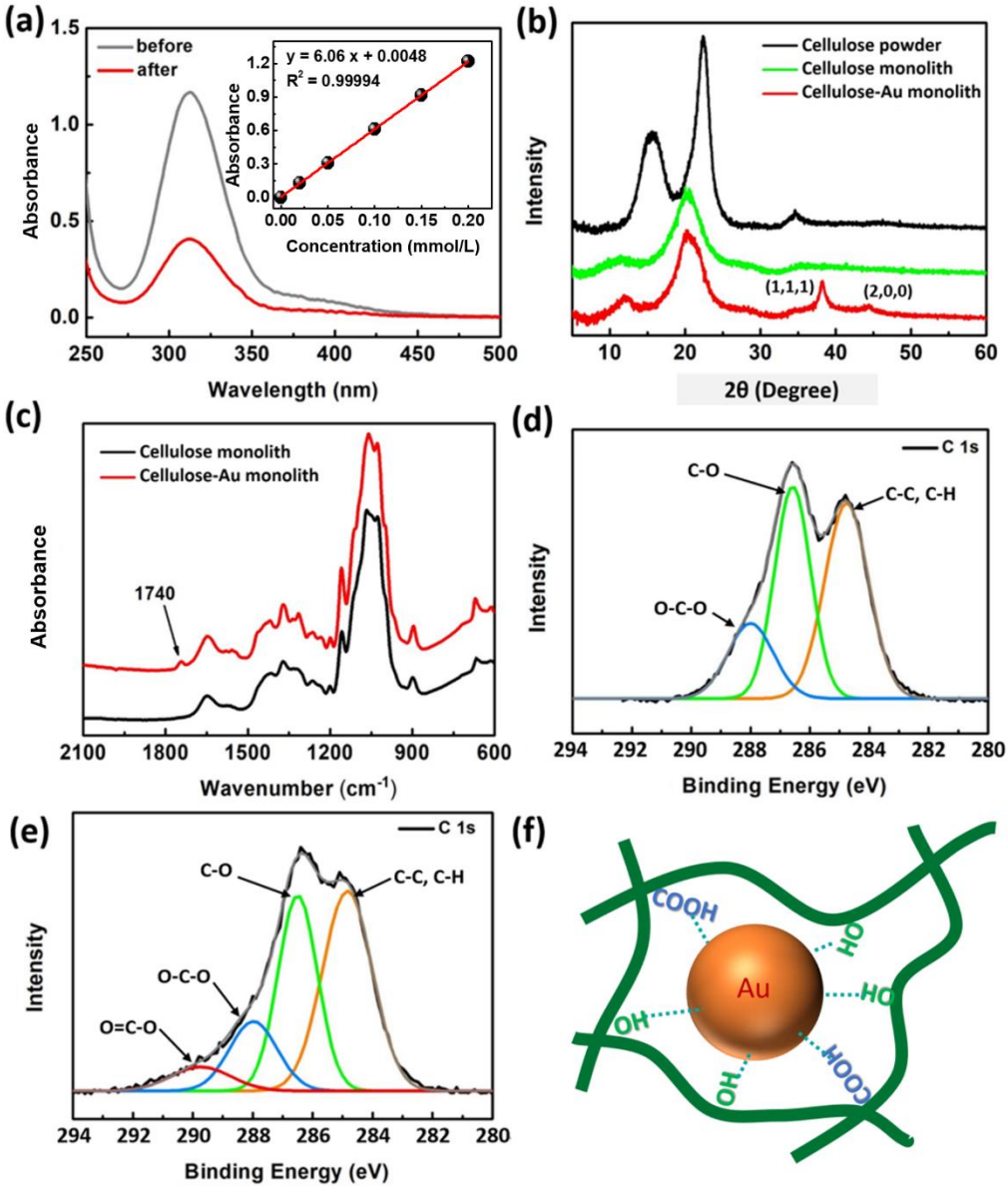

Fig. 3-2 (a) UV-vis spectra of Au ion solution before and after flowing with cellulose. Before reaction: 0.2 mmol/L, 5 mL. The inset figure is the standard curve of the UV-vis absorbance at 312 nm as a function of the concentration of Au ions. The pH of the sample was adjusted to 1 before the test. **(b)** XRD spectra of cellulose powder, cellulose monolith, and cellulose-Au monolith, respectively. **(c)** FTIR spectra of the cellulose monolith and cellulose-Au monolith. **(d)** and **(e)** C1s XPS of the cellulose monolith before and after immobilization. **(f)** Schematic diagram of the interaction between Au NPs and the oxygen-containing groups of cellulose.

monitored by UV-*vis* measurement using the characteristic peak of Au ions around 312 nm at pH=1 (**Fig. 3-2 (a)**). The results indicated that over 60% of Au ions were reduced after 3 h, which was in good agreement with the results obtained from ICP-AES measurements (0.62 μmol). The Au NPs formation was confirmed by XRD measurements. As shown in **Fig. 3-2**

(b), new peaks at 2θ = 38.1° and 44.3°, corresponding to the fcc packing structure of Au(111) and Au(200) planes,[31] respectively, were observed on the spectrum of the monolith after reaction with Au ions, demonstrating a successful preparation of Au NPs on the cellulose monolith. Since no external reducing agent was added during the continuous-flow generation of Au NPs, the cellulose monolith itself must work as a reducing agent, which was confirmed by the FTIR spectra for the observation at 1740 cm^{-1}, which corresponds to the C=O stretching, after the reaction (**Fig. 3-2 (c)**). [18] In addition, the change in the oxidation state was determined by the peak-differentiation-imitation analysis of the C1s XPS. The original cellulose monolith displayed three typical peaks at binding energies of 284.8, 286.6, and 288.0 eV, corresponding to the C–C/C–H bond, C–O single bond, and O–C–O bond of cellulose, respectively (**Fig. 3-2 (d)**).[32] In contrast, the cellulose monolith after the reaction exhibited a relatively lower contribution of C–O bonding and a new peak appearing at the binding energy of 289.7 eV, which could be interpreted by the consumption of C–O bonds and the formation of O–C=O bonds, suggesting that some hydroxyl groups of the cellulose were oxidized to carbonyl groups during the reaction (**Fig. 3-2 (e)**). In general, cellulose does not show reducibility to Au ions at room temperature, because of the high crystallinity and strong hydrogen bonding interaction. The reason for the high reactivity of the monolith may be attributed to the weak hydrogen-bonding network to liberate the free hydroxyl groups due to the monolith structure as well as the alkaline conditions.[33,34] Meanwhile, the pore structure of the cellulose monolith can act as an ideal scaffold for the seeding of Au. During the continuous-flow process, the Au ions were forced to contact the activated hydroxyl groups on the pore surface and reduced by the hydroxyl groups of the cellulose monolith. Both a large number of the hydroxyl groups and the newly formed carbonyl groups may contribute to the immobilization of Au NPs on the surface of the monolith via coordination or electrostatic adsorption. (**Fig. 3-2 (f)**).

3.3.2 Morphology of Au NPs formed on the monolith

The morphology of the obtained Au NPs was observed by TEM (**Fig. 3-3 (a)**). The Au NPs formed on the monolith showed a virtually spherical sphere shape without obvious aggregation. The corresponding statistical histogram illustrated that the size of the formed Au was 12.1 ± 5.5 nm (based on over 300 counts). As a comparison, the Au NPs synthesized by

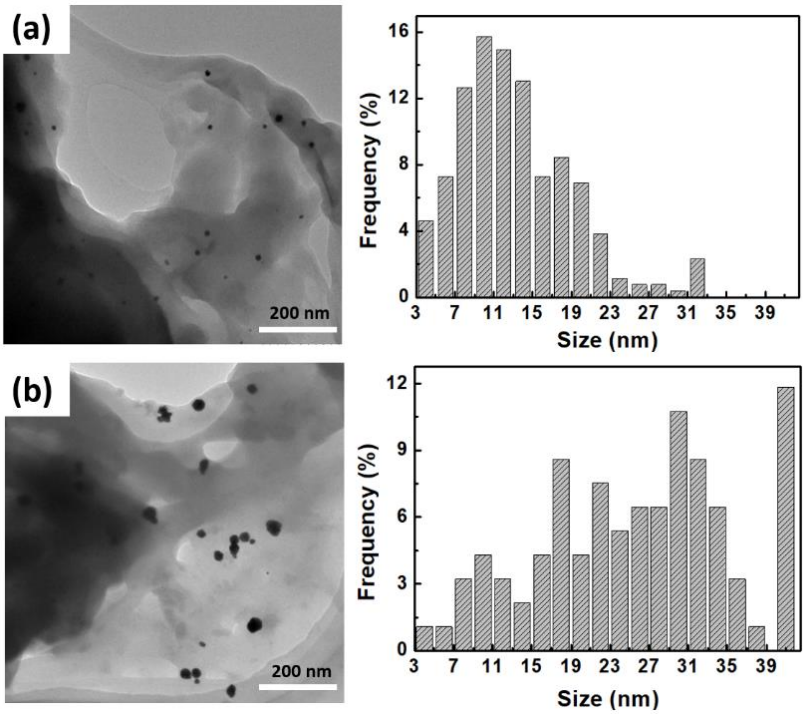

Fig. 3-3 TEM images and the size distribution of the Au NPs loaded on the monolith by **(a)** flow method and **(b)** immersion method.

immersing the monolith in the Au ion solution with the same pH and reaction conditions showed a bigger size (26.4 ± 9.1 nm, based on over 300 counts) and wider size distribution. In addition, the aggregation of the Au NPs was observed in the TEM image **(Fig. 3-3 (b))**. These results indicated that the flow method was more conducive to the homogenous formation of the Au NPs. The continuous-flow process realized a homogeneous concentration distribution of Au ions, as well as achieves the better contact between the Au solution and the large surface of the monolith that bears sufficient reaction sites.

Furthermore, the influences of both the concentration of $HAuCl_4$ and the reaction time were investigated. As shown in **Fig. 3-4 (a)**, the sample prepared by the flow reaction with a low initial Au concentration of 0.05 mmol/L (cellulose-Au-1) led to the smallest size of the Au NPs (NPs are marked in the red circle). To apply for a large throughput in practical use, the concentration of $HAuCl_4$ was increased to 0.2 mmol/L (cellulose-Au-2) and 1 mmol/L (cellulose-Au-3) (**Fig. 3-4 (a-d)**). The results showed that a larger size of Au NPs was formed by increasing the Au concentration. The effect of reaction time was also investigated by extending the reaction time from 3 h to 12 h. Consequently, the NPs exhibited a significantly larger size, as shown in **Fig. 3-4 (e)** and **(f)** (compared to **Fig. 3-4 (b)** and **(c),** respectively). It

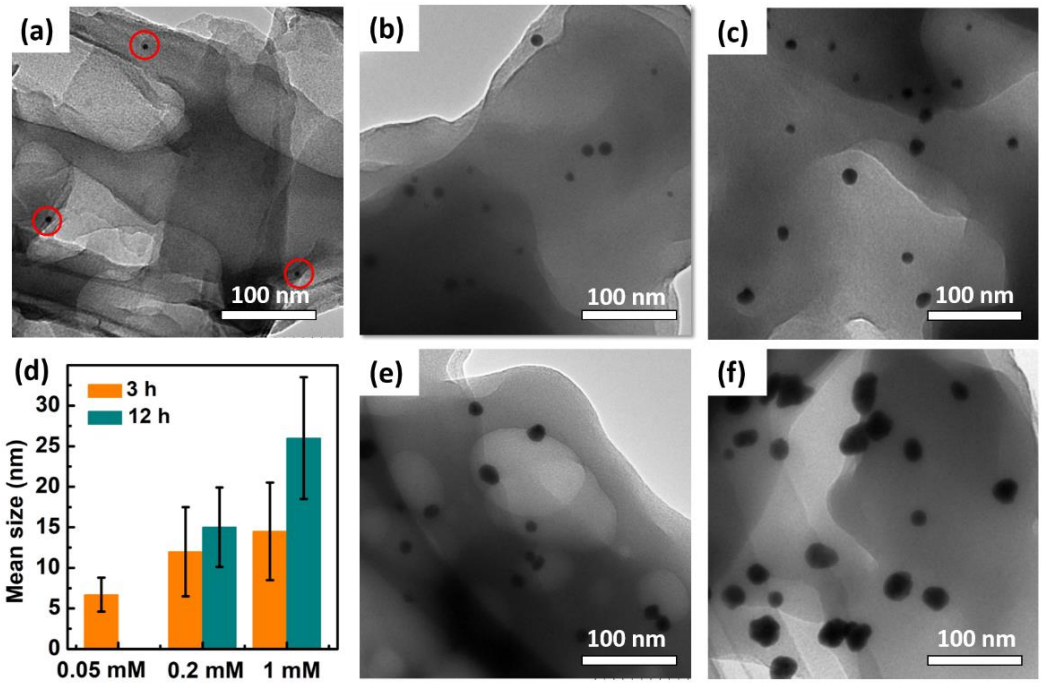

Fig. 3-4 TEM images of Au NPs in cellulose-Au samples with different initial concentrations and reaction times: **(a)** Cellulose-Au-1: 0.05 mmol/L, 3 h. (NPs are indicated by red circle) **(b)** Cellulose-Au-2: 0.2 mmol/L, 3 h. **(c)** Cellulose-Au-3: 1.0 mmol/L, 3 h. **(e)** Cellulose-Au-4: 0.2 mmol/L, 12 h. **(f)** Cellulose-Au-5: 1 mmol/L, 12 h. The mean particle sizes of each sample were accounted and calculated in **(d).**

could be interpreted that the longer reaction time allowed the NPs to grow further by using the formed NPs as seeds and form bigger NPs during the flow process as long as the supply of Au ions was adequate. In particular, the samples that reacted with 1 mmol/L Au ions showed a significantly larger size as the reaction time increased. This might be attributed to the saturation of Au ions, and the monolith cannot provide sufficient reactive sites to form new seeds. The sample that reacted with an initial concentration of 0.2 mmol/L for 3 h (Cellulose-Au-2) was adopted in the later experiments due to its relatively smaller particle size and the shorter time consumption.

3.3.3 Catalytic application of the obtained cellulose-Au monolith

Owing to a large number of oxide-containing groups on the cellulose monolith, the obtained Au NPs were stably anchored on the surface of the monolith and could not be washed out by water.[22, 25] Even after circularly washing the cellulose-Au monolith with 10 mL of deionized water for 3 h, the amount of leached Au NPs was very low (<1 ppm), as measured by ICP-AES. This result prompted us to investigate the cellulose-Au monolith as a catalyst of

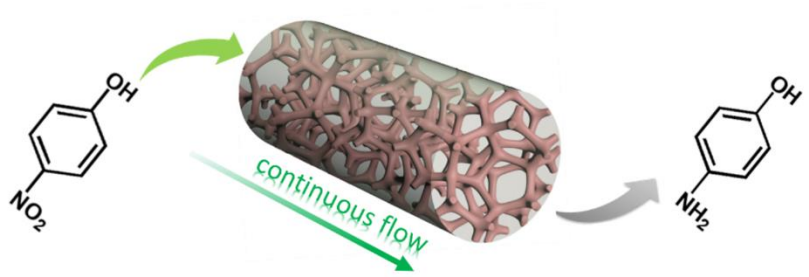

Fig. 3-5 Cellulose-Au monolith used as a continuous-flow reactor for the reduction of 4-NP.

continuous-flowing system. As shown in **Fig. 3-5**, the cellulose-Au-2 was used as a flow reactor, and a peristaltic pump was employed to flow the reactant mixture through the monolith to react under the catalysis of Au NPs (see **Fig. 3-6 (a)**). The $NaBH_4$ reduction from 4-NP to 4-AP was chosen as a model reaction to evaluate the catalytic performance.

In a typical experiment, a mixture of 4-NP (3 mmol/L) and $NaBH_4$ (0.5 mol/L) was flowed through the reactor using the tubing pump flow system. As a result, the yellow color of 4-NP disappeared to become colorless when the flow rate was 3.5 mL/min, suggesting the successful reduction of 4-NP. (**Fig. 3-6 (b)**). The progress of reduction was also monitored by using UV-

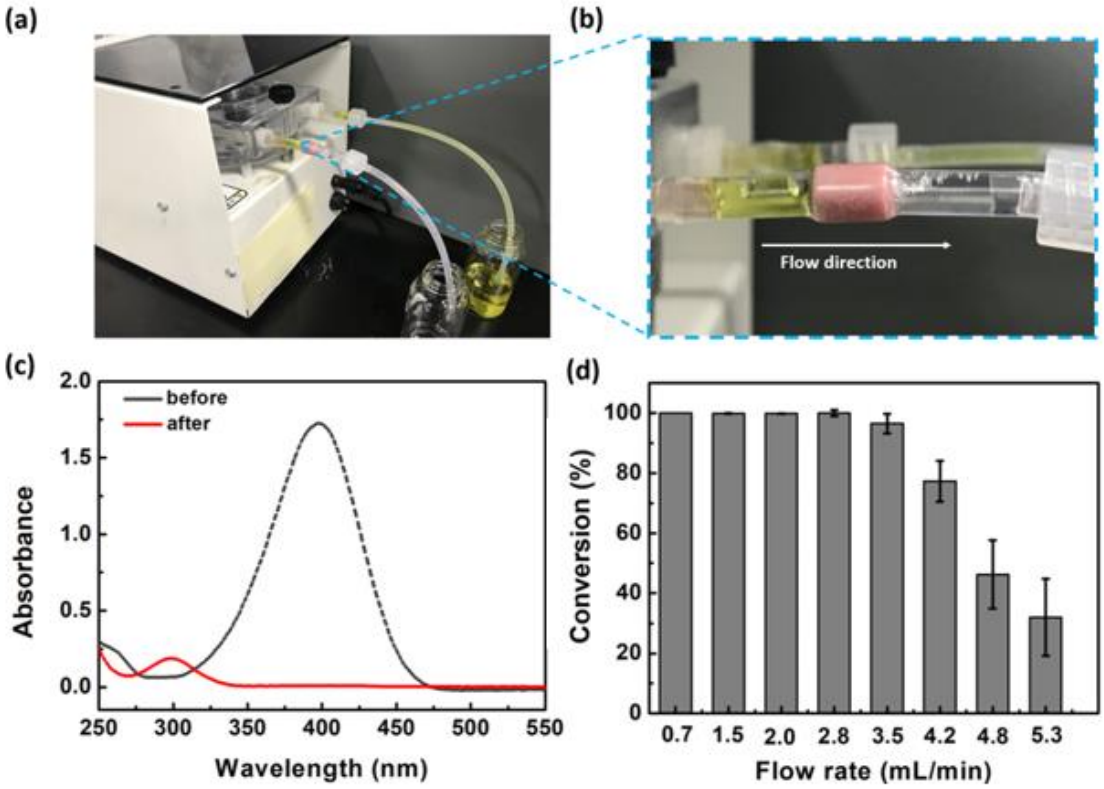

Fig. 3-6 (a) Digital photograph of the flow reactor; **(b)** The close-up photograph of monolith microreactor; **(c)** UV-vis spectra of the reactant solution at a flow rate of 1 mL/min. (diluted by 30 times before test) **(d)** Reaction conversion at the different flow rates.

vis spectroscopy. Result showed the complete disappearance of the signal of 4-NP (400 nm) and the generation of a new peak centered at 300 nm, indicating the formation of 4-AP. (**Fig. 3-6 (c)**) The reduction of 4-NP at the different flow rates was traced through the decay of the UV-*vis* signal at 400 nm. According to the standard curve of 4-NP in water, the concentration of 4-NP remaining in the effluent was determined and then the conversion was calculated. (**Fig. 3-6 (d)**) Considering that the reaction conversion at the flow rate of 3.5 mL/min was about 96 %, the reaction efficiency was calculated to be around 970 h^{-1}.

The good catalytic performance of the as-prepared monolithic cellulose reactor can be attributed to the following reasons: First, the Au NPs were directly supported by the cellulose monolith without adding any other stabilizer or surfactant, and thus the Au NPs exposed a larger free surface and provided more reactive sites for catalysis. Furthermore, the immobilization of Au NPs was realized by a flow method, by which the Au NPs were mainly formed at the pore surface along with the flow routes with good dispersion. This allowed the Au to take part in the reaction sufficiently and avoided the idleness of the catalysts during the flow process. More importantly, the monolithic cellulose, which is different from the bulk or fibrous cellulose, has a special hierarchically porous structure, as shown in **Fig. 3-7**. During the flow reaction, the three-dimensional continuous macro-pores endowed the reactor with good permeability and high throughput capacity, while the numerous micro/mesopores, which

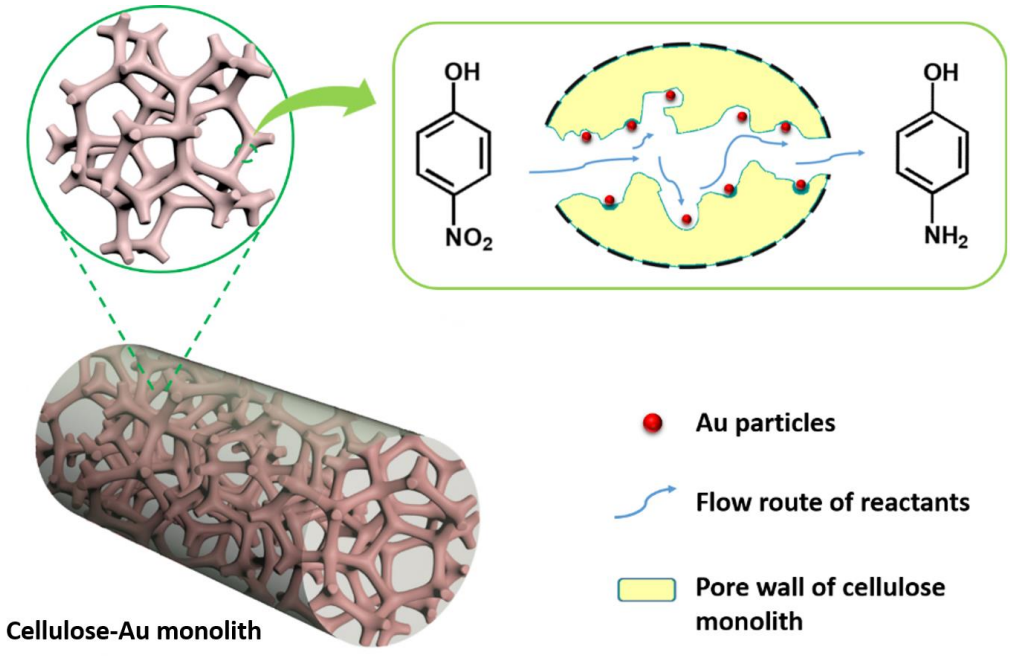

Fig. 3-7. Schematic diagram of monolith microstructure during the continuous-flow reaction.

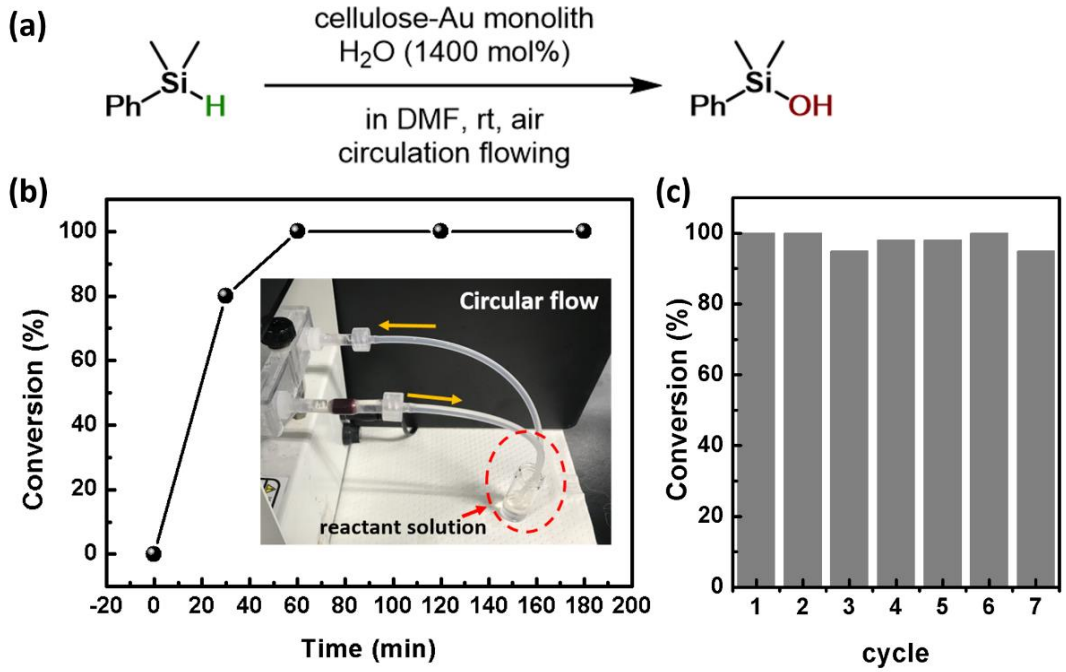

Fig. 3-8 (a) Schematic diagram of oxidation of $PhMe_2SiH$ in DMF; **(b)** Conversion of the reaction as a function of reaction time. Inset was the digital picture of the circular flow process; **(c)** Reusability test of the monolith reactor after 60 min.

contributed to the rough surface of the skeleton, enabled the reactants to be quickly diffused in the monolith and sufficiently contacted with the catalysts. Thereby the monolithic cellulose reactor realized a combination of good flowability and the high-efficiency reaction.

Although most of the bio-materials-based solid supports are not applicable in organic solvents due to their instability and solubility, the cellulose-based materials have high organic solvent tolerance, which is one of their attractive characteristics of them. Furthermore, the high solvent permeability of the monolithic cellulose is preferable for the flow reaction, expanding the utility of the cellulose-Au catalyst. Taking these into consideration, the oxidation of silane to silanol in an organic solvent was investigated as a demonstration (**Fig. 3-8 (a)** and **(b)**). The $PhMe_2SiH$/DMF solution was circularly flowed through the cellulose reactor to react. After 60 min of flowing, the $PhMe_2SiH$ was successfully oxidized to afford the corresponding silanol ($PhMe_2SiOH$) according to the result of ^{1}HNMR measurements (**Fig. 3-9**) To illustrate the durability of the monolith reactor under the reaction conditions, the reusability test was carried out. As shown in **Fig. 3-8 (c)**, the cellulose reactor can be used at least 7 times while retaining the catalytic activity, showing the high stability even in DMF.

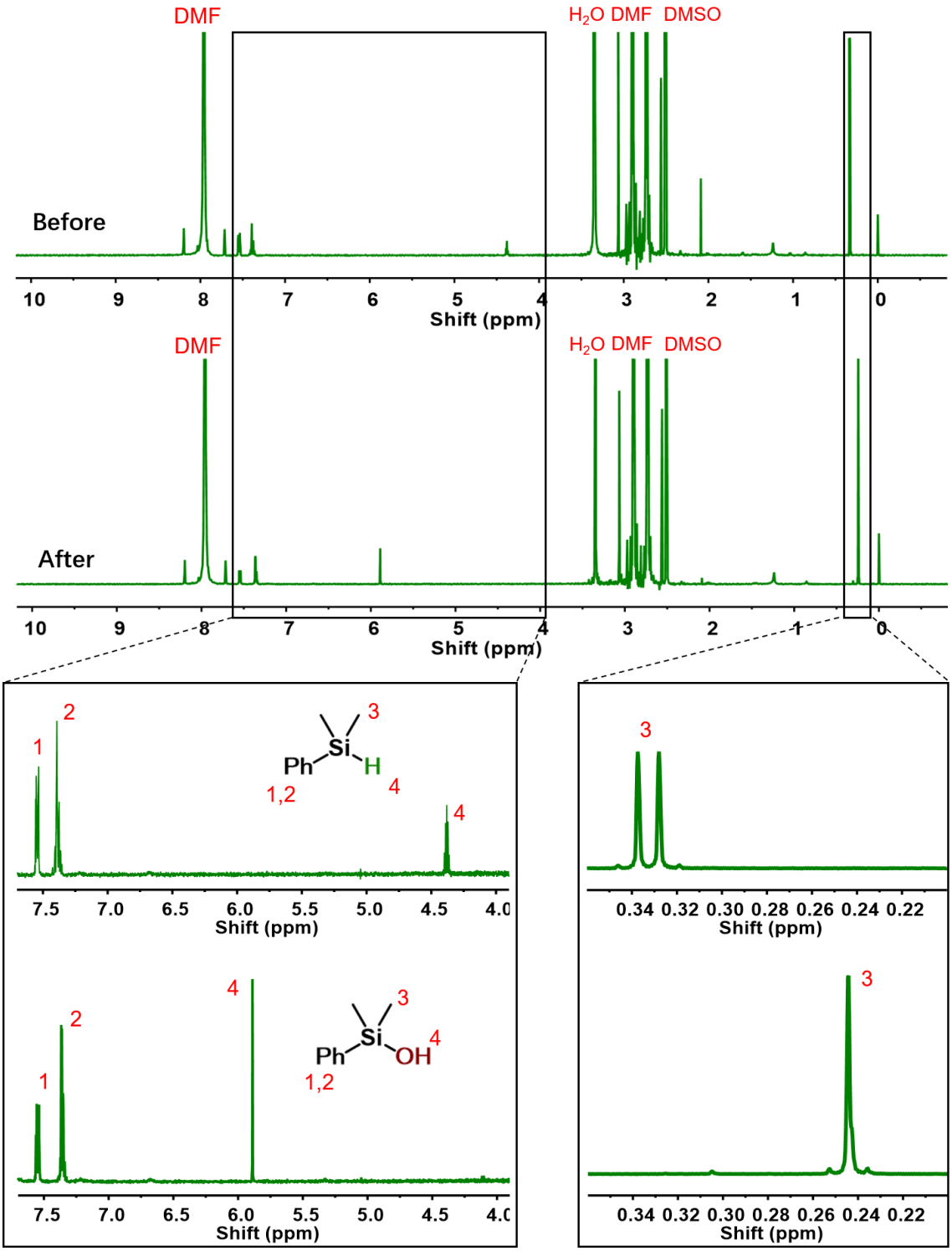

Fig. 3-9 ^{1}H NMR spectra (DMSO-d_6 as solvent) of the dimethylphenlsilane reactant before and after flowing for 60 min, respectively.

3.4 Conclusion

In this chapter, a simple, green, and cost-effective strategy was developed for constructing a high-efficiency cellulose monolith-Au flow reactor. The cellulose monolith prepared using

the facile TIPS method can be directly used to synthesize and stabilize the Au NPs at room temperature without any other surface modification or adding a reduction agent. The results demonstrated that the abundant hydroxide groups on the cellulose endowed the monolith with reducibility to Au ions. Compared to the batch synthesis, the flow reduction was more conducive to the homogeneous preparation of Au NPs with relatively smaller sizes. Moreover, the size of the Au NPs formed on the cellulose monolith can be affected by the reaction conditions including the initial concentration of $HAuCl_4$ and the reaction time. Consequently, the obtained cellulose products could be applied as a green flow reactor in both water and organic solution and showed excellent catalytic efficiency and good stability.

3.5 References

1. L. Han, S. Cai, M. Gao, J. Y. Hasegawa, P. Wang, J. Zhang, L. Shi and D. Zhang, *Chem. Rev.*, 2019, **119**, 10916-10976.
2. H. Yang, Q. Lu, F. Gao, Q. Shi, Y. Yan, F. Zhang, S. Xie, B. Tu and D. Zhao, *Advanced Functional Materials*, 2005, **15**, 1377-1384.
3. N. Moitra, K. Kanamori, T. Shimada, K. Takeda, Y. H. Ikuhara, X. Gao and K. Nakanishi, *Advanced Functional Materials*, 2013, **23**, 2714-2722.
4. L. M. Bronstein, S. Polarz, B. Smarsly and M. Antonietti, *Advanced Materials*, 2001, **13**, 1333-1336.
5. Z. T. Xie, T. A. Asoh and H. Uyama, *Carbohydr. Polym.*, 2019, **214**, 195-203.
6. Y. Li, L. Xu, B. Xu, Z. Mao, H. Xu, Y. Zhong, L. Zhang, B. Wang and X. Sui, *ACS applied materials & interfaces*, 2017, **9**, 17155-17162.
7. C. H. Pelisson, T. Nakanishi, Y. Zhu, K. Morisato, T. Kamei, A. Maeno, H. Kaji, S. Muroyama, M. Tafu, K. Kanamori, T. Shimada and K. Nakanishi, *ACS applied materials & interfaces*, 2017, **9**, 406-412.
8. F. J. Heiligtag, W. Cheng, V. R. de Mendonça, M. J. Süess, K. Hametner, D. Günther, C. Ribeiro and M. Niederberger, *Chemistry of Materials*, 2014, **26**, 5576-5584.
9. K. I. Hadjiivanov and D. G. Klissurski, *Chemical Society Reviews*, 1996, **25**, 61.
10. R. B. Bedford, U. G. Singh, R. I. Walton, R. T. Williams and S. A. Davis, *Chemistry of Materials*, 2005, **17**, 701-707.
11. J. Macanás, L. Ouyang, M. L. Bruening, M. Muñoz, J. C. Remigy and J. F. Lahitte, *Catalysis Today*, 2010, **156**, 181-186.
12. P. K. Jal, S. Patel and B. K. Mishra, *Talanta*, 2004, **62**, 1005-1028.
13. R. J. White, R. Luque, V. L. Budarin, J. H. Clark and D. J. Macquarrie, *Chemical Society Reviews*, 2009, **38**, 481-494.
14. K. M. Koczkur, S. Mourdikoudis, L. Polavarapu and S. E. Skrabalak, *Dalton transactions*, 2015, **44**, 17883-17905.
15. H. Nakao, H. Shiigi, Y. Yamamoto, S. Tokonami, T. Nagaoka, S. Sugiyama and T. Ohtani, *Nano Lett.*, 2003, **3**, 1391-1394.
16. J. Turkevich, P. C. Stevenson and J. Hillier, *Discussions of the Faraday Society*, 1951, **11**, 55-75.
17. J. Van Rie and W. Thielemans, *Nanoscale*, 2017, **9**, 8525-8554.
18. X. Wu, C. Lu, Z. Zhou, G. Yuan, R. Xiong and X. Zhang, *Environmental Science: Nano*,

2014, **1**, 71.

19. D. R. Bhumkar, H. M. Joshi, M. Sastry and V. B. Pokharkar, *Pharm. Res.*, 2007, **24**, 1415-1426.
20. C.-M. Shih, Y.-T. Shieh and Y.-K. Twu, *Carbohydrate Polymers*, 2009, **78**, 309-315.
21. J. Schurz, *Progress in Polymer Science*, 1999, **24**, 481-483.
22. M. Kaushik and A. Moores, *Green Chemistry*, 2016, **18**, 622-637.
23. K. Benaissi, L. Johnson, D. A. Walsh and W. Thielemans, *Green Chem.*, 2010, **12**, 220-222.
24. X. Wu, C. Lu, W. Zhang, G. Yuan, R. Xiong and X. Zhang, *Journal of Materials Chemistry A*, 2013, **1**, 8645.
25. X. Wu, C. Lu, Z. Zhou, G. Yuan, R. Xiong and X. Zhang, *Environmental Science: Nano*, 2014, **1**, 71-79.
26. Y. Zhang, Y. Liu, X. Wang, Z. Sun, J. Ma, T. Wu, F. Xing and J. Gao, *Carbohydr. Polym.*, 2014, **101**, 392-400.
27. T. Saito, S. Kimura, Y. Nishiyama and A. Isogai, *Biomacromolecules*, 2007, **8**, 2485-2491.
28. Y. Xin, Q. Xiong, Q. Bai, M. Miyamoto, C. Li, Y. Shen and H. Uyama, *Carbohydrate polymers*, 2017, **157**, 429-437.
29. P. Tarazona, *Phys Rev A Gen Phys*, 1985, **31**, 2672-2679.
30. P. Tarazona, U. M. B. Marconi and R. Evans, *Mol. Phys.*, 1987, **60**, 573-595.
31. T. Teranishi, I. Kiyokawa and M. Miyake, *Advanced Materials*, 1998, **10**, 596-599.
32. L.-S. Johansson and J. M. Campbell, *Surface and Interface Analysis*, 2004, **36**, 1018-1022.
33. L. Zhang, D. Ruan and J. Zhou, *Industrial & Engineering Chemistry Research*, 2001, **40**, 5923-5928.
34. Z. Hu, Q. Meng, R. Liu, S. Fu and L. A. Lucia, *ACS Sustainable Chemistry & Engineering*, 2017, **5**, 1601-1609.

Chapter 4

Facile fabrication of flow reactor from natural wood and the used cigarette filter

4.1 Introduction

With the increasing policy and awareness of sustainable development and environmental protection, converting the already existed cheap bioresource or daily waste material to valuable functional products through a facile and effective method is highly promising. In daily life, some cellulose-based monolithic materials such as the natural wood and the cigarette filter can be used to fabricated flow catalytic devices after suitable treatment. Unlike the cellulose monolith with a connected porous structure formed in the phase-separation process, the cigarette filter has a typically anisotropic fibrous structure, and the wood material poses a natural channel structure. These structures also endow the materials with good permeability and flowability and represent two commonly used structures in the flow reactors other than the connected porous structure.

Since the method established in Chapter 3 for fabricating cellulose flow reactor using cellulose itself as the reducing agent and supporting materials is conducted at room temperature without tedious chemical modification, it can be easily extended to other cellulose-based porous materials. As the demonstrations, this method was further used in this chapter to convert the natural wood and the used cigarette filter to flow reactors.

This chapter consists of two parts. In the first part, the biofriendly flow reactor with a channel structure was prepared from the natural wood. In the second part, the development of the flow reactor from a used cigarette filter was presented. The obtained flow reactor has excellent permeability and showed potential for the superfast treatment of wastewater.

4.2 Part I. Facile fabrication of flow reactor from natural wood

4.2.1 introduction

The natural wood has a naturally anisotropic structure with a large number of interconnected channels (or vessels) aligned along the growth direction. These aligned channels endow the wood with good permeability and enable the efficient transport of the water and nutrients from root to crown.[1-3] In light of these interesting properties, several efforts [4-7] have been attempted to develop functional devices from wood materials for flow catalytic application. The current methods for decoration of metal catalysts on wood materials are mainly based on two strategies. The first one is to chemically graft functional groups onto the wood and then introduce metal NPs using these functional groups as recipient or ligand.[7] This method allows us to finely design the surface chemical structure of wood, but it usually requires tedious modification steps or large chemical usage. Another method involves the carbonization [4] or hydrothermal treatment [8] of the metal ions precursors on the wood surface. It can directly form metal NPs with low chemical usage and fast speed, while this method relies on the energy-consuming equipment. Moreover, the high-temperature treatment may damage the original structure of wood, and thus it often conducted under the inert gas protection. From the green and sustainable perspective, a more facile and accessible method remains necessary for the efficient fabrication of the wood catalytic device.

In this part, the continuous-flow method in chapter 3 is extended to fabricate the flow reactor from the natural wood, in which the Au NPs are generated and stabilized using the wood itself as reductants and stabilizers in a continuous-flow fashion.

4.2.2 Experiments

Materials: The wood plate with a size of 45 cm × 3.5 cm × 1 cm was purchased from Seria Co.,Ltd., Japan. The Hydrogen Tetrachloroaurate Tetrahydrate powder ($HAuCl_4 \cdot 4H_2O$) with the purity of 99%, and the Sodium Hypochlorite aqueous solution (NaClO, active chlorite content is 8-13 wt%) were purchased from Nacalai Tesque, Inc. Kyoto, Japan. The polyolefin heat-shrinkable tube (THT-8.0N) was purchased from MonotaRO Co.,Ltd. Its inside diameter

was about 4 mm after shrinkage. The 4-NP was supplied by Tokyo Chemical Industry Co., Ltd. The $NaBH_4$ with the purity of 98%, the NaOH with a purity of 97%, and the chemically purified ethanol were provided by FUJIFILM Wako Pure Chemical Corporation, Japan. All the deionized water (18.2 MΩ·cm) used in this experiment was produced by a Merck Milli-Q Direct water purification system.

Fabrication of delignified wood-Au flow reactor: the wood plate was cut to columns with a length of 1.5 cm (along with the growth direction of wood) and a diameter of about 0.7 cm. After manually remove any detached impurity, a wood column was fixed into a shrinkage tube with a length of 4 cm. The delignified wood (dWood) was obtained by circularly flowing the NaClO aqueous solution (without dilution) through the wood to remove lignin using a peristaltic pump and then washed by flowing the deionized water. Subsequently, 5 mL of the 0.2 mmol/L HAuCl4 aqueous solution (in which 1 mL of 1 mol/L NaOH was added to adjust the pH to be around 13) was circularly flowed through the tube for 3 h to generate Au NPs in dWood. The obtained product, named dWood-Au, was used as a flow reactor in catalytic experiments.

Catalytic experiments: the reduction reaction of 4-NP was used to evaluate the catalytic performance of the obtained dWood-Au flow reactor. Specifically, the freshly prepared mixture solution of 1 mmol/L 4-NP and 0.2 mol/L $NaBH_4$ was flowed through the reactor with a certain flow rate to take reaction. Both the influent and effluent solutions were collected and tested by the UV-*vis* experiment to monitor the concentration change of 4-NP. To quantify the concentration, the standard curve of 4-NP in water was previously obtained using the 4-NP solutions with known concentration. The conversion (X_c) of the reaction was calculated by the equation: $X_c = (C - C_0)/C_0$, where C and C_0 are the 4-NP concentration before and after the reaction, respectively. The effect of the flow rate was investigated by changing the flow rate and recorded the X_c at each flow rate.

Characterization: The SEM images were collected using Hitachi S-3000N system at an acceleration voltage of 15 kV. Before observation, the cross-sections of samples were coated with a thin layer of Au by an ion sputter apparatus (E-1010, Hitachi Ltd.). FTIR spectra were

measured by ATR method on a Thermo Scientific (Yokohama, Japan) Nicolet iS5 spectrometer equipped with iD5 ATR attachment. The UV-*vis* absorption spectra were collected using a HITACHI U-2910 spectrophotometer. The absorbance curve was collected at the wavelength from 250 nm to 600 nm. TEM images were recorded using JEOL JEM-2010 at an acceleration voltage of 100 kV. The TEM grids (NP-C15, Okenshoji, Co., Ltd.) were used as received. ICP-AES measurements were carried out using SHIMADZU ICPS-8100 under the flowing of argon gas. The lignin contents of the samples were measured according to literature.[9]

4.2.2 Results and discussion

The balsa wood was used in this experiment to fabricate the flow reactor. As shown in **Fig. 4-1 (a-f)**, it posed a typical anisotropic structure in which the channels with a diameter of 20-30 um can be found along with the growth direction. After manually removing the attached impurities, the wood was cut to a column with a length of 1.5 cm along with the growth direction and a diameter of 0.7 cm at the radial direction, and then fixed into a polyolefin heat-shrinkable tube for flow application. As shown in **Fig. 4-1 (g)**, the NaClO aqueous solution was used to remove the lignin. As a result, the wood gradually faded and became white after about 3 h, indicating the removal of lignin. The component analysis demonstrated that the lignin content was significantly decreased from 24.7% to 6.1% during this flow process. **Fig. 4-1 (h)**. The dWood remained the column shape and good flowability, which enabled the further flow application.

To *in situ* generate the Au NPs on the dWood, the $HAuCl_4$/NaOH aqueous solution (PH was about 13) with an Au ion concentration of 0.2 mmol/L was circularly flowed through the dWood, as shown in **Fig. 4-2 (a** and **b)**). Consequently, the dWood was gradually changed to red, which suggested that the Au ions were reduced to Au NPs and deposited on the cellulose. (**Fig. 4-2 (c)**) According to the analysis in Chapter 3, the cellulose can reduce the Au ions to form Au NPs. Similarly, in this experiment, the reducibility of dWood towards Au ions can be attributed to the large number of cellulose molecules of dWood. To confirm the formation of Au NPs, the obtained sample (dWood-Au) after flowing for 2 h was collected and dried to be tested by TEM experiment. From **Fig. 4-2 (d)**, the NPs with a sphere shape can be observed on

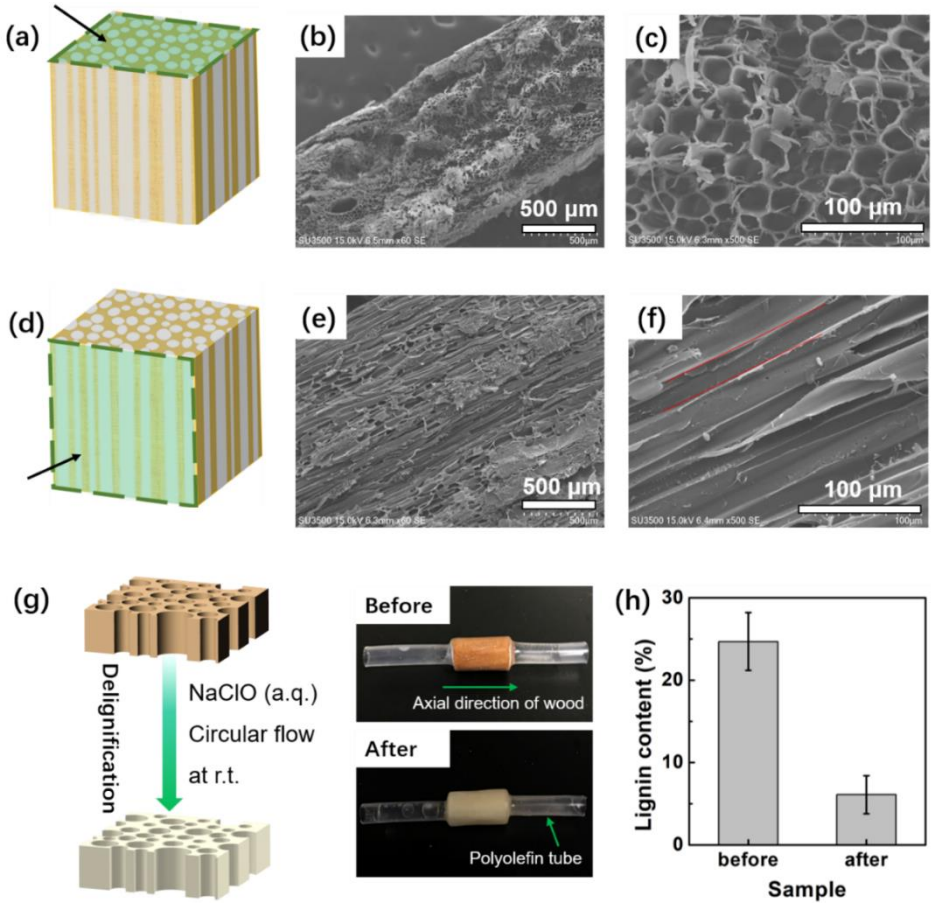

Fig. 4-1 (a) Schematic diagram of the wood (cross-section perpendicular to the growth direction is highlighted in the green dash). **(b, c)** SEM images of the cross-section perpendicular to the growth direction with different magnification. **(d)** Schematic diagram of the cross-section along with the growth direction of wood. **(e, f)** SEM images of the wood at cross-section along with the growth direction with different magnification. **(g)** Delignification of wood by the circular flow of NaClO aq. Digital photos are the wood column fixed in a shrinkage tube before and after delignification, respectively. **(h)** Lignin content of wood before and after delignification.

the Wood. The size and its distribution of the NPs were further counted using Image-J program and the average size was calculated to be 14.5 ± 5.2 nm, as illustrated in **Fig. 4-2 (e)**.

According to the result of ICP-AES measurements, the content of Au atoms deposited on the dWood was about 0.55 μmol. These Au NPs will serve as heterogeneous catalysts for the flow catalytic application. SEM images in **Fig. 4-2 (f** and **g)** revealed that the obtained dWood-Au kept the channel structure after the deposition of Au NPs, which would work as the pathway of reactants in the flow catalytic application. Different from the carbonization or hydrothermal strategies, the continuous-flow method was carried out at room temperature, which avoided the energy-consuming steps and prevented the structure of wood from damage at high-temperature.

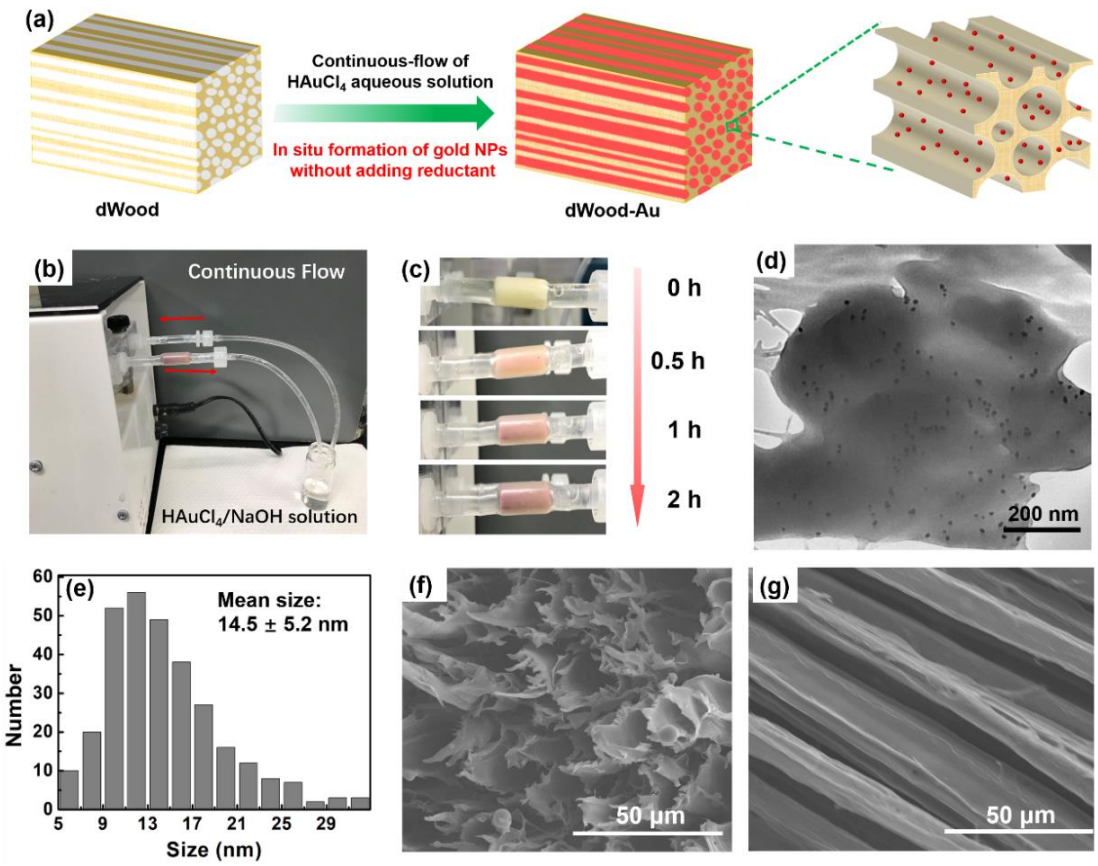

Fig. 4-2 (a) Scheme of the continuous-flow generation of Au NPs on the channel of wood. **(b)** Digital picture of the continuous flow system. **(c)** Digital pictures of the wood during the reaction process. **(d)** TEM image of the wood-Au sample. **(e)** Size distribution of the produced Au NPs. **(f)** and **(g)** are the SEM images of dWood-Au at the radial direction and axial direction, respectively.

Moreover, since the NPs were formed during the flow process, they are mainly located along with the flow route, but not homogeneously dispersed in the whole sample. This may reduce the "dead catalysts" that cannot contact the reactants and improve the overall usage efficiency of catalysts in the practical flow application.

The obtained dWood-Au was applied as a flow reactor as illustrated in **Fig. 4-3 (a)**. The reduction reaction of 4-NP, one of the commonest pollutants in wastewater, was applied in this experiment to access the catalytic performance of the reactor. Briefly, the fresh mixture of 4-NP (1 mmol/L) and $NaBH_4$ (0.2 mol/L) aqueous solution flowed through the reactor with a flow rate of 1 mL/min to reaction under the catalysis of Au NPs. It can be seen in **Fig. 4-3 (b** and **c)**, the color of the mixture solution changed from yellow to colorless after flow through the reactor, proving the successful degradation of 4-NP by the reactor. To quantitatively investigate the reduction process, UV-*vis* measurements were conducted to monitor the

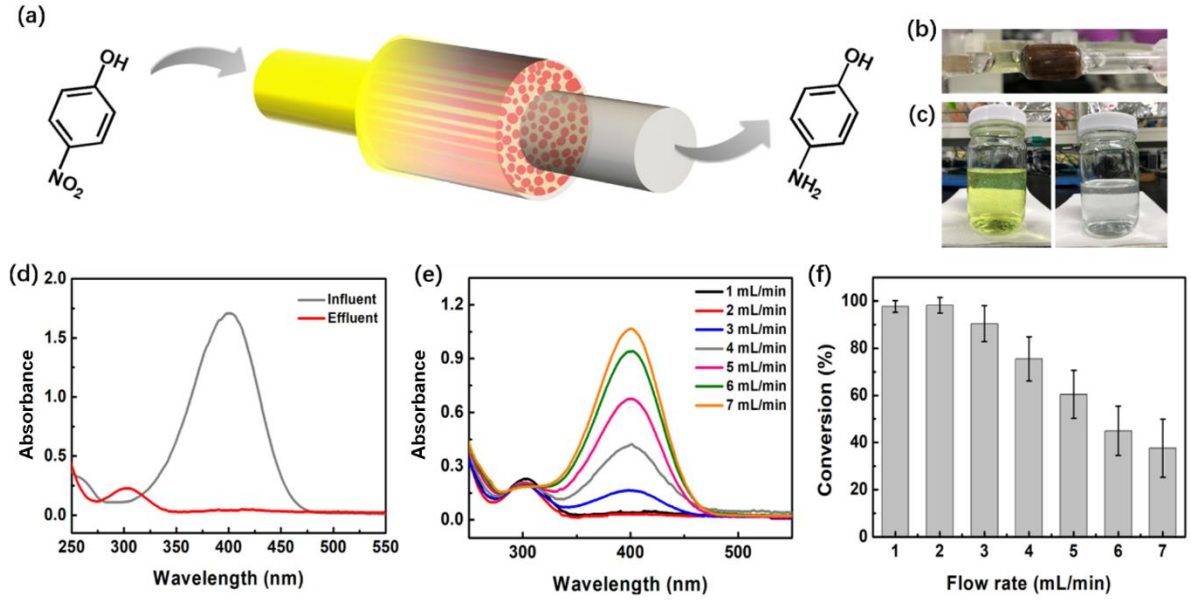

Fig. 4-3 (a) Schematic picture of the flow catalytic process. **(b)** Magnified photo of the flow reactor, which shows the color change of 4-NP after flow through the reactor. **(c)** Digital photos of the reactants solution before and after reaction **(d)** UV-vis spectra of the 4-NP before and after reaction with a flow rate of 1 mL/min. **(e)** UV-*vis* spectra of the solution outflow from the reactor with different flow rate. **(f)** Conversion of the 4-NP in the flow reaction at different flow rate.

concentration change of 4-NP in influent and effluent by detecting the characteristic peak at 400 nm, as displayed in **Fig. 4-3 (d)**. This peak disappeared at the spectrum of the solution outflow from the reactor with a flow rate of 1 mL/min. Furthermore, the effect of the flow rate on the catalytic performance was studied in **Fig. 4-3 (e)**. Under a relatively slow flow rate (≤ 2 mL/min), the 4-NP was not detected in the effluents, while at higher flow rate the 4-NP cannot be totally degraded and thus remained in the outflow solution. According to the standard curve, the conversion (X_c) of the reaction was calculated and listed in **Fig. 4-3 (f)**. The conversion reached almost 100 % when the flow rate was below 2 mL/min, while decreased as the flow rate further enhanced. Despite it, the conversion remains over 40 % even at a flow rate of 7 mL/min. Subsequently, the catalytic efficiency (defined as the moles of reactant catalyzed by per mole of Au atoms per hour) was calculated to be about 280 h^{-1}, which was as the same order as the current reported results [10-13], demonstrating the practicality of the obtained dWood-Au as an effective flow reactor.

4.2.3 Conclusion

In summary, this part reported a facile continuous-flow method for developing a flow reactor from natural wood. The Au NPs were reductively generated in the channels of wood using the dWood itself as a reducing agent. This method avoided the tedious chemical modification of wood and energy-consuming treatment. The obtained bWood-Au can be used as an effective flow reactor for the degradation of 4-NP.

4.3 Part II. Facile fabrication of flow reactor from the used cigarette filter

4.3.1 Introduction

The cigarette filter (CF), as ubiquitous plastic waste in the daily life, was long regarded as a headache for environmental protection since the annual disposed CF around the world was up to 5.6 trillion, [14] and it was difficult to biodegrade in the ecosystem. [15] Fortunately, different from the casually littered plastics that were usually mixed or contaminated by other wastes, the CF was mainly discarded in the designated smoking areas, [16] making the collection and utilization of CF practicable and convenient.

Taking concern of the special physical and chemical structure, the CF was deemed as a suitable material for fabricating a fast-speed flow reactor. On one hand, the CF is generally a cellulose acetate column with a typical anisotropic structure, in which a large number of fibers with a “Y” shape in cross-section are bunched up and aligned along with the axial direction. On the other hand, the cellulose acetate of CF fibers can be deacetylated to be biodegradable cellulose, and the abundant amount of hydroxyl groups on the cellulose was able to reduce metal ions and stabilize the formed metal NPs under alkaline condition.

In this part, the recycled CF was deacetylated to cellulose filter and then applied to reduce Au ion by a continuous flow process at room temperature without adding any reducing agent or surfactant. The obtained filter was applied as a continuous flow reactor and showed ultrafast

flow catalytic ability for the reductive removal of 4-NP and the degradation of dyes in water. This work provided a clean method to covert the waste CF to a useful flow reactor with the minimal usage of chemicals and the least modification steps, and the product showed great potential for the fast water treatment.

4.3.2 Experiments

Materials and chemicals: The CFs were collected from the used cigarette buttes of the PEACE-Super Light cigarettes (Japan Tobacco Inc., Japan) after consumed by the laboratory mates. The covering paper and tobacco ash remained on the CF were manually detached. $HAuCl_4 \cdot 4H_2O$ was provided by Nacalai Tesque, Inc. Kyoto, Japan, and the purity was 99 %. The 4-NP were purchased from Tokyo Chemical Industry Co., Ltd. The $NaBH_4$ and the NaOH with a purity of 97% were purchased from FUJIFILM Wako Pure Chemical Corporation, Japan. Other chemicals including the methanol and ethanol were all chemically purified and used as received.

Preparation of flow reactor from CF: The CF were firstly soaked in 200 mL of deionized water for 12 h, and then washed with 100 mL ethanol under ultrasonication for 3 h to remove impurities. During the washing process, the solution was exchanged to fresh ethanol every hour and repeated 3 times. After dried in vacuum, the obtained CF with a length of about 27 mm was fixed in a heat-shrinkable tube (the diameter of the CF column was about 5 mm after fixed in the shrinkable tube). Subsequently, 40 mL of 0.5 mol/L NaOH/methanol solution was circularly flowed through the tube by a peristaltic pump with a flow rate of 3 mL/min to react with CF for 3 h. As a result, the CF was deacetylated to be a cellulose filter (hCF).

After washing with 200 mL deionized water for 3 h, the obtained hCF was applied to react with $HAuCl_4$ solution to synthesize the Au NPs on its fibers. In detail, 5 mL of $HAuCl_4$ aqueous solution (0.2 mmol/L, pH was adjusted to be around 13 with 1 mol/L NaOH aqueous solution) circularly flowed through the hCF with a flow rate of 3 mL/min for 5 h. During this process, the Au NPs gradually formed in hCF. After washing with 200 mL of deionized water, the obtained filter (hCF-Au) was applied as a flow reactor.

Catalytic performance test of the obtained flow reactor: The reduction of 4-NP was used to evaluate the catalytic performance of the obtained hCF-Au flow reactor. In this experiment, the 0.5 mmol/L 4-NP and the freshly prepared 0.25 mol/L $NaBH_4$ were mixed and immediately flow through the reactor with a certain flow rate to take reaction under the catalyzation of Au NPs. The effluent solution was collected to test the concentration of the remained 4-NP by UV-*vis* measurements. (The samples were diluted by 5 times with deionized water to be tested.)

The leaching of Au NPs in the flow reactor was further investigated as follows: 5 mL of the deionized water was circularly flowing through the reactor with the flow speed of 60 mL/min to wash the hCF-Au filter. After washing for 3 h, 3 mL of the washing solution was collected and added into 3 mL of the mixed aqueous solution of 4-NP (0.5 mmol/L) and $NaBH_4$ (0.25 mol/L). The obtained mixture solution was stored at room temperature for 3 days. If it contained the leached Au NPs, the yellow color of the solution would be gradually fade during the storage. On the other hand, the reusability was tested by flow 100 mL of 0.5 mmol/L 4-NP reactants solution through the reactor with 5 mL/min to take reaction, and the effluent was collected to calculate the conversion based on UV-*vis* measurement. This experiment was repeatedly conducted with the same condition, and the conversions in each cycle were recorded. To avoid the effect of the remained reactants in the flow reactor, the flow reactor was washed by 30 mL of deionized water before reuse.

Characterization: The FTIR measurements were conducted on a Thermo Scientific Nicolet iS5 spectrometer with an iD3 ATR attachment to detect the chemical composition of the CF, hCF, and hCF-Au. The micromorphology of the original CF and the hCF were observed by the SEM (Hitachi S-3000N) at a voltage of 15 kV. Before the measurement, the samples were coated with a thin layer of Au using an ion sputter apparatus (E-1010, Hitachi Ltd. Co.). In the synthesis process, the deposition amount of Au ions was determined by the UV-*vis* spectrophotometer (Hitachi, U2910) based on the concentration change of the Au ions in flow solution before and after the reaction. The date at the wavelength from 250 nm to 600 nm were collected. Before the test, the pH of the solution was adjusted to be 1 with the 1 mol/L HCl

aqueous solution. The concentration of UV specimen was determined according to the peak intensity and calibrated based on the volume change caused by the pH adjustment. The standard $HAuCl_4$ aqueous solutions with the concentration of 0.02, 0.05, 0.10, and 0.20 mmol/L were previously tested respectively as references. The ICP-AES-8100 (Shimadzu, Japan) was also employed to confirm the Au loading of products. The sample was dissolved in 20 mL of aqua regia to be tested. To investigate the size and its distribution of the formed Au NPs in hCF-Au, the TEM (JEOL JEM-2010) was applied using an acceleration voltage of 100 kV. The samples were ground to powder and then dispersed in the methanol. a little drop of the obtained suspension was deposited on the copper grid (NP-C15, Okenshoji, Co., Ltd., used as received) to be tested after completely drying. The surface chemical composition before and after reaction with Au ions was studied by XPS (JEOL JPS-9010MC) with monochromatized Al-Kα radiation. The spectra were collected at fixed analyzer pass energies of 160 eV and 10 eV, respectively. The resulted binding energy was calibrated setting the C1s peak of C-H (sp^3) carbon at 284.8 eV. The permeability of the samples was tested by flowing the deionized water with different flow rates and recording the corresponding average backpressure. According to these results, the permeability was calculated based on Darcy's Law [17].

4.3.3 Results and discussion

The CFs were collected and used for flow catalytic application in this work. As shown in **Fig. 4-4 (a)**, a used CF generally consists of the wrapping paper, remained tobacco ash, and the CA fibers massed together. After detaching the paper/ash and repeatedly washing according to the previously reported method,[18] the obtained clean CF showed a white color. The SEM images in **Fig. 4-4 (b** and **c)** illustrated that the CF posed an anisotropic structure, in which the CA fibers with a typical "Y"-shaped cross-section were aligned along with the axial direction. Such a special structure endowed the CF with good permeability and made the ultrafast flow application of CF possible. It is known that the CA materials are not biodegradable and soluble in many organic solvents such as DMF and acetone, which is not conducive to the development of green and stable flow reactor. To remove this obstacle, the CF was fixed in a shrinkable tube, and the NaOH/methanol solution was circularly flowed through the filter by a peristaltic pump

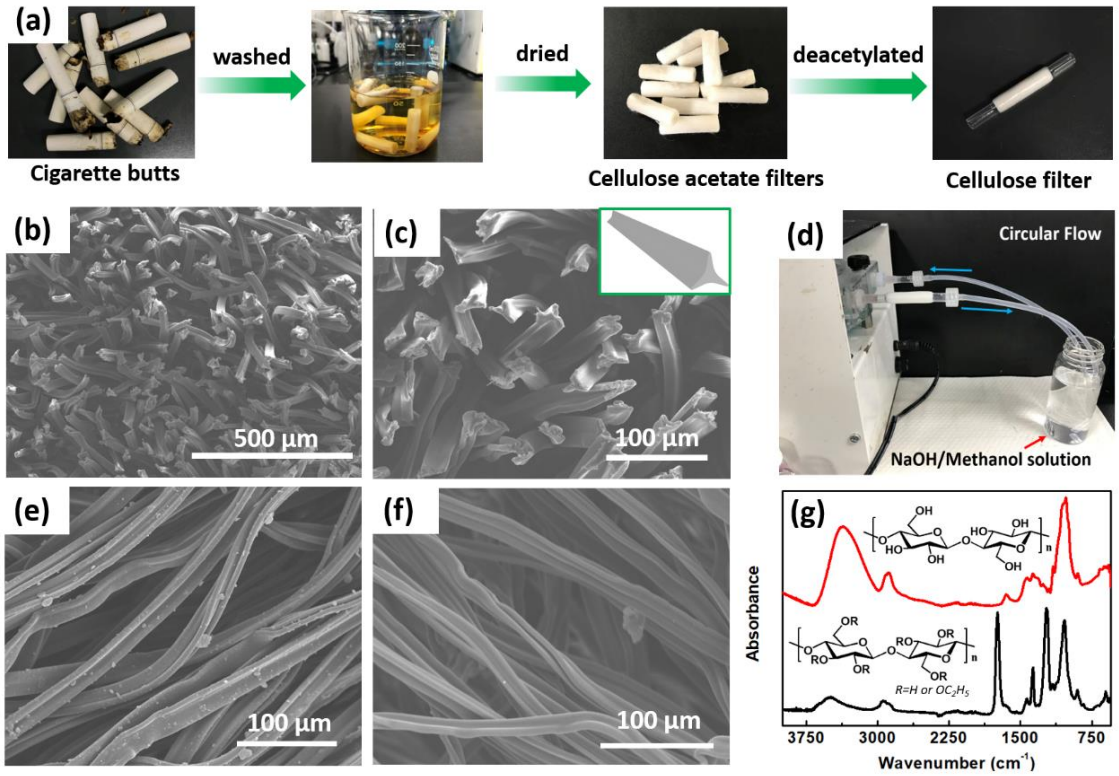

Fig. 4-4 (a) The preparation process of cellulose filters from CFs. **(b** and **c)** The SEM images of the CF at the radius direction. Inset is the schematic picture of the CF fiber with a "Y" shape. **(d)** Digital picture of the continuous-flow hydrolyzation of CF using a peristaltic pump. (**e** and **f**) SEM images of the filter fibers before and after deacetylation. **(g)** FTIR spectra of the sample before and after deacetylation. (inset is the corresponding chemical structure).

(see **Fig. 4-4 (d)**). During this procedure, the CF was gradually deacetylated to be a cellulose filter (hCF). It should be noted that the deacetylation treatment would not destroy the structure of CF since this process was conducted in ethanol at relatively mild room temperature. As shown in **Fig. 4-4 (e** and **f)**, the hCF kept the anisotropic structure of CF with light shrinkage. To confirm the success of this reaction, the FTIR spectra of CF and hCF were collected and compared in **Fig. 4-4 (g)**, it can be found that the characteristic peaks of CA at 1232 cm^{-1} and 1743 cm^{-1}, which originated from the acetate groups, disappeared at the hCF spectrum. Meanwhile, the hCF showed an intensified peak around 3300 cm^{-1}, suggesting that the CA was hydrolyzed to be cellulose. Different from the CA, the cellulose was regarded as a biodegradable and chemical resistant material.

The continuous-flow method was applied to achieve the synthesis and immobilization of Au NPs on hCF, in which the hCF worked as both reducing and stabilizing agents as illustrated

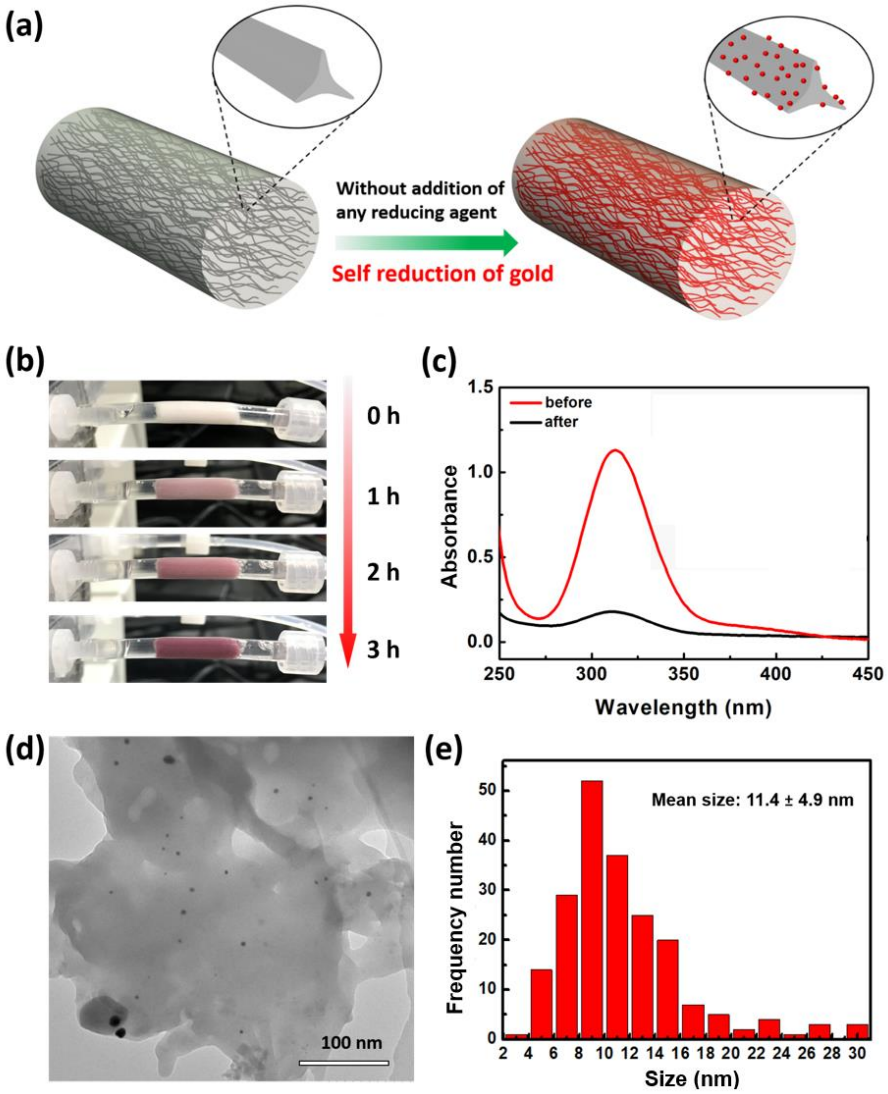

Fig. 4-5. (a) The scheme of the continuous-flow synthesis of Au NPs on hCF without addition of any other reductant. **(b)** The color change of hCF during the continuous flow process. The reddish appearance of hCF indicated the formation of Au NPs on hCF. **(c)** UV-*vis* spectra of the Au solution before and after the flow reaction with hCF. (**d**) The TEM images of hCF-Au, in which the sphere Au NPs can be observed. **(e)** The size and its distribution of the Au NPs on hCF-Au based on the TEM observation.

in **Fig. 4-5 (a)**. In this experiment, the mixed $HAuCl_4$/NaOH aqueous solution was circularly flowed through the hCF to take reaction. As an interesting result, the hCF was gradually changed to be reddish and the red color became darker in the flow process, which indicated the formation of Au NPs on hCF (**Fig. 4-5 (b)**). It should be noted that the solution kept colorless during the whole flow reaction, suggesting that Au NPs were immobilized by the hCF but not dispersed in solution.

The UV-*vis* experiments were conducted to monitor the concentration change of Au ions

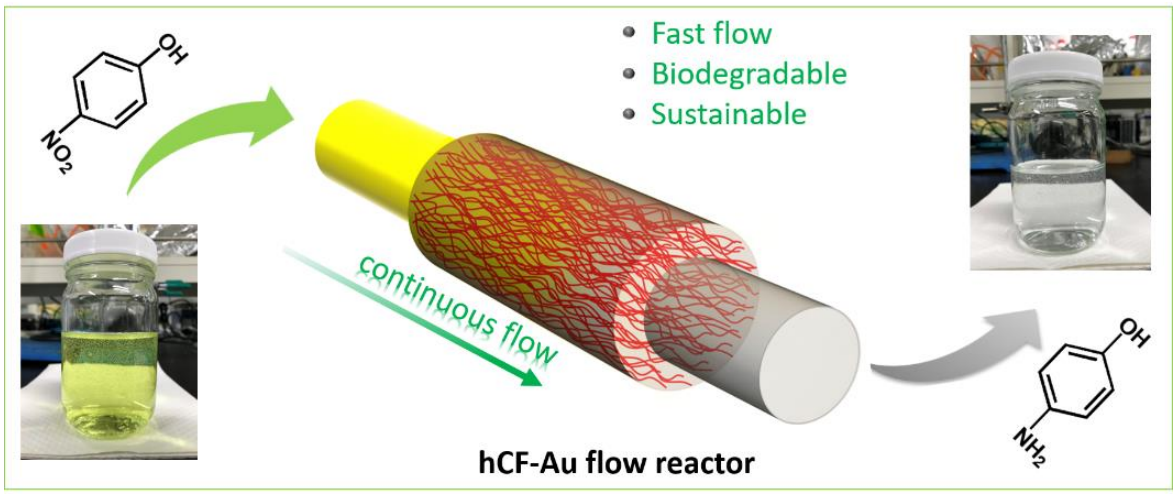

Fig. 4-6. The scheme of the obtained hCF-Au flow reactor and its application in the continuous flow reduction of 4-NP.

in solution before and after the reaction. Results (**Fig. 4-5 (c)**) demonstrated that the Au ions were reduced during the reaction, and the amount of the exhausted Au ions was calculated to be around 80% based on the standard curve. This coincided with the result of ICP-AES measurement (76%). To confirm the formation of Au NPs, the obtained sample (hCF-Au) was observed by TEM. As shown in **Fig. 4-5 (d)**, the Au NPs with a sphere shape were found in the image and no aggregation was observed. Furthermore, the size and its distribution of the formed Au NPs were accounted for and analyzed by Image-J program. Results (**Fig. 4-5 (e)**) demonstrated that the average size was around 11.4 nm (about 200 counts). All these results above demonstrated that the Au NPs were successfully synthesized and supported by the hCF.

As elucidated in **Fig. 4-6,** the hCF-Au was fixed in a shrinkable tube and then used as a continuous-flow reactor. The reduction of 4-NP was employed as a model reaction to evaluate the catalytic performance of hCF-Au product. In this experiment, the peristaltic pump was employed to flow the reactants (the freshly prepared mixture solution of 0.5 mmol/L 4-NP and 0.25 mol/L $NaBH_4$) through hCF-Au filter with certain flow rate to take reaction under the catalysis of the Au NPs. As shown in **Fig. 4-7 (a)**, when the flow speed was set to 5 mL/min, the color of the solution was changed from yellow to colorless after the reaction, indicating the successful reduction of 4-NP. The reaction process can also be monitored by UV- *vis* experiments using the characteristic peak of 4-NP at around 400 nm. This peak was disappeared and a new peak at 312 nm emerged after flow through the hCF-Au filter, which confirmed the

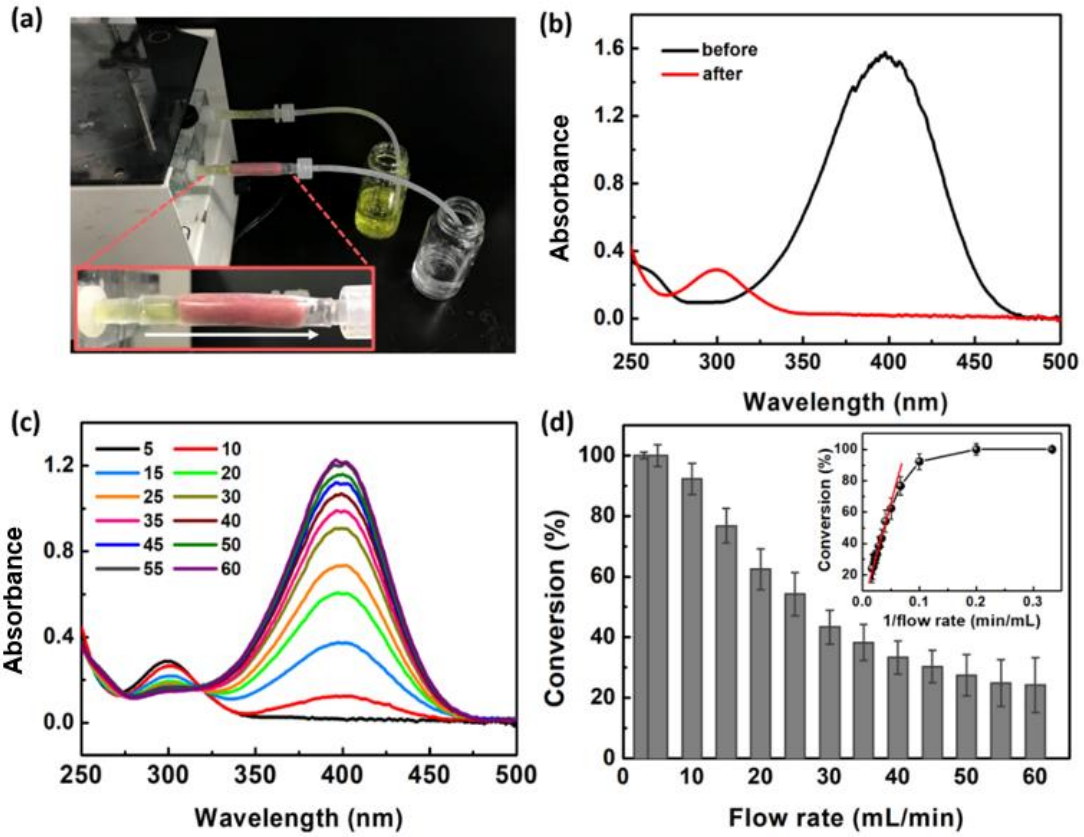

Fig. 4-7. (a) The digital picture of the flow reactor in the catalytic process. (Inset was the magnified picture of the reactor. The yellow solution was reduced to colorless after flow out from reactor). **(b)** The UV-*vis* spectra of the reactants solution before and after flow through the hCF-Au reactor. (The samples were diluted by 5 times to be tested.) **(c)** The UV-*vis* spectra of the reactants solution after flow through the reactor with various flow rate (mL/min). (The samples were diluted by 5 times to be tested.) **(d)** The conversion of 4-NP calculated based on the UV-*vis* results. Inset is the conversion as a function of 1/flow rate.

complete reduction of 4-NP and the formation of corresponding product 4-AP. (**Fig. 4-7 (b)**)

The effect of the flow rate on the catalytic reaction was investigated as shown in **Fig. 4-7 (c)**. It can be found that the 4-NP was completely reduced when the flow rate was below 5 mL/min, while under a faster flow rate the 4-NP cannot be totally reacted and its characteristic peak remained. The concentration of 4-NP in each effluent solution was further determined according to the standard curve in Chapter 1. As shown in **Fig. 4-7 (d)**, the reaction efficiency was almost 100 % at a low flow rate (< 5 mL/min). When applied to a faster flow speed, the flow reactor still worked. The reactor can endure the flow rate of 60 mL/min without damage, which suggested that the hCF-Au flow reactor can be employed for ultrafast catalytic applications such as the high-throughput water treatment. Although the reactor still worked at

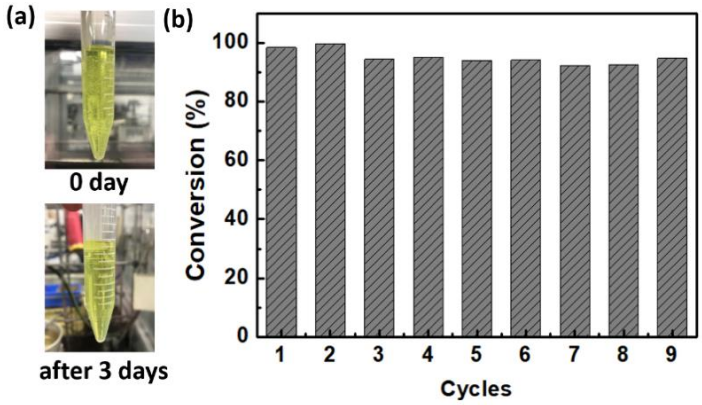

Fig. 4-8. (a) The digital picture of the mixture solution of 4-NP and washing water. **(b)** The stability of the flow reactor.

over 60 mL/min, the reaction conversion is further decreased. This decrease of the conversion at a high flow rate can be interpreted by the insufficient contact of reactants with Au NPs. At such a speed, the majority of the reactants passed through the reactor without enough time to take reaction. To quantitatively investigate the catalytic efficiency, the inset in **Fig. 4-7 (d)** plots the relationship between conversion and 1/*v*, and the TOF was estimated based on the slope of the fitting line of the low *1/v* region (v > 15 mL/min). The result indicated that the TOF was about 370 h^{-1}, which was relatively high compared with the results in other works, [10-13] suggesting that the hCF-Au flow reactor can work under ultrafast speed without the sacrifice of catalytic efficiency.

To clarify the stability of the reactor, the leaching of Au was tested by a simple experiment. The deionized water after circularly flow through the hCF-Au with a flow rate of 60 mL/min for 3 h was collected and added into the mixed reactants solution of 4-NP (0.5 mmol/L) and $NaBH_4$ (0.25 mol/L). The result showed that the yellow color of 4-NP did not fade even kept it for 3 days (**Fig. 4-8 (a)**), indicating the leaching of Au NPs during the flow process was ignorable, otherwise, the 4-NP would be reduced by the leached Au NPs in water. Furthermore, the reusability was studied by repeatedly catalyzing the reaction of 4-NP aqueous solution. In each cycle, 100 mL of 4-NP was treated and the conversion was tested by UV-*vis* experiments. As recorded in **Fig. 4-8 (b)**, the conversion kept over 90 % even after repeat for 9 times.

The ultrafast throughput capacity of the obtained flow reactor can be interpreted by the special anisotropic structure. As shown in **Fig. 4-9 (a)**, the cellulose fibers aligned and bunched

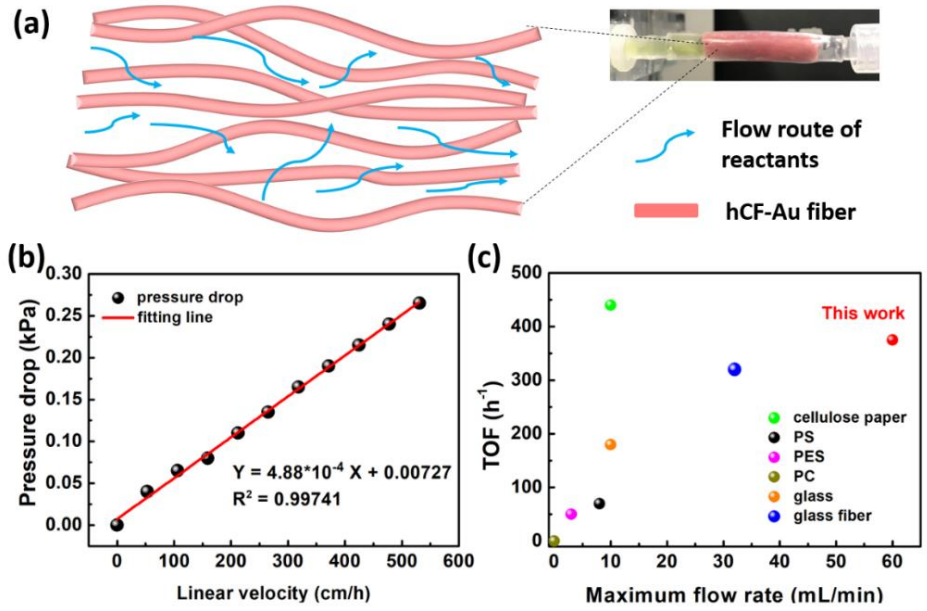

Fig. 4-9 (a) The scheme of the flow routes in the hCF-Au reactor. **(b)** The pressure drop of the hCF-Au reactor at different of linear velocity. **(c)** The TOF and the maximum flow rate of the hCF-Au reactor and other catalytic flow reactor reported in other works.

together in the axial direction. When the reactant solution was pumped into the filter, it progressed between the surface of fibers with very low flow resistance. During this process, the influent solution would weave between the large number of hCF-Au fibers (about 3×10^4 cm^{-2}, based on SEM observation) and frequently contact the Au NPs on the fibers to take reaction. As a result, the 4-NP was gradually reduced to 4-aminophenol. **Fig. 4-9 (b)** plotted the pressure drop of the obtained hCF-Au reactor as a function of the linear velocity (equal to the flow rate divided by the cross-sectional area). Accordingly, the permeability coefficient was calculated to be around 1.4×10^{-10} m^2. It was much higher than common porous cellulose materials [19]. The good permeability of the reactor resulted from the special structure of the CF, which was remained after modification. Beside of the permeability, the catalytic performance was of crucial importance for the flow reactor as well. To intuitively compare the catalytic performance, **Fig. 4-9 (c)** presented the TOF as well as the maximum flow rate of the obtained product and other flow systems made from the materials such as the cellulose paper, glass fibers, polycarbonate (PC) membranes, polyethersulfone (PES) hollow fibers, and the polysulfone (PS) hollow fibers. [10-13] The glass and glass fibers catalytic systems have a low cost. The catalytic reactors made from PES and PS hollow fibers pose a well-designed hollow structure for flow,

but their catalytic activity is relatively low. The cellulose paper catalytic system showed high activity, while its maximum flow rate is only 10 mL/min. Compared with these reactors, the hCF-Au exhibits an evident improvement of the flow rate without the sacrifice of the catalytic efficiency.

From the economical perspective, the hCF-Au reactor had a relatively low cost since it was made from the waste cigarette filter and the fabrication process did not involve expensive organic chemicals or solvents. Although the Au as a noble metal is expensive, the usage of the $HAuCl_4$ in this experiment for synthesis Au NPs was very low (1 μmol), thus the product was not very costly even taking into the account of Au NPs. Considering that the reactor can be reused, the hCF-Au flow reactor was cost-effective. Actually, the organic pollutants can also be degraded by other methods such as the electrochemistry process [20], ultrasonic degradation [21], photocatalysts [22]. However, the electrochemistry process and ultrasonic degradations are usually energy-consuming. The photocatalytic degradation method uses solar light or UV light as energy to degrade the pollutants and thus its operating cost is very low. Nevertheless, the photocatalysts are usually limited by the relatively low efficiency. Compared with these processes, the hCF-Au reactor showed relatively high catalytic efficiency and low cost. Based on the analysis above, the hCF-Au flow reactor has a potential in water treatment.

4.3.4 Conclusion

The CF was recycled to fabricate an ultrafast flow reactor. After removing the impurities, the obtained CF was deacetylated to prepare hCF. And then the facile continuous-flow strategy was employed to immobilize the Au NPs on the surface of the fibers of hCF, in which the Au ions were directly reduced by hCF. The Au NPs formed on the surface of hCF showed a sphere shape with an average size of 11.4 nm. The obtained hCF-Au was applied as a flow reactor for the reduction of 4-NP. The result indicated that the TOF of the reactor was about 370 h^{-1} for the reduction of 4-NP. Owing to the anisotropic structure of hCF, the obtained flow reactor showed a high permeability and ultrafast flow catalytic ability. This product may have great potential for superfast water treatment.

4.4 References

1. P. Kitin and R. Funada, *IAWA Journal*, 2016, **37**, 315-331.
2. John S. Sperry, *Int. J. Plant Sci.*, 2003, **164**, S115-S127.
3. L. A. Berglund and I. Burgert, *Adv. Mater.*, 2018, **30**, e1704285.
4. Y. Wang, G. Sun, J. Dai, G. Chen, J. Morgenstern, Y. Wang, S. Kang, M. Zhu, S. Das, L. Cui and L. Hu, *Adv. Mater.*, 2017, **29**.
5. H. Guo, P. Warnicke, M. Griffa, U. Muller, Z. Chen, R. Schaeublin, Z. Zhang and M. Lukovic, *ACS Nano*, 2019, **13**, 14337-14347.
6. B. Chen, A. Gsalla, A. Gaur, Y. H. Lui, X. Tang, J. Geder, M. Pruessner, B. J. Melde, I. L. Medintz, B. Shafei, S. Hu and J. C. Claussen, *ACS Applied Nano Materials*, 2019, **2**, 4143-4149.
7. Z. Yang, H. Liu, J. Li, K. Yang, Z. Zhang, F. Chen and B. Wang, *ACS applied materials & interfaces*, 2020, **12**, 15002-15011.
8. S. He, C. Chen, G. Chen, F. Chen, J. Dai, J. Song, F. Jiang, C. Jia, H. Xie, Y. Yao, E. Hitz, G. Chen, R. Mi, M. Jiao, S. Das and L. Hu, *Chemistry of Materials*, 2020, **32**, 1887-1895.
9. M. Zhu, J. Song, T. Li, A. Gong, Y. Wang, J. Dai, Y. Yao, W. Luo, D. Henderson and L. Hu, *Adv. Mater.*, 2016, **28**, 5181-5187.
10. L. Ouyang, D. M. Dotzauer, S. R. Hogg, J. Macanás, J.-F. Lahitte and M. L. Bruening, *Catalysis Today*, 2010, **156**, 100-106.
11. A. S. Peinetti, L. P. De Leo, G. A. Gonzalez and F. Battaglini, *J. Colloid Interface Sci.*, 2012, **386**, 44-50.
12. H. Koga, N. Namba, T. Takahashi, M. Nogi and Y. Nishina, *ChemSusChem*, 2017, **10**, 2560-2565.
13. J. He, W. Ji, L. Yao, Y. Wang, B. Khezri, R. D. Webster and H. Chen, *Adv. Mater.*, 2014, **26**, 4151-4155.
14. H. Moriwaki, S. Kitajima and K. Katahira, *Waste Manag*, 2009, **29**, 1192-1197.
15. J. Puls, S. A. Wilson and D. Hölter, *J. Polym. Environ.*, 2010, **19**, 152-165.
16. A. L. Roder Green, A. Putschew and T. Nehls, *Journal of Hydrology*, 2014, **519**, 3466-3474.
17. S. Whitaker, *Transport in Porous Media*, 1986, **1**, 3-25.
18. F. Huang, Y. Xu, B. Peng, Y. Su, F. Jiang, Y.-L. Hsieh and Q. Wei, *ACS Sustainable Chemistry & Engineering*, 2015, **3**, 932-940.

19. Z. Yang, T.-A. Asoh and H. Uyama, *Bull. Chem. Soc. Jpn.*, 2019, **92**, 1453-1461.
20. L. Ma, M. Zhou, G. Ren, W. Yang and L. Liang, *Electrochim. Acta*, 2016, **200**, 222-230.
21. M. Dukkanci and G. Gunduz, *Ultrason. Sonochem.*, 2006, **13**, 517-522.
22. C.-C. Wang, J.-R. Li, X.-L. Lv, Y.-Q. Zhang and G. Guo, *Energy Environ. Sci.*, 2014, **7**, 2831-2867.

Concluding remarks

In this thesis, the monolithic cellulose with a hierarchically porous structure was prepared by TIPS, and its application as the catalyst matrices was investigated. Three efficient strategies have been developed to construct catalytic flow devices based on the monolithic cellulose.

In Chapter 1, The cellulose monolith was prepared by the TIPS method. The obtained cellulose monolith had a hierarchically porous structure with adjustable pore size and an excellent shape resilience under compression. A surface modification strategy was used to functionalize the monolith surface with bPEI. The Pd nanoparticles were synthesized on the skeleton of the cellulose monolith through a Pd ions absorption process followed by the chemical reduction of $NaBH_4$. The obtained cellulose-Pd monolith was applied as a flow reactor for continuously catalyzing the reduction reaction of 4-nitrophenol. The result showed that the flow reactor has an enhanced catalytic efficiency rather than cellulose nanocrystals-supported Pd catalysts and showed good stability. The higher catalytic activity can be interpreted by the special hierarchically porous structure, in which the Pd NPs are distributed along the flow route. In the flow process, the reactant was forced to flow in the interconnected pores and sufficiently contact with the catalysts to take reaction. Moreover, the bPEI-modified monolith can also be applied to other flow applications such as the bacteria capture in water, due to the good bio-infinity of bPEI molecules.

On the other hand, in Chapter 2, the PVP-stabilized Au NPs with a narrow size distribution were transferred on cellulose monolith as catalysts without surface modification. After the removal of the attached PVP by washing with the $NaBH_4$ solution, the obtained sample can be used as a flow reactor in water. The particle size of the Au NPs remained during the deposition and PVP-removing process. Moreover, the removal of the PVP led to the enhanced catalytic activity of Au NPs. This method realized the facile deposition of the readymade Au catalysts and avoided the chemical modification of the cellulose monolith surface, which provided a facile approach to introduce the well-designed metal NPs on cellulose monolith for flow reaction.

Furthermore, Chapter 3 reported a simple strategy to generate and support the Au NPs on cellulose monolith under a continuous-flow condition. In this method, the cellulose monolith not only acted as supporting material but also worked as the reducing agent. The reducibility of cellulose monolith can be attributed to a large number of the hydroxyl groups on cellulose monolith, which will reduce Au ions under alkaline condition. The effects of the reaction condition on the particle size were investigated. The result showed the flow condition favors to form smaller AuNPs with relatively homogeneous size distribution rather than the batch condition. It avoided the surface modification process and needed not external reducing agent and stabilizer. Thus, the obtained monolith-Au reactor had a simple chemical composition and can be used in both water and organic solvent such as DMF with good stability. Moreover, since this method was simple and conducted at room temperature, it can be easily applied to other monolithic cellulose.

Finally, the method in chapter 3 was further extended to other cellulose-based monolithic material including the natural wood material and the used cigarette filter, which was described in Chapter 4. The Au NPs were successfully synthesized and immobilized on the interconnected channel structure of wood after delignification. The obtained wood-Au materials can be used as a green and biofriendly reactor. Besides the wood material, the used cigarette filter was also recycled to fabricate the flow reactor. The cigarette filter after deacetylation was applied to generate and support Au NPs. Due to its superior permeability, the obtained cigarette filter-Au reactor can be used for fast water treatment. Unlike the cellulose monolith with a connected porous structure formed in the phase-separation process, the cigarette filter has a typically anisotropic fibrous structure, and the wood material poses a natural channel structure, which are two commonly used structures in the flow reactors other than the connected porous structure. Both these experiments confirmed that the continuous-flow method for generation metal NPs using monolithic cellulose as a reducing agent has good applicability and showed great potential for developing cellulose-based flow catalytic devices.

In summary, the thesis developed three efficient strategies for fabricating flow catalytic devices. The research in this thesis demonstrated the monolithic cellulose material has a great

potential for the application of catalyst matrix. The methods established in this thesis may provide guidance for the future development of sustainable flow reactors based on monolithic cellulose materials.

List of publications

Chapter 1

Monolithic cellulose supported metal nanoparticles as green flow reactor with high catalytic efficiency

Zheng-Tian Xie, Taka-Aki Asoh*, Hiroshi Uyama*

Carbohydrate Polymers, **2019**, *214*, 195-203.

Amine-functionalized cellulose monolith for efficient bacterial capture

Xinnan Cui, **Zhengtian Xie**, Yoshihiro Yamaguchi, Taka-Aki Asoh*, Hiroshi Uyama*

Colloid and surface B: biointerfaces (submitted)

Chapter 2

Facile deposition of narrow-dispersed gold nanoparticles on monolithic cellulose

Zheng-Tian Xie, Yuta Uetake, Taka-Aki Asoh*, Hidehiro Sakurai, Hiroshi Uyama*

in preparation

Chapter 3

Dual roles of cellulose monolith in the continuous-flow generation and support of gold nanoparticles for green catalyst

Zheng-Tian Xie, Taka-Aki Asoh*, Yuta Uetake, Hidehiro Sakurai, Hiroshi Uyama*

Carbohydrate Polymers, **2020***, 247*,116723

Chapter 4

Superfast flow reactor derived from the used cigarette filter for the degradation of pollutants in water

Zheng-Tian Xie, Taka-Aki Asoh*, Hiroshi Uyama*

Journal of Hazardous Materials, **2020**, *400*,123303.

Facile fabrication of flow reactor from natural wood

Zheng-Tian Xie, Taka-Aki Asoh*, Hiroshi Uyama*

Chemistry letters **2020**, *49*, X

Acknowledgments

This study was carried out from 2017 to 2020 at Department of Applied Chemistry, Graduate School of Engineering, Osaka University. During the 3 years, I have received a lot of assistant from many people around me. Upon the completion of this thesis, I am grateful to those who have offered me encouragement and support.

First of all, profound gratitude should go to my supervisor Prof. Hiroshi Uyama for his continuous guidance and suggestions on my study. Thanks for his kind help during the research project design, experiment supporting, and manuscripts revising. He also provided me the valuable opportunities to attend academic conferences including the internal and international ones, which allowed me to share my research with other researchers. My eyesight was broadened and my research taste was improved in these communication experiences. I also sincerely thank him for the important advice and recommendations in my future career.

Besides my supervisor, I would like to thank the rest of my thesis committee: Prof. Masaya Nogi and Prof. Hidehiro Sakurai, for their insightful comments and their donation of time. I owe my sincere thanks to Prof. Hidehiro Sakurai and Assist. Prof Yuta Uetake for their suggestions and help in my experiments and scientific paper writing. I learned a lot during the discussion with them. I also thank Prof. Susumu Kuwabata and Assist. Prof. Taro Uematsu, for the assistant in the SEM experiments.

I also want to express my heartfelt appreciation to Assoc. Prof. Taka-Aki Asoh for his help in my research. Thank him for the manuscripts revising, inspirations, and experience sharing. He taught me the philosophy for overcoming the problem and encouraged me to build a strong heart when confronted with the challenge on the route of pursuing doctor degree. All these will be a great help to my future academic research and daily life.

I am grateful for the kind help and expert suggestions from Prof. Takashi Tusjimoto (Teikyo University of Science), Assist. Prof. Yu-I Hsu. Dr. Yasushi Takeuchi and Dr. Xinnan Cui. Their help played an important role in the smooth conduction of my research work.

Special thanks also send to Ms. Yoko Uenishi and Ms. Tomoko Shimizu for their warm-hearted support in the laboratory affairs and the kind help in my daily life.

My appreciation also goes to the previous and current fellows in the laboratory: Dr. Yu Shu, Dr. Tomonari Kanno, Dr. Qidong Wang, Dr. Zhaohang Yang, Dr. Masatoshi Kato, Mr. Chen Qian, Ms. Yankun Jia, Mr. Shunsuke Mizuno, Mr. Toshiki Tamiya, Mr. Bozhi Chen, Mr. Naharullah Bin Jamaluddin, Mr. Raghav Soni, Ms. Hanyu Wen, Ms. Yanting Lyu, Mr. Akihide Sugawara, Mr. Mark Adam Malaluan Ferry, Ms. Yan Wang, Mr. Luwei, Zhang, Ms. Meng Wei, Mr. Yusuke, Hinamoto, Mr. Haoyan Zhou, Ms. Lulu Huang, etc. Thanks for their kind-hearted help both in my research and daily life.

I would like to thank the scholarship support from China Scholarship Council (CSC) for my academic study and stay in Japan.

Finally, I want to express my appreciation to my family and my girlfriend. Thanks for their endless love, support, and understanding.

July 2020

XIE Zhengtian